PALAMIDIS KYRIAKOS

Simulation and techno-economic analysis of an alkaline electrolyser for green hydrogen production

SCHOOL OF MECHANICAL ENGINEERIGN

Sector: Thermal Engineering

Supervisor: Sotirios Karellas, Professor NTUA

Athens 2024

ΠΑΛΑΜΙΔΗΣ ΚΥΡΙΑΚΟΣ

ΣΧΟΛΗ ΜΗΧΑΝΟΛΟΓΩΝ ΜΗΧΑΝΙΚΩΝ

Μοντελοποίηση και τεχνοοικονομική ανάλυση παραγωγής πράσινου υδρογόνου μέσω αλκαλικής ηλεκτρόλυσης

Τομέας: Θερμότητας

Επιβλέπων: Σωτήριος Καρέλλας, Καθηγητής ΕΜΠ

Αθήνα 2024

Acknowledgements

This particular thesis was conducted at the Laboratory of Thermal Processes within the school of Mechanical Engineering at the National Technical University of Athens (NTUA).

I would like to express my warm gratitude to Professor Sotiris Karellas, who entrusted me with such an interesting topic. Furthermore, my collaboration with the Ph.D. candidate Nikos Skordoulias was pivotal and flawless. He guided me through all aspects of the thesis, dedicating a significant amount of his time, for which I am grateful.

Throughout the thesis, I received substantial support from my family, friends and my girlfriend Natalia and I sincerely thank them for it.

The completion of this specific thesis signifies the end of the chapter of my academic years. During this time, my brother and fellow student, Gabriel Palamidis, was constantly by my side, offering advice and guidance. Finally, this journey wouldn't have been the same, filled with memories, if it weren't for my friends and future colleagues from the university.

Ευχαριστίες

Η συγκεκριμένη διπλωματική εργασία εκπονήθηκε στο εργαστήριο Θερμικών Διεργασιών του τμήματος Μηχανολόγων Μηχανικών του ΕΜΠ.
Για την εκπόνηση της διπλωματικής μου εργασίας θα ήθελα αρχικά να ευχαριστήσω θερμά τον καθηγητή Σωτήρη Καρέλλα που με εμπιστεύτηκε με την ανάθεση ενός τόσο ενδιαφέροντος θέματος. Ύστερα καταλυτική και άψογη ήταν η συνεργασία μου με τον υποψήφιο διδάκτορα Νίκο Σκορδούλια, ο οποίος με καθοδήγησε σε όλες τις πτυχές της εκπόνησης της εργασίας αφιερώνοντας πολύ από τον χρόνο του και προς τούτο του είμαι ευγνώμων.
Κατά την διάρκεια της εκπόνησης της εργασίας έλαβα πολύ στήριξη από την οικογένεια μου, τους φίλους μου και την κοπέλα μου Ναταλία και για αυτό τους ευχαριστώ θερμά.
Με την εκπόνηση της συγκεκριμένης διπλωματικής σηματοδοτείται το τέλος του κεφαλαίου των φοιτητικών μου χρόνων στο οποίο δίπλα μου ήταν διαρκώς ο αδερφός μου και συμφοιτητής Γαβριήλ Παλαμίδης προσφέροντας μου συμβουλές και καθοδήγηση. Τέλος το ταξίδι αυτό δεν θα ήταν το ίδιο και γεμάτο αναμνήσεις εάν δεν είχα δίπλα μου τους φίλους και μελλοντικούς μου συνάδελφους από το πανεπιστήμιο.

Declaration of responsibility for plagiarism and theft of intellectual property:

I have read and understood the rules on plagiarism and how to properly cite sources contained in the Guide to Writing Dissertations. I declare that, to the best of my knowledge, the content of this Thesis is the product of my own work and there are references to all the sources I have used.

The views and conclusions contained in this thesis are those of the author and should not be interpreted as representing the official positions of the School of Mechanical Engineering or the National Technical University of Athens.

Kyriakos Palamidis

Υπεύθυνη δήλωση για λογοκλοπή και για κλοπή πνευματικής ιδιοκτησίας:

Έχω διαβάσει και κατανοήσει τους κανόνες για τη λογοκλοπή και τον τρόπο σωστής αναφοράς των πηγών που περιέχονται στον οδηγό συγγραφής Διπλωματικών Εργασιών. Δηλώνω ότι, από όσα γνωρίζω, το περιεχόμενο της παρούσας Διπλωματικής Εργασίας είναι προϊόν δικής μου εργασίας και υπάρχουν αναφορές σε όλες τις πηγές που χρησιμοποίησα.

Οι απόψεις και τα συμπεράσματα που περιέχονται σε αυτή τη Διπλωματική εργασία είναι του συγγραφέα και δεν πρέπει να ερμηνευθεί ότι αντιπροσωπεύουν τις επίσημες θέσεις της Σχολής Μηχανολόγων Μηχανικών ή του Εθνικού Μετσόβιου Πολυτεχνείου.

Κυριάκος Παλαμίδης

Contents

Abstract

Over the last few years, it has become increasingly clear that in order to address the climate crisis, the penetration of renewable energy sources in much larger shares of the energy mix is a one-way street. Nevertheless, the thoughtfulness of RES raises the issue of finding ''energy batteries'' that will contribute to the flexibility of systems and the decarbonization of hard to abate sectors. Hydrogen seems to be able to play this role by taking the form of a green fuel, which can be produced through water electrolysis using renewable electricity. The aim of this thesis is to carry out the modelling, the simulation and techno-economic analysis of an alkaline electrolyser for green hydrogen production.

Hydrogen, as a green fuel, possesses high thermal energy per unit of mass and a similar interchangeability ratio to many conventional fuels. On the flip side, it contains very low energy per unit of volume and raises safety issues. Depending on the method of hydrogen production, it is often divided into different colors that indicates how environmentally friendly it is, with green standing out as the friendliest coming from the electrolysis of water from renewable electricity. Alkaline electrolysis is the most mature technology. Another crucial factor of hydrogen lifecycle is its storage. Hydrogen can be stored as a solid, liquid or a gas with the last being the most common.

For the simulation of the electrolysis system Aspen Plus^{TM} was utilized and to properly simulate the behavior of the alkaline stack, Aspen Custom Modeler was used. There, the semi-empirical equations that describe the behavior of a 15 kW experimental electrolyser from the original paper of Sanchez et al., were used. The validation of the stack was successful since the results from the created component matched perfectly with the results from the original paper. Subsequently, an integrated 1.5 MW electrolysis system was developed by adding a cooling system with a fan and water refrigerant, the purification system that isolates hydrogen, which enters the two-stage compressor system to produce the final 200 bar and 25 Celsius hydrogen. The simulation was solved for three different stack pressures (5,7 and 10 bars) and four inlet stack temperatures (50,60,70 and 80 Celsius). The mixture that gets into the stack consists of 65% w/w H_2O and 35% w/w KOH electrolyte. The results from the 12 different simulations for power input ranging from 250 to 1500 kW, affecting the load, were transferred to Excel for a system behavior analysis. Comparing the system's results with 1.5 MW commercial alkaline electrolyser revealed that hydrogen production was in line. However, the efficiency and water amount did not show significant correlation.

The results from the simulations aided in extracting performance charts for different loads, stack pressures and inlet stack temperatures. Overall, the system operates more efficiently at lower stack pressures and higher stack inlet temperatures. When the inlet stack temperature increases, more hydrogen is being produced and less energy is being consumed in the cooling system while stack pressure reduction result to smaller amount of hydrogen returning to the stack although more energy is being consumed on the compressors.

Ultimately at 5 bar and 80 Celsius, the highest system efficiency of 54.9% is observed, for current density of 0.33 A/cm^2 that leads to the generation of 12.93 kg/hr of hydrogen. The highest electrical consumption arises from the electrolyte, followed by the cooling system, the compressors and finally the pumps.
Conducting a simple techo-economic analysis of the system, three different scenarios of electrical supply from photovoltaics (PV), wind turbines and the electrical grid were examined, resulting the Levelized Cost Of Hydrogen (LCOH). Wind turbines, due to their lower electricity production cost and higher capacity factor than photovoltaics, lead to the lowest LCOH at 6.6 €/kg, while PV lead to 10.6 €/kg. For the grid connection scenario, the system operation was found to be more efficient for 4000 hours annually, producing hydrogen at a cost of 9.8 €/kg, which is 2.2 €/kg cheaper than the 8000 annual operating hours scenario. In the case of operating under the worst temperature and pressure conditions, the LCOH increased by 1-1.7 €/kg. Finally, by calculating the LCOH for cases where the system is connected to renewable energy sources in a 2030 construction scenario, where the electricity production costs are expected to further decrease, and the capital costs of the alkaline stack electrolysers are expected to decrease as well, the LCOH calculated at 5.2 €/kg and 7.9 €/kg for the wind turbine and the PV connection scenarios, respectively. In capital costs the biggest influence comes from the stack which is followed by the compressors and finally the supply of deionized water. In operational costs, the primary role is played by the cost of electricity, followed by the stack, the compressor, the storage and finally the supply of deionized water.

Περίληψη

Κατά την διάρκεια των τελευταίων ετών γίνεται ολοένα και πιο φανερό ότι για την αντιμετώπιση της κλιματικής κρίσης η διείσδυση των ανανεώσιμων πηγών ενέργειας σε πολύ μεγαλύτερα ποσοστά του ενεργειακού μείγματος είναι μονόδρομος. Ωστόσο, η στοχαστικότατα που χαρακτηρίζει τις ΑΠΕ θέτει το θέμα εύρεσης <<μπαταριών>> ενέργειας που θα βοηθήσουν στην ευελιξία των συστημάτων και στην απανθρακοποίηση ιδιόμορφων τομέων της ενέργειας. Τον ρόλο αυτό φαίνεται να μπορεί να παίξει το υδρογόνο παίρνοντας την μορφή ενός πράσινου καυσίμου που μπορεί να παραχθεί από την ηλεκτρόλυση του νερού με χρήση ανανεώσιμου ηλεκτρισμού. Σκοπός της παρούσας διπλωματικής εργασίας είναι να διεξάγει την μοντελοποίηση και τεχνοοικονομική ανάλυση της παραγωγής πράσινου υδρογόνου μέσω αλκαλικής ηλεκτρόλυσης.

Το υδρογόνο ως πράσινο καύσιμο διαθέτει πολύ υψηλά ποσά θερμότητας ανά μονάδα μάζας και παρόμοιο δείκτη εναλλαξιμότητας με πολλά από τα συμβατά καύσιμα ενώ από την άλλη διαθέτει πολύ χαμηλή ενέργεια ανά μονάδα όγκου και δημιουργεί ζητήματα ασφαλείας. Ανάλογα με την μέθοδο παραγωγής του υδρογόνου, συχνά χωρίζεται σε διαφορετικά χρώματα που χαρακτηρίζουν και το πόσο φιλικό προς το περιβάλλον είναι, με το πράσινο να είναι πολύ φιλικό προς το περιβάλλον έχοντας παραχθεί από ανανεώσιμο ρεύμα και νερό. Αυτή η μέθοδος παραγωγής ονομάζεται ηλεκτρόλυση και η πιο ώριμη τεχνολογία ηλεκτρόλυσης είναι η αλκαλική. Σημαντικός παράγοντας στον κύκλο ζωής του υδρογόνου είναι και η αποθήκευσή του η οποία μπορεί να γίνει σε στερεή υγρή και αέρια μορφή με την τελευταία να είναι η πιο σύνηθες.

Για την μοντελοποίηση χρησιμοποιήθηκε το πρόγραμμα Aspen Plus™ με την βοήθεια του Aspen Custom Modeler στο οποίο δημιουργήθηκε ένα εξειδικευμένο στοιχείο που προσομοιώνει με ακρίβεια την αλκαλική ηλεκτρόλυση νερού με χρήση ημι-εμπειρικών εξισώσεων που έχουν αναπτυχθεί κατά την ανάλυση πειραματικού συστήματος ηλεκτρόλυσης ισχύος 15 kW. Η δημιουργία αυτού του στοιχείου κρίθηκε επιτυχής καθώς ήρθε σε πλήρη επαλήθευση με τα αποτελέσματα που προέκυψαν από την αρχική προσομοίωση του Sanchez. Στην συνέχεια δημιουργήθηκε ένα ολοκληρωμένο σύστημα ισχύος 1.5 MW προσθέτοντας το σύστημα ψύξης με ανεμιστήρα και ψυκτικό μέσο νερό, το purification system που απομονώνει το υδρογόνο το οποίο ύστερα εισέρχεται στο διβάθμιο σύστημα των συμπιεστών για να παραχθεί τελικά υδρογόνο πίεσης 200 bar και 25 Celsius. Το μοντέλο αυτό επιλύθηκε για τρεις διαφορετικές πιέσεις ηλεκτρόλυσης 5,7 και 10 bar και για τέσσερις θερμοκρασίες μείγματος εισαγωγής στον ηλεκτρολύτη 50,60,70 και 80 Celsius. Το μείγμα αυτό αποτελείται από 65% κατά βάρος H_2O και 35% κατά βάρος ηλεκτρολύτη KOH. Επιλύοντας τα 12 διαφορετικά σενάρια για εισαγωγή ισχύος 250-1500 kW η οποία επηρεάζει το φορτίο, προέκυψαν αποτελέσματα που μεταφέρθηκαν στο excel για να μελετηθεί η συμπεριφορά του συστήματος. Συγκρίνοντας τα αποτελέσματα του συστήματος

ηλεκτρολύτες παρόμοιας ισχύος της αγοράς φάνηκε πως η παραγωγή υδρογόνου συμβαδίζει, ωστόσο η απόδοση και η ποσότητα νερού δεν είχαν ιδιαίτερη αντιστοιχία.
Τα αποτελέσματα από την επίλυση των συστημάτων βοήθησαν στην εξαγωγή διαγραμμάτων λειτουργίας για διαφορετικό φορτίο, πιέσεις ηλεκτρόλυσης και θερμοκρασίες εισαγωγής στον ηλεκτρολύτη. Συνολικά το σύστημα λειτουργεί πιο αποδοτικά για χαμηλότερες πιέσεις ηλεκτρόλυσης και υψηλότερες θερμοκρασίες εισαγωγής ηλεκτρόλυσης καθώς η αύξηση της θερμοκρασίας έχει σαν αποτέλεσμα ο ηλεκτρολύτης να λειτουργεί πιο αποδοτικά παράγοντα περισσότερο υδρογόνο και καταναλώνοντας λιγότερη ενέργεια στο σύστημα ψύξης, ενώ η μείωση της πίεσης προκαλεί την επιστροφή μικρότερων ποσών υδρογόνου στον ηλεκτρολύτη παρόλο που προκαλεί αύξηση στην κατανάλωση του διβάθμιου συμπιεστή. Έτσι τελικά για 5 bar και 80 Celsius παρατηρείται ο μεγαλύτερος βαθμός απόδοσης συστήματος 54.9% για πυκνότητα ρεύματος 0.33 A/cm^2 με 12.93 kg/hr παραγόμενο υδρογόνο. Η μεγαλύτερη ηλεκτρική κατανάλωση προκύπτει από τον ηλεκτρολύτη και ύστερα ακολουθούν το σύστημα ψύξης, οι συμπιεστές και τέλος οι αντλίες.
Διεξάγοντας μια απλή τεχνοοικονομική ανάλυση του συστήματος κατά την οποία εξετάστηκαν τρία διαφορετικά σενάρια ηλεκτρικής τροφοδότησης από φωτοβολταϊκά, ανεμογεννήτριες και το ηλεκτρικό δίκτυο προέκυψαν τα σταθμισμένα κόστη του υδρογόνου. Οι ανεμογεννήτριες λόγω του φθηνότερου κόστους παραγωγής ηλεκτρικής ενέργειας και υψηλότερου βαθμού εκμεταλλευσιμότητας από τα φωτοβολταϊκά οδηγούν στο χαμηλότερο σταθμισμένο κόστος υδρογόνου 6.6 €/kg ενώ τα φωτοβολταϊκά 10.6€/kg. Για το σενάριο σύνδεσης με το δίκτυο κρίθηκε πιο αποδοτική η λειτουργία του συστήματος για 4000 ώρες ετησίως όπου παράγεται υδρογόνο με κόστος 9.8 €/kg που είναι 2.2 €/kg φθηνότερο από το σενάριο 8000 ωρών λειτουργίας ετησίως. Σε περίπτωση λειτουργίας του συστήματος στις χειρότερες συνθήκες θερμοκρασίας και πίεσης το σταθμισμένο κόστος αυξάνεται κατά 1-1.7 €/kg. Τέλος κάνοντας τους υπολογισμούς για τα σταθμισμένα κόστη για τις περιπτώσεις σύνδεση του συστήματος με ΑΠΕ σε περίπτωση κατασκευής το 2030, όπου τα κόστη παραγωγής ηλεκτρικής ενέργειας και τα κεφαλαιουχικά κόστη του αλκαλικού ηλεκτρολύτη αναμένεται να μειωθούν περαιτέρω, υπολογίστηκαν σταθμισμένα κόστη 5.2 €/kg και 7.9 €/kg για το σενάριο σύνδεσης με ανεμογεννήτρια και φωτοβολταϊκά αντίστοιχα. Στα κεφαλαιουχικά κόστη μεγαλύτερη βαρύτητα έχει ο ηλεκτρολύτης και ακολουθεί το σύστημα συμπίεσης και τέλος της αποθήκευσης σε φιάλες αέριου υδρογόνου, ενώ στα λειτουργικά κόστη το κύριο ρόλο παίζει το κόστος της ηλεκτρικής ενέργειας και ακολουθούν ο ηλεκτρολύτης, ο συμπιεστής, η αποθήκευση και τέλος η προμήθεια απιονισμένου νερού.

1. Introduction

On this chapter the context, the purpose and the structure of the thesis are displayed.

1.1 Climate change and plans towards carbon neutrality

The quality of human life has always been related to the energy consumption [1]. During the last centuries energy consumption has raised dramatically as Figure 1 demonstrates.

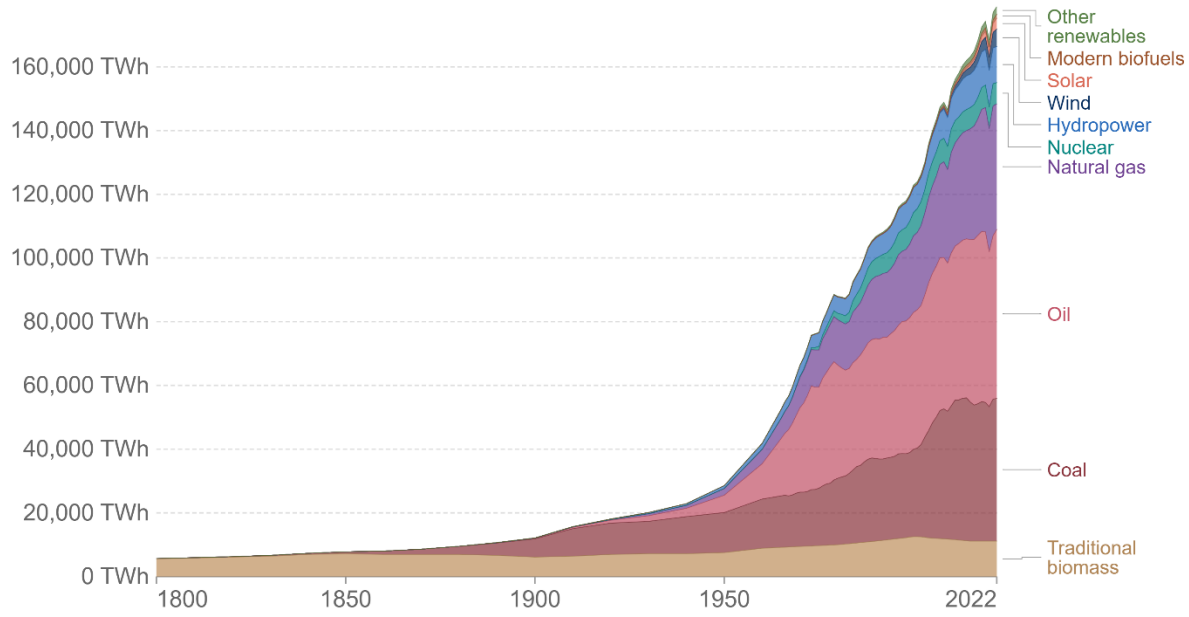

Figure 1: Global primary energy consumption by source for the period 1800-2022 [2].

However, the way modern societies produce their energy is not sustainable due to the rise of the temperature that comes with the increased CO_2 and other greenhouse gases concentration on the atmosphere. The CO_2 concentrations for the last 800 thousand and 60 years are presented on Figure 2 and Figure 3.

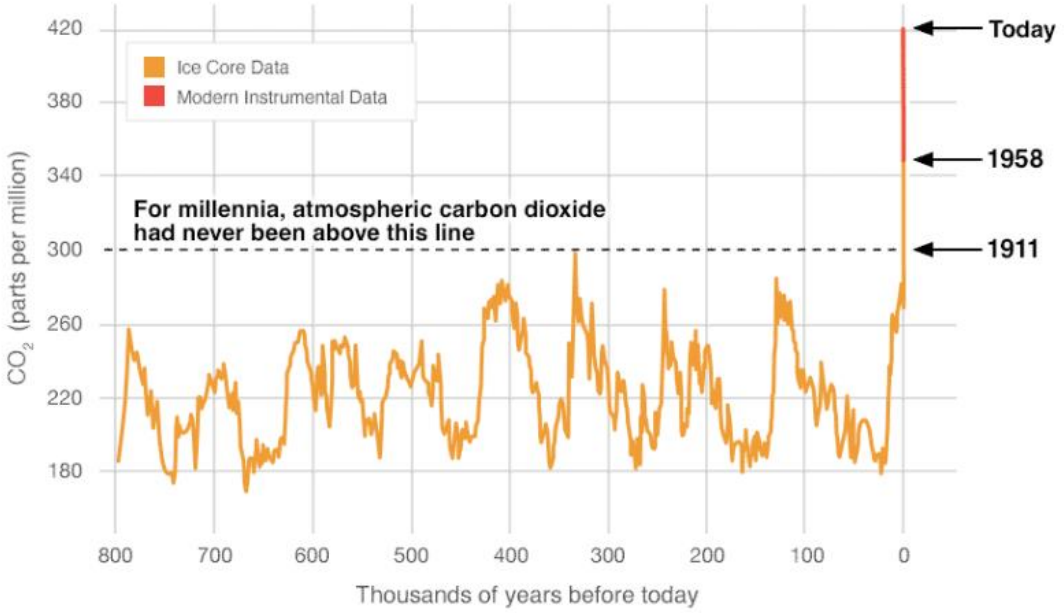

Figure 2: Concentration of CO_2 in the atmosphere during the last 800 thousand years [3].

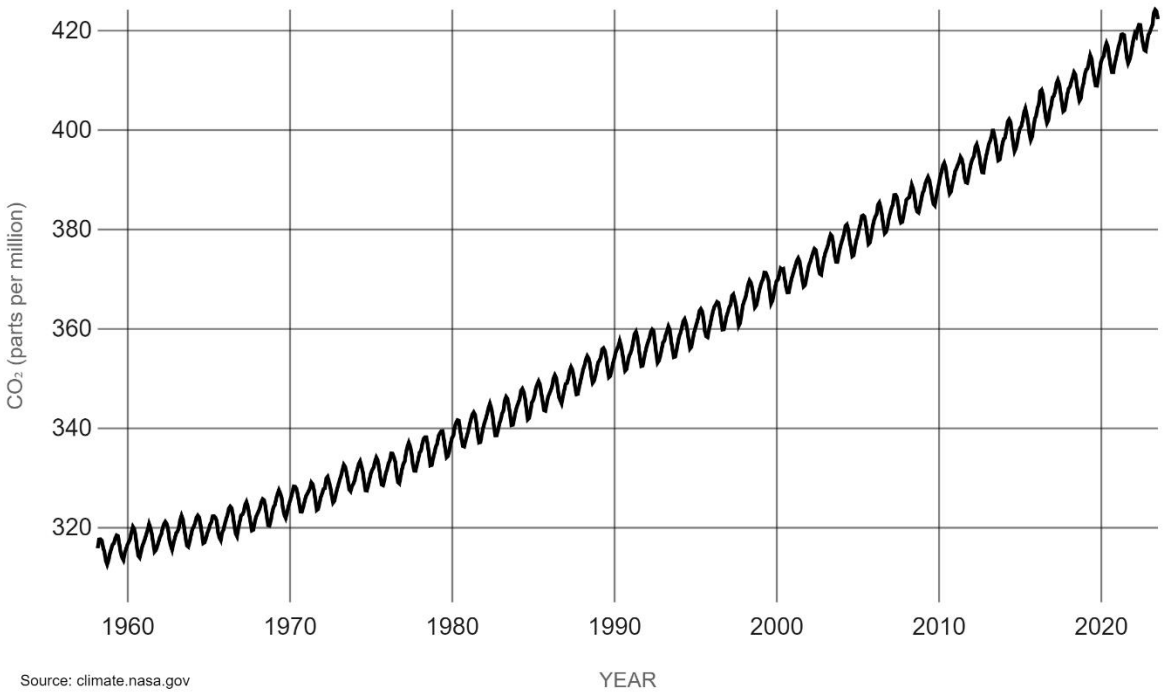

Figure 3: Concentration of CO_2 in the atmosphere during the last decades [3].

First Svante Arrhenius noted that increased concertation of carbon dioxide and water vapor in the atmosphere would result in a warming of the planet [4], [5]. Ever since, much research has been done connecting greenhouse gases with global warming. Already average global surface temperature has been raised around 0.9 Celsius compared to the average temperature of the period 1951-1980 as Figure 4 illustrates.

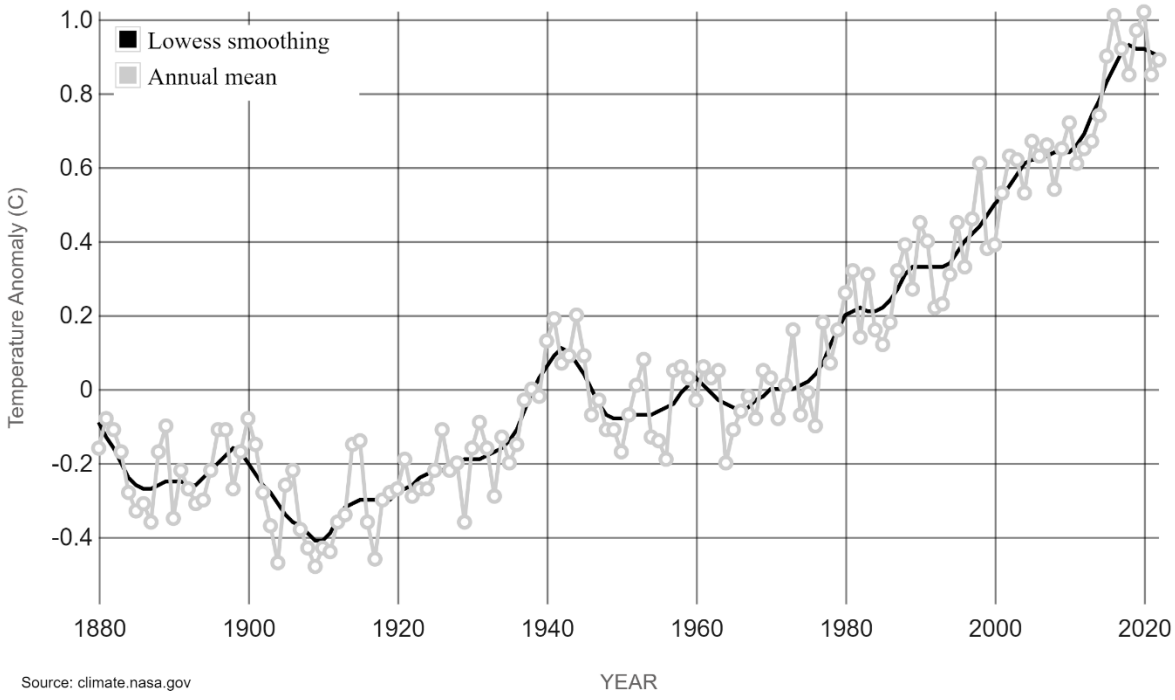

Figure 4: Global surface temperature compared to the long-term average from 1951 to 1980 [6].

Global warming can turn on a list of consequences that is known as climate change. There are facts connecting climate change with various potential catastrophic impacts on the air, water, plants, animals, and human beings. Quality of drinking water, change in hydrological cycle and impacts on wildlife. Economy could also be influenced importantly because marine economy, wool industry, water recourses, land carrying capacity and animal health would be affected due to temperature rise and water quality and availability. Human health will be affected as well due to the increase of heat stress, flooding changes in disease transmission and malnutrition [7].

In order to avoid the catastrophic results of the climate change countries have started taking action. The most recent and important action is the Paris agreement, which set the goal of limiting the global warming under 2 Celsius with the more specific target of the 1.5 Celsius, comparing to pre-industrial levels, and it was signed from 196 countries. To keep global warming to 1.5°C, greenhouse gas emissions must peak no later than 2025 and then fall by 43% by 2030 [8].

All 27 EU member states agreed to make the EU the first climate-neutral continent by 2050. To get there, they agreed to cut emissions by at least 55% by 2030, compared to 1990 levels. To do so multiple targets, such as energy saving have been given. One of the most important targets is the binding renewable target for 2030 which has been set to at least 42,5% of the total energy mix. That implies doubling the existing share of renewable energy in the EU [9].

Therefore, the importance of renewable energy technologies is major for the energy portfolio of the forthcoming decades since the sustainability of energy generation is critical. Although one of the biggest challenges is their stochastic character which relates to their availability and intermittency [10]. This constraint can be addressed by energy storage solutions. One of the most promising technologies that can tackle this problem is the electrolysis of water to produce hydrogen. More specific, energy surplus from renewable sources can be used to produce hydrogen that can later be used when there is energy demand in order to supply the system with the necessary electricity through the opposite process of electrolysis on fuel cells or it can also be used as a green fuel on plenty hard to electrify sectors such as transportation, heating and industry. A possible hydrogen ecosystem is illustrated below.

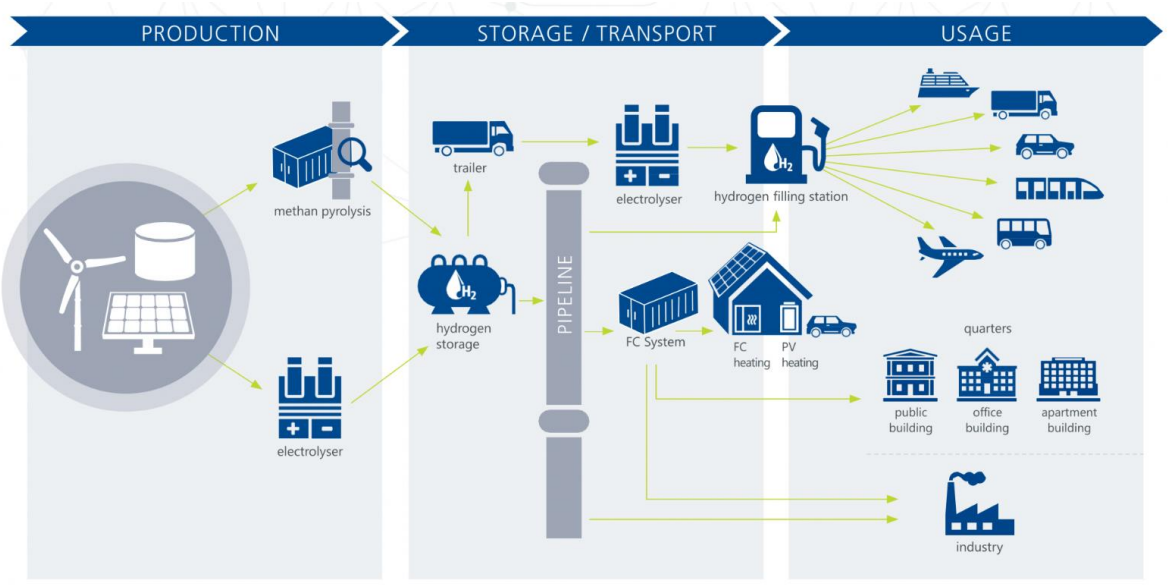

Figure 5: Possible hydrogen ecosystem [11]

In Europe there are already ambitious plans about hydrogen that aim to a climate neutral Europe. Those plans are mentioned below and visualized on Figure 6.

-Till 2024: installation of at least 6 GW of renewable hydrogen electrolysers in the EU, and the production of up to 1 million tons of renewable hydrogen.

-2025-2030: hydrogen needs to become an intrinsic part of our integrated energy system, with at least 40 GW of renewable hydrogen electrolysers and the production of up to 10 million tonnes of renewable hydrogen in the EU.

-2030 and onwards: renewable hydrogen will be deployed at a large scale across all hard-to-decarbonize sectors.

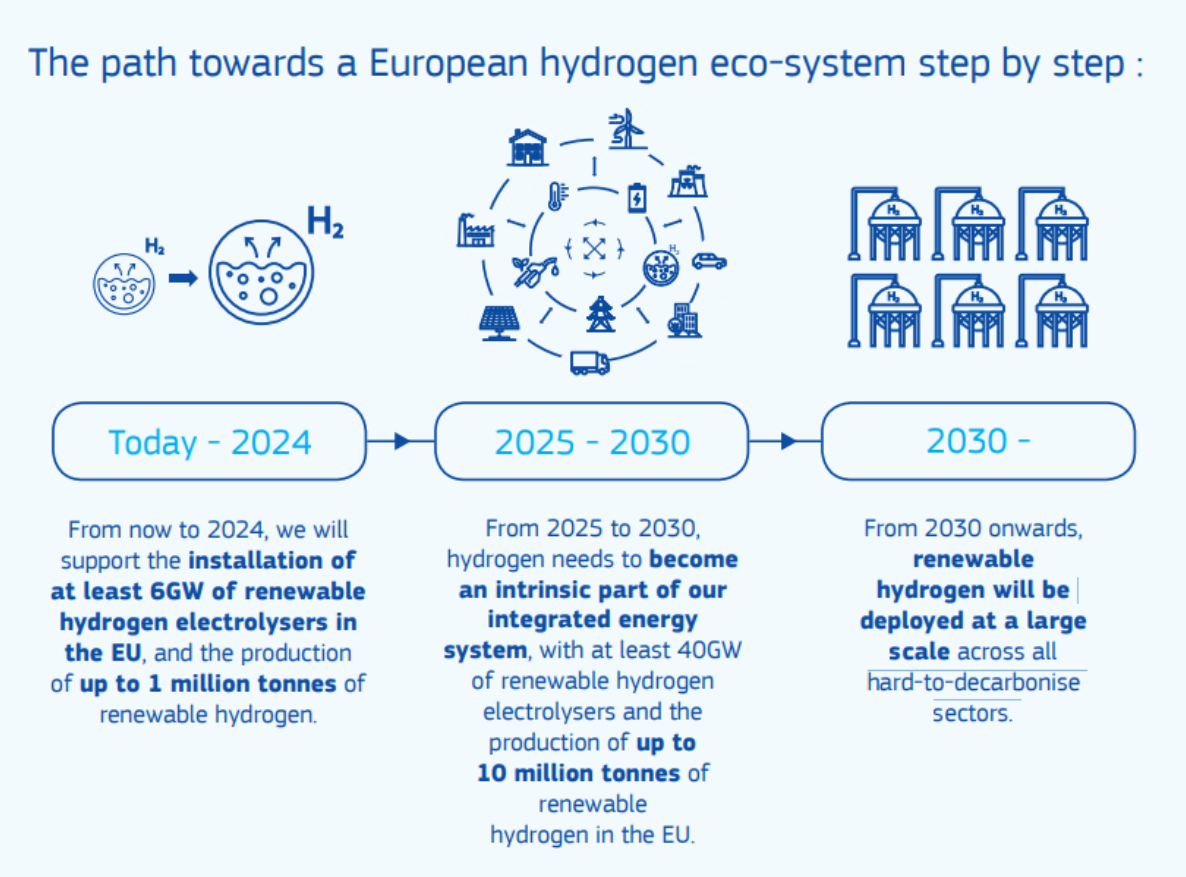

Figure 6: The path towards a European hydrogen eco-system step by step [12].

The presence of hydrogen is considered highly important on the energy mix of the next decades in order to achieve net zero systems, thus it is going to be widely communicated and

implemented by the states and the communities. Whether the percentage of this mix will be very high or not is questionable. Although hydrogen producing technologies such as water electrolysis are probably going to be very important for the stability of renewable energies and the decarbonizing of hard to abate sectors, while further evolution of such technologies is crucial.

1.2 Purpose

The purpose of this diploma thesis is to carry out a simulation and a techno-economic study of an alkaline electrolyser with the use of Aspen Plus™ commercial software. The novelty of the thesis is the development of the electrolyser stack on the Aspen Custom Modeler that allows the study of a 1.5 MW power scale system for different loads and conditions. In this way important variables such as the efficiency and the hydrogen production are calculated with great accuracy and the behavior of the system for different operating parameters can be studied with great precision. Moreover, the amount of hydrogen production for different loads is used to calculate the LCOH for different scenarios of electricity supply. If one wanted to use the power form renewable energy sources to produce hydrogen from electrolysis, due to their stochasticity, detailed knowledge of the electrolyser performance during different circumstances would be necessary. Since the simulation is quite detailed, real-life projects that have been globally undertaken to achieve a carbon-neutral future could be simulated accurately with the appropriate adaptation of the model.

1.3 Thesis Structure

This thesis has the following structure:
In *Chapter 1,* an introduction to the energy problem and why hydrogen could play a crucial role in it are discussed. This introduction leads to the purpose of the thesis, which is then followed by the structure of the following chapters.
In *Chapter 2*, a literature review takes place. The information that is mentioned in this chapter is the properties of hydrogen, its pros and cons as a fuel, the different methods to produce hydrogen, especially water electrolysis, and its different technologies with more details about the alkaline water electrolysis, and finally the hydrogen storage methods.
In *Chapter 3,* a simulation of an alkaline electrolyser system takes place in the Aspen Plus software. For the simulation of the stack, where the electrolysis of the water takes place, a custom model is developed on the Aspen Custom Modeler.
In *Chapter 4*, the results from the simulation are studied to export some basic charts that describes the behavior of the system at different temperatures, pressures and loads. A simple techno-economic analysis for the calculation of the LCOH for three different primary sources of electricity takes place.

In *Chapter 5*, the conclusion with the most important results from the thesis and some proposals for future work takes place.
Chapter 6 ensures that the writer understands the rules of plagiarism and how to properly cite the sources that are used.
Chapter 7, 8 and *9* includes the list of abbreviations, tables and graphs that are contained.
Chapter 10 includes the code annex from the Aspen Custom Modeler.
Chapter 11 includes all the references that were cited.

2. Literature Review

On this chapter a literature review takes place. The hydrogen properties, different kind of hydrogen definitions depending on the production method and the state-of-the-art technologies for green hydrogen production are presented. The electrolysis phenomenon and the thermodynamic equations that describe its operation are described. Next there is more extended research on the alkaline electrolysis that is used in this thesis and in the end a broader assessment on the various storage methods of hydrogen.

2.1 Hydrogen properties

At normal temperature, hydrogen is colorless, odorless, tasteless, and nonpoisonous. It burns with a pale blue flame and is highly flammable. It plays a vital role in sustaining life on Earth by combining with oxygen to form water. It is also the lightest element, with the lightest molecule being its diatomic molecule (H_2). Although it is very common in nature, it is very difficult to find it in its pure form. The reason for that is the combination that it makes with other elements. It is mostly found in water (H_2O), ammonia (NH_3), sugar ($C_{12}H_{22}O_{11}$) and in each hydrocarbon (C_nH2_{n+2}, C_nH_{2n}, C_nH_{2n-2}, etc.). It has atomic number 1, atomic weight 1.008 g/mol, molecular weight 2.016 g and density 0.09 grams per liter at standard pressure. In Table 1 some of the most important thermodynamic properties of hydrogen compared to methane which is the main component of natural gas are shown.

Table 1: Hydrogen and Methane Physical Properties [13]

Parameter	Unit	Hydrogen (H_2)	Methane (CH_4)
Molecular Weight	*[g/mol]*	2,016	16,04
Mass density (gas, at 0 C, 1 atm)	*[kg/Nm³]*	0,09	0,72
Boiling Point (1 atm)	*Celsius*	-252,9	-162
Lower Heating Value (LHV)	*MJ/kg*	120	50
	MJ/Nm³	11	36
Higher Heating Value (HHV)	*MJ/kg*	142	55,5
	MJ/Nm³	13	40
Flame Velocity in Air	*cm/s*	265-325	37-45
Flammability Limits	*Volume content in air*	4-75%	5,3-15%
Autoignition Temperature	*Celsius*	571	540
Flame Temperature in Air	*Celsius*	2045	1875
Ignition Energy	*mJ*	0,02	0,29

2.2 Hydrogen as a fuel

One of the reasons hydrogen has gained so much attention is that it could play the role of a green fuel since it does not emit greenhouse gases when it is burned. After hydrogen is produced it can then be transported in various ways and utilized on plenty applications such as domestic heating and cooking as well as for power generation on gas turbines or in a fuel cell producing electricity. One of the most efficient ways to transport hydrogen is in the form of gas via the already used pipeline in mixtures with natural gas. However, there are many challenges that need to be overcome for hydrogen to be used widely as an energy carrier.

$$2H_2 + O_2 \rightarrow 2H_2O \quad (1)$$

2.2.1 Advantages

- Equation (1) shows the combustion equation of hydrogen. It is obvious that no greenhouse gasses are emitted during the combustion of hydrogen.
- Moreover, hydrogen can be produced through electrolysis of water which is in abundance in our planet.
- Higher Heating Value of hydrogen is almost 3 times bigger compared to natural gas making it very efficient [14].
- As Figure 7 demonstrates, hydrogen has similar Wobbe index to many of the already used fuels. In equation (2) the formula of Wobbe index is shown, where HHV [MJ/Nm^3] is the Higher Heating Value and S_g [dimensionless] is the quotient of the air density and the density of the fuel [15]. When the Wobbe index of a gas increase, the volume of the gas flowing through a given cross-section in a given time will grow, as will the heating value per unit of gas [16]. Consequently, Wobbe index is a way to categorize the fuels depending on their heat transfer and can demonstrate whether two fuels can be used in the same burning applications. That gives hydrogen the possibility to be used as a fuel in mix with other already used fuels or on its own. In this way already used systems could be used with some modifications while a decrease in the emissions would be observed [17].

$$W_0 = \frac{HHV}{\sqrt{S_g}} \quad (2)$$

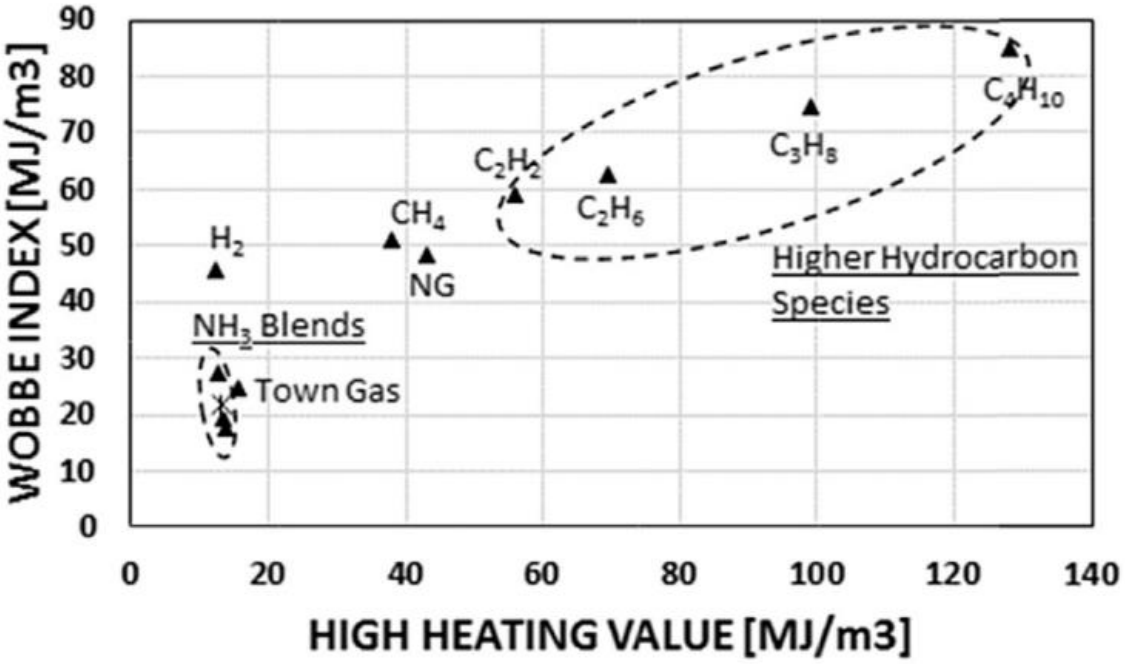

Figure 7: Wobbe index of hydrogen compared to other traditional gaseous fuels [18].

2.2.2 Disadvantages

- On the other hand, as Figure 7 demonstrates hydrogen has similar Wobbe index to other hydrocarbon fuels but very smaller energy volumetric density which implies a larger volumetric fuel flow rate. Storing the hydrogen under increased pressure or at extremely low temperatures as a liquid could play key role to tackle this problem [19].
- The wide ignition range of hydrogen increases the danger of auto-ignition in the premixing area. This could be even more challenging for the systems with high air inlet temperatures such as highly efficient gas turbines. To address this issue complex burning designs are necessary that increase the cost.
- The increased flame velocity in comparison with natural gas increases flashback risks which again is challenging for high air inlet temperature systems. To avoid this problem systems that detect and avoid flashbacks need to be applied.
- Hydrogen has also different thermoacoustic properties than natural gas. Higher flame speed, smaller ignition delay and distinct flame stabilization are observed in hydrogen. Therefore, flame shapes, positions and reactivity are different. This increases the risk in the dynamic area of the combustion in gas turbines that use high percentages of

hydrogen in their fuel. Therefore, combustion instabilities, flashback, and lean blow out will be even more possible to happen during transient operation [20].

- High levels of NOx can be generated through the combustion of hydrogen due to the high flame temperature that comes from the increased flame speed. NOx is toxic and dangerous both for the human and the environment [21].
- In the whole cycle of hydrogen, it is necessary to compress it, although there are some problems that occur such as that the already used centrifugal compressors of natural gas do not work well with hydrogen because of the low molecular mass and the existence of leaks [21].
- When hydrogen leaks, it can result in jet fire or explosion. Both are dangerous for humans and the surroundings. Although HyHouse study that was held from Kiwa and partners in 2015 concluded that when hydrogen leak takes place in domestic environment (small low-pressure leak) the risks are similar to natural gas leaks [22].
- Because of the small size of hydrogen atoms, it is possible for hydrogen to penetrate on the lattice of a wide variety of working materials that are used on the hydrogen ecosystem from the production till the exploitation of the end user. This penetration is called hydrogen embrittlement and significantly reduce the mechanical properties (plasticity, toughness and strength) of the materials and can result to a series of dangerous events that affect the lifecycle of the ecosystems [23], [24]. A lot of research is taking place to better understand the conditions under which the effect is taking place. Some of the most important factors affecting the embrittlement of the pipelines are the hydrogen blending ratio, the pressure, the material strength, and others [24].

2.3 The colors of hydrogen

Hydrogen can be created using a variety of primary energy sources, feed stocks (fuels) and methods. One of the broadest methods that hydrogen is being promoted to the society is through its color. The color of hydrogen can give basic information about the combination of primary energy, feed stock and routes that are being used. Yet hydrogen production is a complex issue with many new studies and technologies evolving. Figure 8 summaries the main colors of hydrogen.

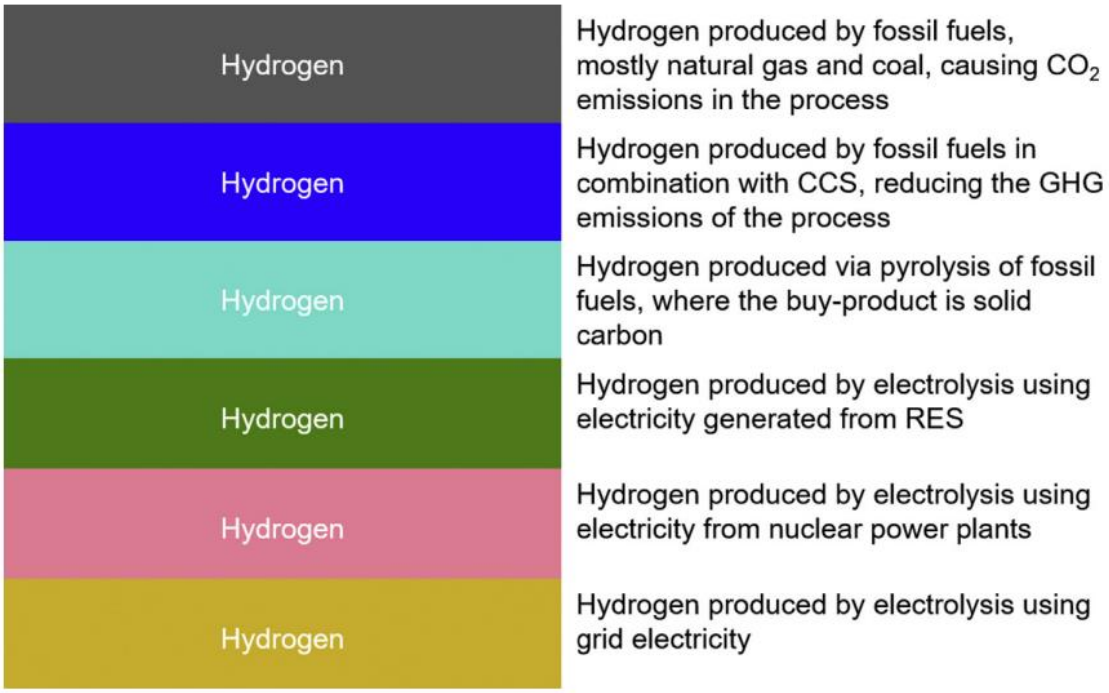

Figure 8: The colors of hydrogen [25].

2.3.1 Grey Hydrogen

- Grey Hydrogen from Steam Reforming of Methane (SMR):

The main process that produces grey hydrogen is through the steam reforming of methane (SMR). Steam reforming contains the reforming, water-gas shift (WGS) and hydrogen purification processes. It is carried out at high temperatures and precious metals or nickel-based materials are being used as catalysts [26]. As a fuel, natural gas, and different compositions of methane with a wide variety of hydrocarbons and naphtha can also be used [27]. The reaction of reforming for methane is endothermic (Equation (3)) and produce syngas of H_2 and CO while water shift reaction is exothermic (Equation (4)) and convert CO to CO_2 and H_2 [21].

$$CH_4 + H_2O \rightarrow CO + 3H_2, \Delta h = +206\ kJ/kmol \quad (3)$$

$$CO + H_2O \rightarrow CO_2 + H_2, \Delta h = -41kJ/kmol \quad (4)$$

After the shift reaction, hydrogen is separated and transferred outside the reaction system through hydrogen-selective membrane. The following Figure 9 demonstrate schematically the production of grey hydrogen from steam methane reforming.

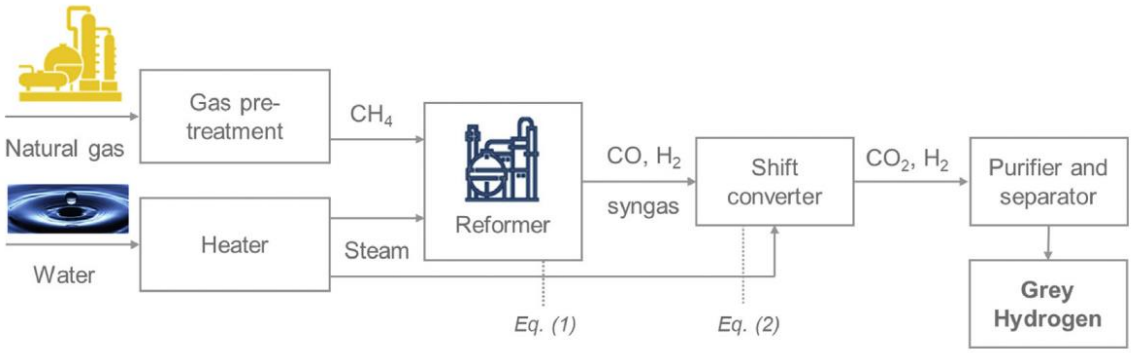

Figure 9: Steam reforming of natural gas (SMR) [25].

- Grey or Black-Brown Hydrogen from coal gasification (CG):

Grey hydrogen can be produced from the coal gasification as well with the use of different kind of coal (lignite, sub-bituminous coal, bituminous and anthracites) and different kind of gasification methods (fixed bed, moving bed, fluidized bed, entrained flow, and plasma gasification). In general, dry coal, under high temperature reacts with oxygen and steam to produce syngas of H_2 and CO_2 as the equations (5) and (6) demonstrate. In some cases, hydrogen produced from coal gasification is also called as black or brown hydrogen depending on whether the feed stock is bituminous or lignite respectively [28].

$$C + O_2 \rightarrow CO_2 \quad (5)$$

$$C + H_2O \rightarrow CO_2 + H_2 \quad (6)$$

- Grey Hydrogen from Partial Oxidation (POX) and Autothermal Reforming (ATR):

Partial oxidation (POX) of methane (POM) and oil products can also produce grey hydrogen, with the advantage of the absence of external heat, because of the exothermic nature of the

oxidation. Although pure oxygen is required. For methane partial oxidation takes place (equation (7)) and water gas shift follows (equation (4)).

$$CH_4 + 0.5O_2 \rightarrow CO + 2H_2 \quad (7)$$

Autothermal reforming (ATR) can also produce grey hydrogen and it is a combination of reforming and partial oxidation using the necessary heat of reforming from the partial oxidation. This method is not yet available on large scale [26]. The following Figure 10 shows the production of hydrogen from coal schematically.

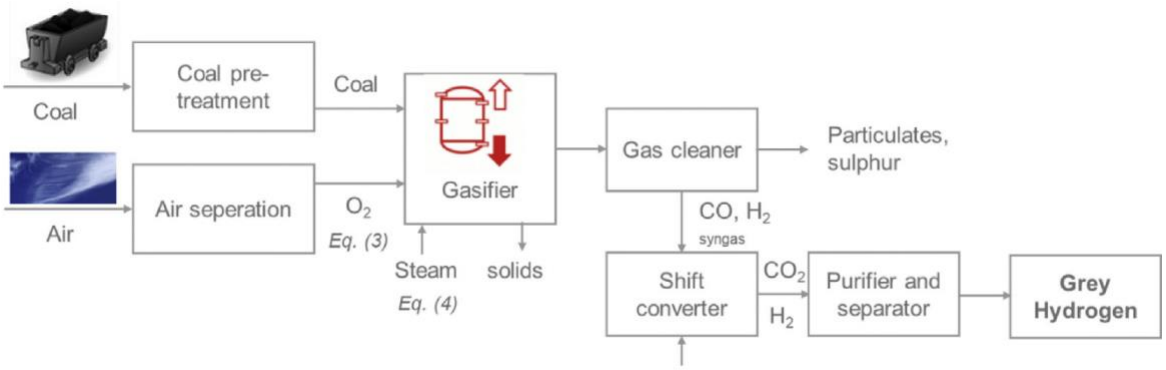

Figure 10: Coal Gasification (CG) production process [25].

2.3.2 Blue Hydrogen

When after the final stage of hydrogen separation on steam methane reforming carbon capture and stored (CCS) or used (CCU) system is being added hydrogen is called blue and around half of the CO_2 emissions can be avoided [29], although cost is rising significantly. The captured CO_2 could be injected into geological reservoirs or the ocean [27]. Figure 11 demonstrates a CCUS system that can be added after an SMR process.

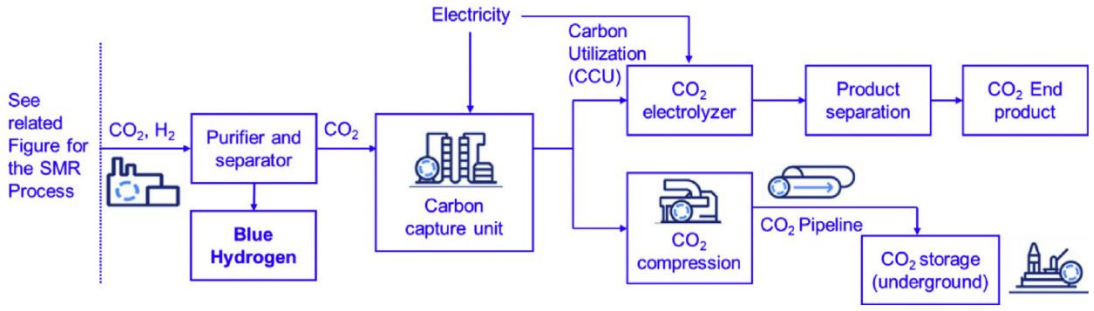

Figure 11: Carbon Capture and Utilization (CCU) and Carbon Capture and Storage (CCS) schematic demonstration for the SMR production of H_2 [25].

2.3.3 Turquoise Hydrogen

Turquoise hydrogen is being produced from the pyrolysis of methane. Pyrolysis is a method that decomposes thermally a hydrocarbon source. For methane at atmospheric pressure, the reaction takes place at 980 Celsius while an air and water free environment is necessary [27]. The equation that describes the thermal pyrolysis of methane is the following:

$$CH_4 \rightarrow 2H_2 + C \quad (8)$$

2.3.4 Green Hydrogen

Green hydrogen refers to hydrogen that is produced using renewable energy sources through water electrolysis. Generally, electrolysis involves splitting water into hydrogen and oxygen using an electric current. Sometimes green hydrogen is also called “clean hydrogen”, “renewable hydrogen”, or “low-carbon hydrogen”. This technology will be analyzed in greater detail in the sub-chapter 2.4.

2.3.5 Purple Hydrogen

Purple hydrogen is the hydrogen that is produced by electrolysis using electricity that is generated from nuclear power plants. European strategies do not promote it that much but different regions such as Russia and China are more likely to use it as a useful alternative.

2.3.6 Yellow Hydrogen

Yellow hydrogen refers to hydrogen that is produced using grid electricity through water electrolysis. Sometimes, in the literature yellow hydrogen is referred to as purple hydrogen.

2.3.7 Other colors and methods

Renewable hydrogen can also be produced from biomass processing. It is not fully specified yet if hydrogen produced from biomass should be considered green. Biomass is organic matter coming from plant and animal material (energy crops, crop residues, wood from forests, forest residues, grass, industrial residues, animal and municipal waste, etc.) and is considered a renewable fuel because the CO_2 that is released during its combustion was earlier captured by living organisms [27]. Biological or thermochemical methods can be used to produce hydrogen from biomass. Biological includes bio-photolysis, dark fermentation, and photo fermentation, while thermochemical includes pyrolysis, gasification, combustion, and liquefaction. The most mature technology of biomass processing for hydrogen production is the thermochemical method of gasification [25]. During this procedure different gasification agents such as steam, oxygen, and air can be used, while steam results the biggest H_2/CO ratio [26]. Biomass steam gasification is a very complex procedure but in general it is endothermic, and it can be described from the following equation:

$$Biomass + H_2O \rightarrow H_2 + CH_4 + CO + CO_2 + Tar + Char \quad (9)$$

Where, tar refers to sticky-viscous remaining substances and char is the solid residue that is left behind.

Some new colors in the literature are aqua and white hydrogen. Aqua refers to hydrogen produced from oil with a procedure that is claimed to not emit any carbon, while white hydrogen refers to hydrogen produced from concentrated solar energy that directly split the molecules of water.

2.3.8 Hydrogen Production Data

Global hydrogen production reached around 95 Mt in 2022, a 3% increase over 2021. Figure 12 demonstrates that during 2022, 62% of the produced hydrogen came from natural gas without CCUS, 21% came from unabated coat mainly located in China, 16% was produced as a by-product at refineries and other petrochemical processes by naphtha reforming that was later used mainly in other refinery and conversion processes and only 0.7% (around 1Mt) was low-emission hydrogen from which 0.6% came from fossil fuels with CCUS and 0.1% came from water electrolysis. Although hydrogen produced from water electrolysis was below 100 kt (around 47 kt) in 2022, a 35% growth rate compared to 2021 was observed when 35 kt of green hydrogen was produced. In a similar way water electrolysis increased by 20% from 2020 to 2021 [30], [31].

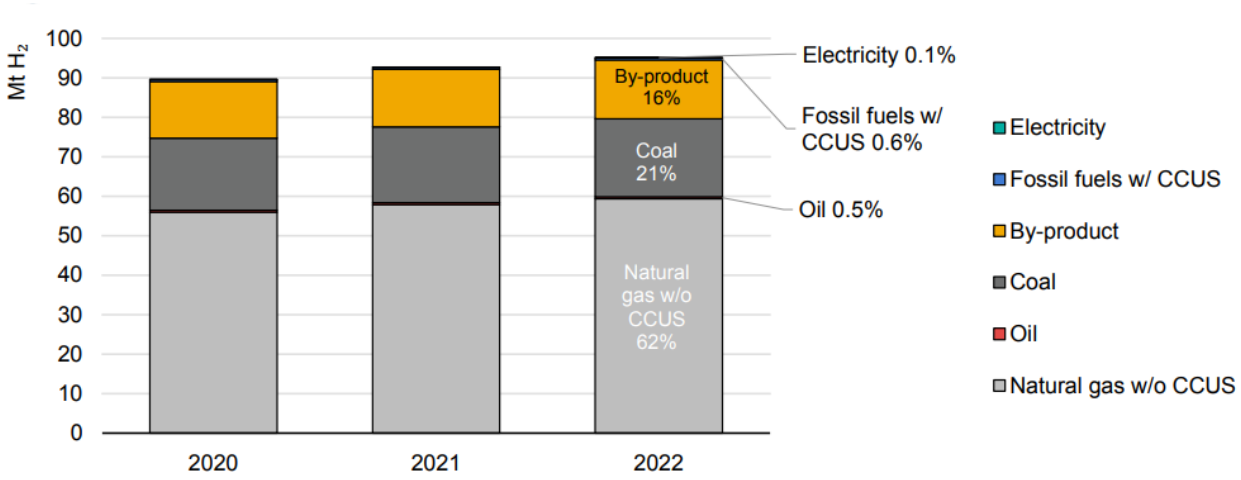

Figure 12: Global hydrogen production depending on its source for 2020, 2021, and 2022 [31].

Although these data do not seem very promising, it is important to be mentioned that the announced projects of low emission hydrogen production are rising with very high rates, aiming to reach even more than 20 Mt of H_2 by 2030, if all the announced projects for hydrogen produced from water electrolysis and fossil fuels with CCUS come to realization. That implies a 30% increase (16 Mt H_2 by 2030) in the announced low-emission hydrogen projects compared to 2021.

Water electrolysis accounted for only about 0.1% of worldwide hydrogen production in 2022. However, the installed capacity of electrolysis is rapidly increasing, reaching 700 megawatts (MW) by the end of 2022, an increase of 190 MW, or 20%, over 2021. Until the end of 2023 it is possible that installed could reach more than 2000 MW based on the projects that are under construction or have reach the Final Investment Decision (FID) as Figure 13 demonstrate in a graphic way [30], [31].

Figure 14 shows that till 2030 global electrolyser capacity could reach 420 GW when projects in the early stages of development are also included. According to the announced projects, global installed electrolyser capacity might reach 175 GW by 2030, a 30% increase over the 2022 Global Hydrogen Review announcements.

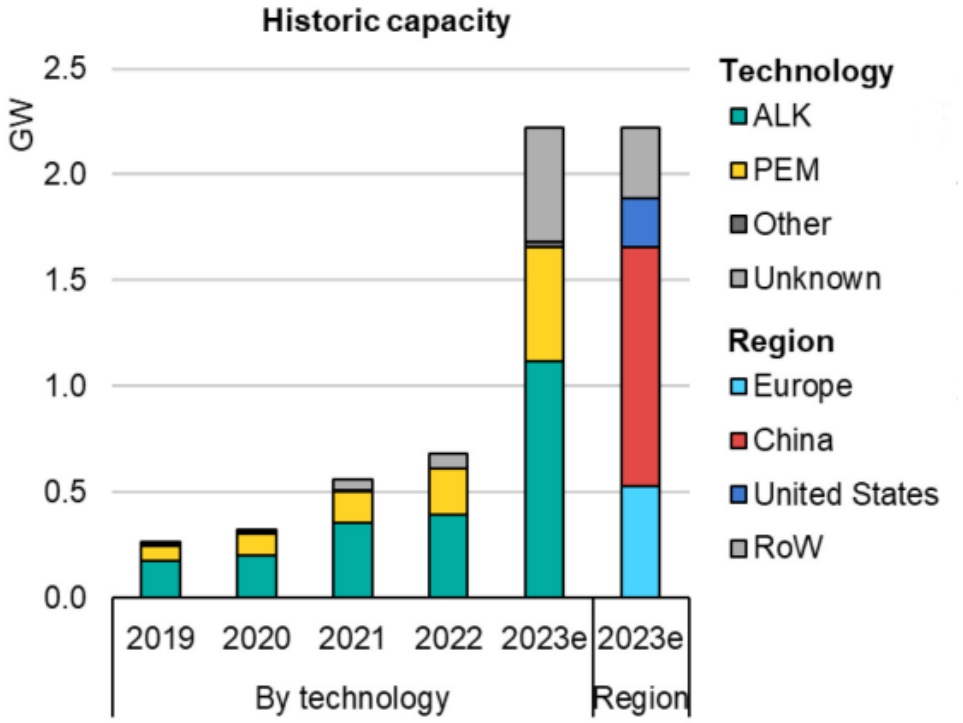

Figure 13: Global electrolyser capacity for the period 2019-2023 by technology, region and size based on announced projects [31].

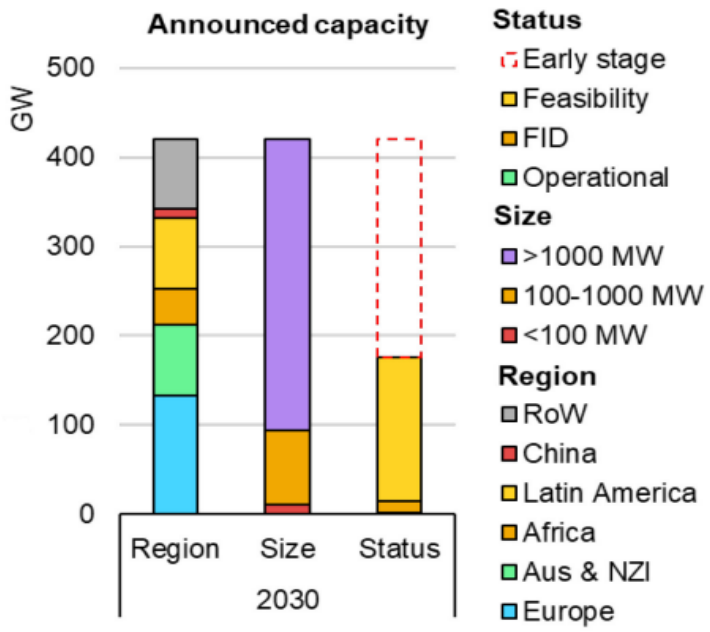

Figure 14: Global electrolyser capacity by 2030 by technology, region and size based on announced projects (including early stage) [31].

When it comes to water electrolysis-based hydrogen generation initiatives, Europe and Australia are in the lead. Other powers of energy are also very committed to hydrogen. The plan of China for hydrogen production till 2050 depending on the production method is illustrated in Figure 15. China target to be carbon neutral till 2060 and expect to produce 10 million tons of hydrogen annually [32] .

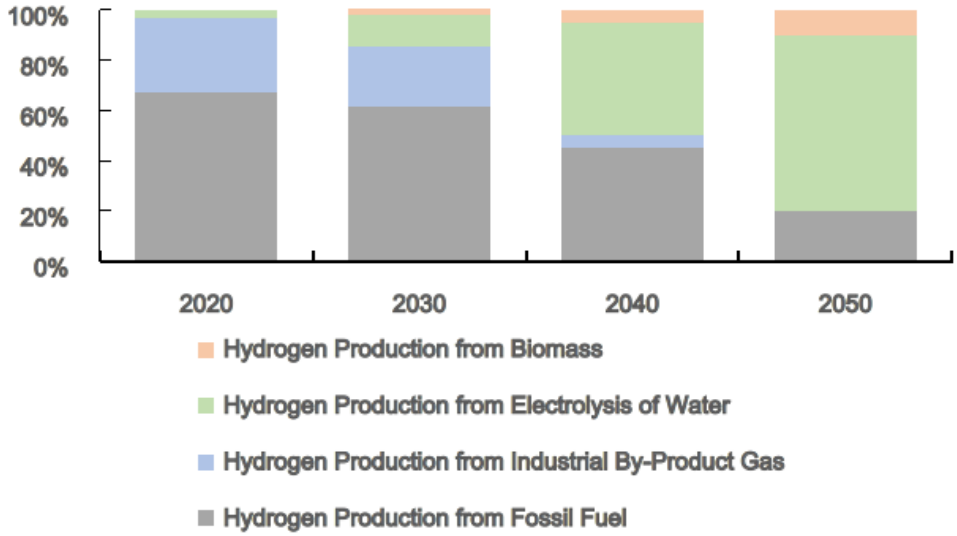

Figure 15: Hydrogen supply in China [32].

Since electrolysis could play such an important role at the future of hydrogen market and because the purpose of this thesis is to provide a simulation and techno-economic analysis of an alkaline electrolyser, an overall review of the electrolysis technology will take place on the next sub-chapter.

2.4 Water Electrolysis

2.4.1 General principles and thermodynamics of water electrolysis

The following analysis for the general principles and thermodynamics of water electrolysis is based on the chapter 9 (Renewable hydrogen production by water electrolysis) of the book Sustainable Fuel Technologies Handbook [33].

The electrolysis of water is a process that has been known for many years. By applying a specific amount of energy (electric current and heat) on the molecules of water it splits into oxygen and hydrogen. This process that occurs can be characterized as oxidation-reduction and the chemical equation is the following.

$$H_2O \rightarrow H_2 + \frac{1}{2}O_2 \qquad (10)$$

An electric power source is used to apply a direct current through a set of electrodes. The positive electrode (+) is referred to as the anode, where the oxygen evolution reaction (OER)

takes place, while the negative electrode (-) is called the cathode, where the hydrogen evolution reaction (HER) occurs. Within these electrodes, there is a transfer between electrons and ions. Negative ions, also known as anions, donate electrons to the anode (+) and positive ions or cations, accept electrons from the cathode (-).

Electrolysis belongs to endothermic reactions requiring external energy supply in order to be produced. This energy needs to have the form of electricity or heat and can be calculated by using the laws of thermodynamics, while assuming that the reaction is reversible. The equation is the following.

$$\Delta H = \Delta G + T * \Delta S \quad (11)$$

ΔH is the total enthalpy that needs to be supplied in order for the molecules of the water to be divided, ΔG is the free energy of Gibbs and represents the electric energy that is applied and ($T * \Delta S$) is the energy expressed as entropy, which is irreversible and represents the thermal energy that is provided. For normal conditions (25 °C and 1 bar) the values that activate the electrolysis of the molecules are visible on Table 2.

Table 2: Activation energy of electrolysis for normal conditions

Δh^0	285.88	[kJ/mol]
Δg^0	237.23	[kJ/mol]
$T*\Delta s^0$	48.65	[kJ/mol]

In order for electrolysis to occur a wide range of combinations of thermal and electrical energy can be applied. While increasing the thermal energy input, the demand for electricity is decreasing and even more in the steam area as Figure 16 demonstrates. The water vaporization results in a sharp decline in the total energy demand while the pressure does not change the total energy demand.

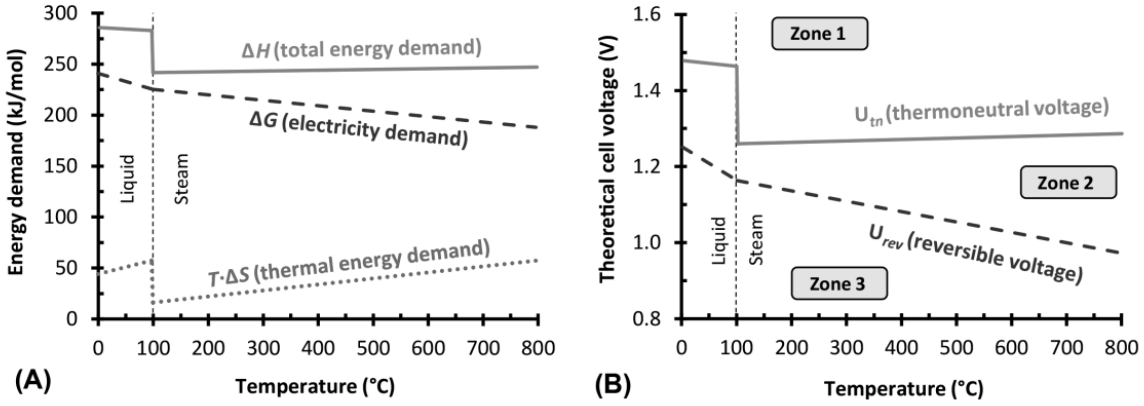

Figure 16: (A) The influence of temperature on energy demand of water electrolysis at 1 bar and (B) Reversible and thermoneutral voltage versus temperature at 1 bar.

- ***Minimum cell voltage and Thermoneutral voltage***

The minimum voltage that needs to be required for the electrolysis to initiate is called reversible or equilibrium cell voltage (V_{rev}). In thermodynamic terms, the effort required to execute this procedure under conditions of constant temperature and pressure corresponds to the change in Gibbs free energy (ΔG). This equation, if there is usage of electricity only and not heat also, can be expressed as follow:

$$V_{rev} = \frac{\Delta g}{z * F} \tag{12}$$

Where V_{rev} [V] stands for the reversible voltage, z [$2e^-$] stands for the number of electrons that being transferred in the water electrolysis and F [96500 C/mol] is the Faraday constant.

For normal or equilibrium conditions (25 °C, 1 bar) if the equation (12) is used, the reversible potential for standard conditions [V_{rev}^0] is obtained and it has the value of V_{rev}^0=1.229 V. That value implies that conditions are ideal, and no resistances exist. In different case reversible voltage is obtained from the Nernst equation:

$$V_{rev} = V_{rev}^0 + \frac{R * T}{z * F} * \ln\left(\frac{p_{O_2}^{1/2} * p_{H_2}}{\alpha_{H_2O}}\right) \tag{13}$$

Where p_{H2} and p_{O2} stands for the partial pressure of the reaction products, α_{H20} is the water activity and R represents the absolute gas constant with the value of 8.314 J/(K*mol).

Thermoneutral voltage is the minimum voltage that is required in order for the electrolysis to occur under adiabatic conditions. In this case heat is not absorbed or generated and the electric current is the only energy source. Equation (14) gives the thermoneutral voltage from which the thermoneutral voltage for standard conditions can be calculated as V_{tn}^{0}=1.48 V.

$$V_{tn} = \frac{\Delta h}{z * F} \tag{14}$$

The distinction between reversible and thermoneutral voltage is called thermal or entropic voltage and it signifies the minimal overvoltage compared to the reversible voltage that is necessary to initiate water dissociation in an electrolytic cell. In equilibrium conditions it takes the value of 0.25 V.

- ***Theoretical operating ranges***

As Figure 16 B shows according to the theoretical applied voltage to the cells of the electrolyser three different occasions-zones occur.

The first zone is when the applied voltage exceeds the thermoneutral voltage of the particular temperature and pressure and then the electrolysis will take place while the surplus energy converts to heat that needs to be retrieved from the refrigeration system. The second zone is when the applied voltage stands between the reversible and thermoneutral voltage. In this scenario thermal energy needs to be applied as well and the last zone is when the applied voltage is smaller than the thermoneutral of the operating conditions resulting the electrolysis to be impossible. The following Table 3 sums up those three zones when external voltage V is applied to the electrolyser.

Table 3: The three different zones of electrolysis.

Zone 1	$V>V_{tn}$	Heat that needs to be removed	$(V-V_{tn})*I$
Zone 2	$V_{rev}<V<V_{tn}$	Necessary thermal energy that needs to be applied for the electolysis to take place	$(V_{tn}-V)*I$
Zone 3	$V<V_{rev}$	electrolysis is impossible	

- ***Overpotentials***

In real conditions for the electrolysis to take place the necessary potential that needs to be applied is greater than the reversible voltage and the thermoneutral voltage as well. The reason for that is the existence of irreversibilities and in order to include them in the analysis they can take the form of overpotentials η^V. The main overpotentials are activation, ohmic and concentration or diffusion and the following table analyzes the cause as well as the equation that can be used to calculate them and the conditions that affect them.

Table 4: Cause, calculation and conditions that affect the overpotentials of water electrolysis.

Overpotential	Cause	Calculation	Conditions
Activation	Activation energy of electrochemical reactions	Butler-Volmer	Suitable catalyst and increased operating temperature can reduce it
Ohmic	Ionic, electric and contact between the parts resistance	Ohm's law	Proportional to the current density and depend on materials, design and temperature
Concentration-diffusion	Mass transport due to diffusion	Nernst equation	Under increased concentration and high current densities it is more intense

After the influence of the overpotentials the necessary voltage applied to the electrolyser is the following

$$V = V_{rev} + (\eta_{act}^V + \eta_{ohm}^V + \eta_{conc}^V) \quad (15)$$

Plotting the cell voltage versus the current density for different temperatures produce the polarization curve of an electrolyser in which the influence of the different overpotentials is shown (Figure 17). Depending on the current, some overvoltages is more intense than other.

At low current densities activation overpotentials are the most dominant, at intermediate levels ohmic overpotentials predominance and linear correspond is observed, while at intense current densities a high slope is observed due to the dominance of the concentration overpotentials. The intense current density zone should be avoided for a better efficiency to be achieved, while the increase of the temperature is desirable if the materials can handle it.

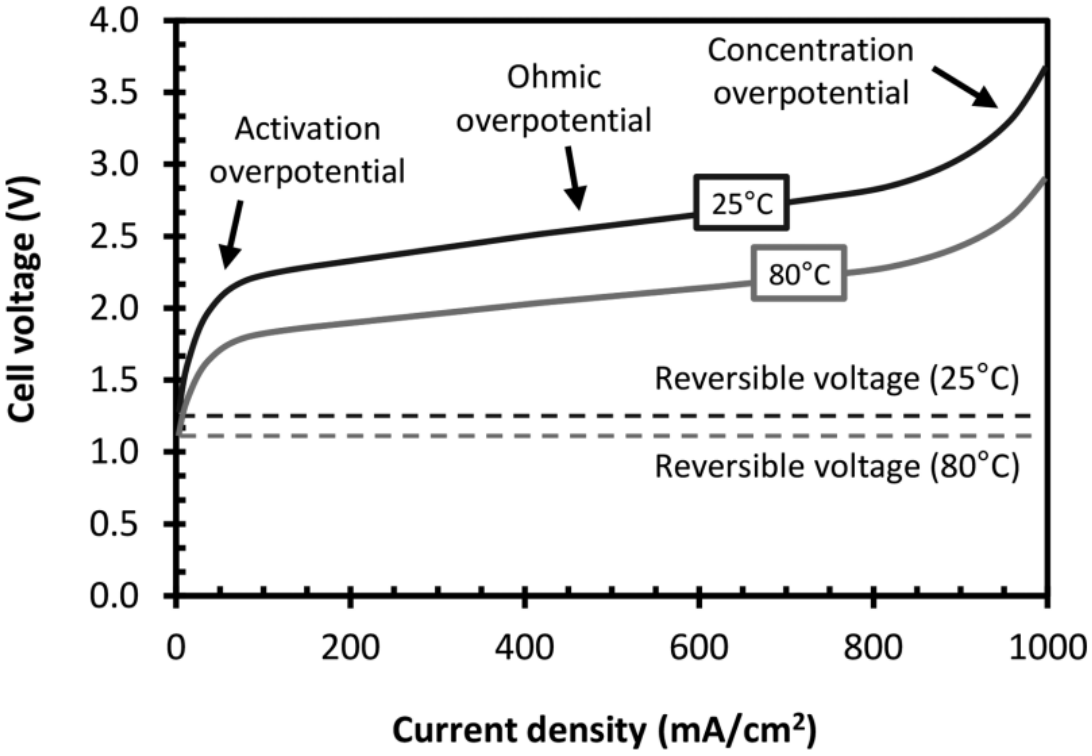

Figure 17: Polarization curve (i-V) of an electrolysis cell at different temperatures (smaller than 100 Celsius).

- ***Theoretical hydrogen production***

To calculate the theoretical production of hydrogen the faraday law can be used (equation (16)) with the increase of electrical current causing higher hydrogen generation.

$$\dot{m}_{prod,th} = \left(\frac{M}{F * z}\right) * I \qquad (16)$$

Where z [2e$^-$] represents the number of electrons F [96.500 C/mol] stands for the Faraday constant, M [g/mol] is the molecular weight of the substance and I [A] is the electrical current. To achieve the desired levels of hydrogen production, an electrolysis stack containing several electrolysis cells is required.

- ***Voltage, Faraday, and overall efficiency***

The relationship between the thermoneutral voltage (V_{tn}) and the real voltage (V) applied to the electrolysis cell is characterized as ***voltage efficiency (η_V)***

$$\eta_V = \frac{V_{tn}}{V} \tag{17}$$

A smaller voltage efficiency means that the overpotentials are greater, while it is possible for the voltage efficiency to be higher than the unit in the case that thermal energy is supplied to the system. The following Figure 18 (A) illustrates that higher current density and smaller operating temperatures reduce voltage efficiency.

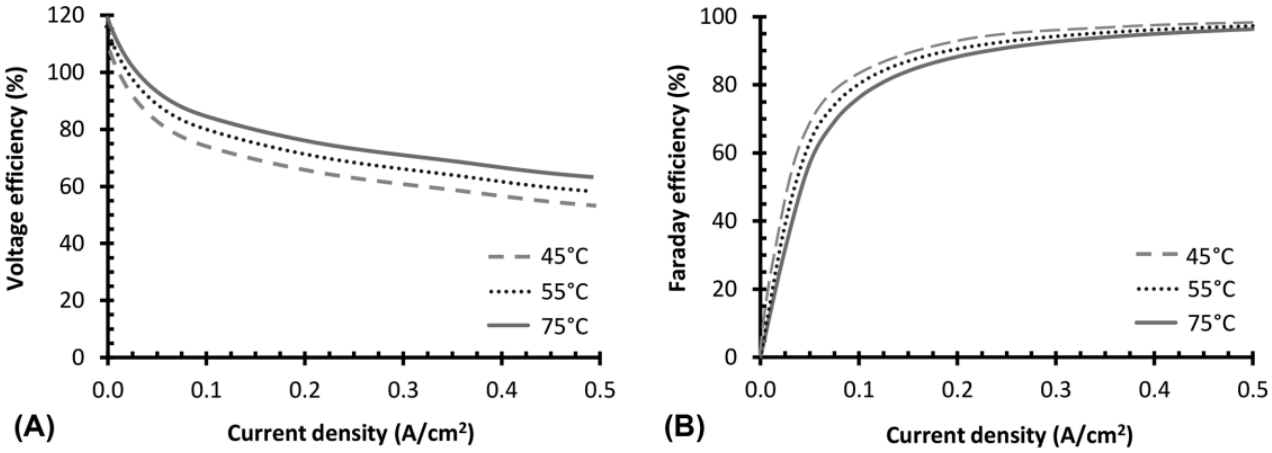

Figure 18: Voltage and Faraday efficiency versus the current density for different temperatures (smaller than 100 Celsius).

Current or Faraday efficiency (η_F) is a measure of the theoretical electrical current (I_{th}) required for the electrolysis reaction in comparison to the actual current flowing through the cell (I). This parameter indicates the portion of the current circulating through the cell that is not directly involved in the electrolysis process. Utilizing the Faraday law outlined in equation

(16), this efficiency be represented as the ratio between the actual volume of H_2 produced and the theoretical volume of H_2.

$$\eta_F = \frac{I_{th}}{I} = \frac{\dot{m}_{prod,real}}{\dot{m}_{prod,th}} \quad (18)$$

As Figure 18 (B) illustrates higher current density and lower operating temperatures result to greater faraday efficiency.

Overall efficiency

The relationship between the change in process enthalpy and the total energy provided to the electrolysis cell for each mole of H_2 generated determines the overall efficiency (η_{tot}). When the only energy source is the electricity supplied to the cell terminals, and no external thermal energy is applied to the cell, the efficiency is equal to

$$\eta_{tot} = \eta_F * \eta_V \quad (19)$$

In the following section, a small review of the four main electrolyser technologies (Alkaline, PEM, SOEC, AEM) will take place. Most of them work under low operating temperatures but the new technology of SOEC works under high temperatures and in a very efficient way. Also depending on the pH electrolysis can be carried out in acid or basic medium where anions (H^+) and cations (OH^-) respectively are responsible for the ionic transport. During the electrolysis an oxygen evolution reaction (OER) is taking place on the anode and a hydrogen evolution reaction (HER) occurs in the cathode. Depending on the different technology different reactions, electrolytes, separators and catalysts exist, while the efficiency, the cost, the purity of the produced hydrogen, the lifetime and other features are also different. The efficiency of an electrolyser is defined from the next equation (20).

$$\eta_{electrolyser} = \frac{\dot{m}_{H_2} * LHV}{P_{input}} \quad (20)$$

2.4.2 Alkaline electrolyser

Alkaline water electrolysis is the most mature, cheap, and commercially developed technology of water electrolysis. It is commonly used for large-scale applications of hydrogen production. Nickel oxides are used for the anode and cobalt for the cathode. NaOH and KOH

are the most used electrolytes with the second to be used the most preferable. In the Figure 19 the technology is schematically displayed, while the reactions that take place in anode to produce oxygen and in the cathode to produce hydrogen are shown on equation (21) and (22) respectively. Between the two electrodes and the hydroxyl ions a separating porous diaphragm is placed that is made of ceramic oxide materials (asbestos and polymers). The diaphragm allows the movement of hydroxyl ions from cathode to the anode. Cathode operating temperatures are 65-100 Celsius, the cell operating voltage is 1.8-2.4 V and the efficiencies are between 60-80%. Alkaline electrolysers have the advantage of being able to work at low temperatures and not requiring catalysts to activate and create hydrogen, while because of the existence of an alkali solution, alkaline electrolyser electrode corrosion is regarded as the most serious obstacle [33], [34].

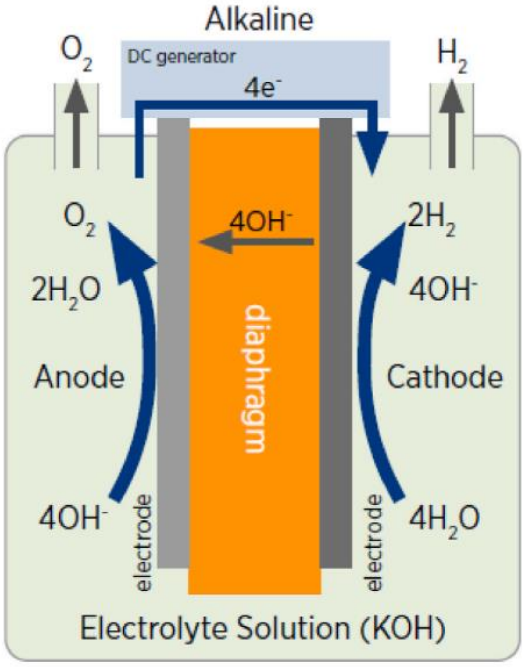

Figure 19: Alkaline water electrolysis [34].

$$Anode: 4OH^- \rightarrow 2H_2O + O_2 + 4e^- \quad (21)$$

$$Cathode: 4H_2O + 4e^- \rightarrow 2H_2 + 4OH^- \quad (22)$$

2.4.3 PEM electrolyser

High-purity hydrogen (>99,99%) at ranges of temperature between 70-90 Celsius can be produced through Proton Exchange Membrane (PEM) electrolysis. For the anode and cathode catalyst materials IrO_2 and Pt are most commonly used, respectively. Figure 20 shows that during PEM electrolysis hydrogen cations H^+ are produced in the anode (equation (23) and transferred through a solid membrane to the cathode where hydrogen is produced (equation (24)). The membrane is most commonly made from Nafion or other perfluorosulfonic acids (Fumapen, Flemion, Aquivion etc) or polymers as well. Compared to alkaline electrolysis, PEM is faster due to the combination of the electrolyte's acidic nature and the metallic surfaces of the electrodes. The operation is also safer and various pressure can occur between anode and cathode side. This allows anode to work under atmospheric pressure while cathode works under higher pressures. On the other hand, scaling up for large-scale (MW) applications is a challenge and the production cost is rising due to the noble metals that are used as catalysts on the electrodes. Efficiency is increasing to 70-80% while current density is also increasing [33], [34].

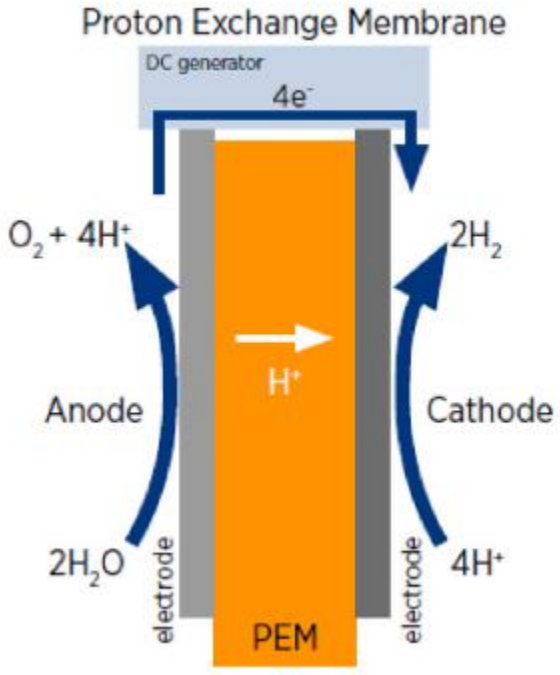

Figure 20: PEM water electrolysis technology [34].

$$Anode: 2H_2O \rightarrow O_2 + 4H^+ + 4e^- \quad (23)$$

$$Cathode: 4H^+ + 4e^- \rightarrow 2H_2 \quad (24)$$

2.4.4 SOEC electrolyser

Solid Oxide Electrolyser (SOEC) works under higher temperatures (900-1000 Celsius) and greater efficiencies. Electrodes are made from nickel and due to higher temperatures operation without the use of precious metals that work as catalysts is possible. Figure 21 demonstrate the electrolysis of SOEC where produced anions O^{2-} immigrate from the cathode to the anode where oxygen is produced (equation (25)). In the cathode the water with electrons react to produce hydrogen (equation (26)). Waste heat, nuclear energy and other heat inputs can be used for the temperature to be increased while this makes possible voltages lower than the thermoneutral to be enough (Zone 2 of Figure 16 (B)). On the other hand, higher temperatures reduce the SOEC lifetime due to the increased electrolyte degradation and only operations with power range of kilowatts exist yet [33], [34].

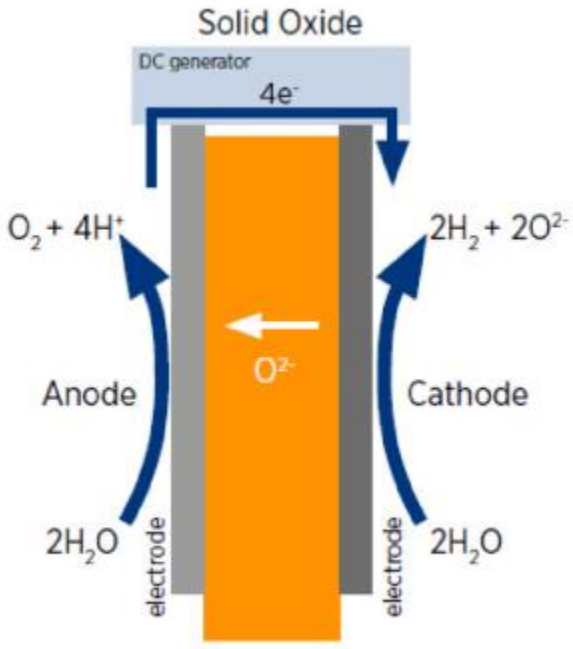

Figure 21: SOEC schematic diagram [34]

$$Anode: 2O^{2-} \rightarrow O_2 + 4e^- \quad (25)$$

$$Cathode: 2H_2O + 4e^- \rightarrow 2H_2 + 4H^+ + 2O^{2-} \quad (26)$$

2.4.5 AEM electrolyser

Anion Exchange Membrane (AEM) electrolyser has the same electrolysis mechanism as alkaline electrolysis but instead of a porous diaphragm, a membrane is responsible for the transmission of the OH^- from the cathode to the anode (Figure 22). This approach combines the strengths of both alkaline and PEM electrolysers. Additionally, inexpensive catalyst materials that are not noble metals can be employed in AEM cells, reducing the overall cost of hydrogen production. AEM performance is hindered by weak catalyst activity and low membrane conductivity. Further research is needed to improve AEM water electrolysis, especially in membrane materials, cell costs, and efficiency [33], [34].

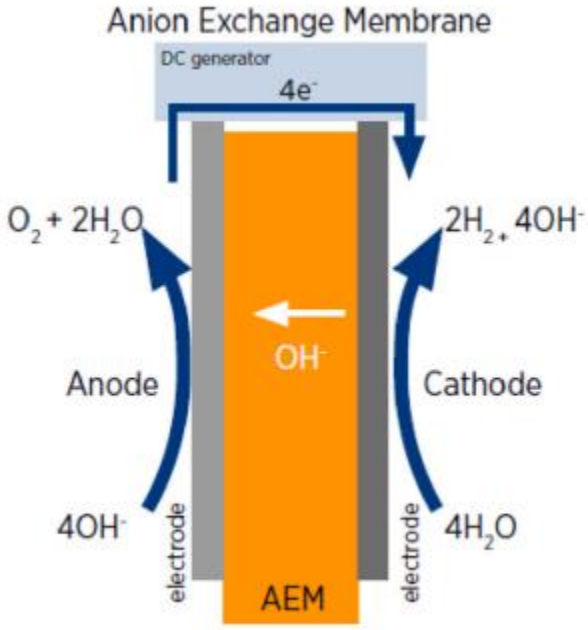

Figure 22: AEM water electrolysis technology [34].

$$Anode: 4OH^- \rightarrow 2H_2O + O_2 + 4e^- \quad (27)$$

$$Cathode: 4H_2O + 4e^- \rightarrow 2H_2 + 4OH^- \quad (28)$$

On the following Table 5 and Table 6 a comparison of technical features and the advantages and disadvantages of each technology are shown. SOEC and AEM electrolysers are currently in the research and development stage and are not as advanced as alkaline and PEM technologies. AEM technology offers cost benefits and stable hydrogen production, but substantial development is required for large-scale industrial use. Additionally, different water electrolysis methods face distinct challenges, such as cell performance, durability, membrane materials, catalysts, and costs.

Table 5: Technical features of standard water electrolysis methods [34].

Specification	Alkaline	PEM	SOEC	AEM
Technology maturity	Mature	Commercial	R&D	R&D
Cell temperature, °C	65–100	70–90	900–1000	50–70
Cell pressure, bar	25–30	30–80	<30	−30
Current density, mA/cm^2	200–500	800–2500	300–1000	200–500
Cell voltage, V	1.8–2.4	1.8–2.2	0.95–1.3	1.8–2.2
Voltage efficiency, %	50–70.8	48.5–65.5	81–86	39.7
Specific system energy consumption, kWh/Nm^3	4.5–7.5	5.8–7.5	2.5–3.5	4.8–5.2
Hydrogen production, Nm^3/hr	<760	0.265–30	–	0.25–1
Stack lifetime, hr	10, 000	<20,000	<40,000	NA
Electrolyte	20–30% KOH	Perflurosulfonated acid (PFSA)	Yttria-stabilized zirconia (YSZ)	DVB polymer support with KOH or $NaHCO_3$
Separator	Asbestos, NiO, ZrO_2, stabilized with PPS mesh	PFSA (e.g., Nafion)	Solid electrolyte	quaternary ammonia polysulfone (QAPS)
Charge carrier	OH^-	H^+	O_2^-	OH^-
OER catalyst	Ni-coated perforated stainless steel	Ir/Ru oxide	Perovskite-type	CO_3O_4
HER catalyst	Ni	Platinum	Ni/YSZ	Ni
Hydrogen purity, (vol%)	99.3–99.9	99.999	–	99.99
Capital cost (€/kW_{el})	1000–1200	1860–2320	>2000	NA

(R&D: research and development, NA: not available)

Table 6: Benefits and drawbacks of usual water electrolysis techniques [35].

Electrolysis technology	Advantages	Disadvantages
Alkaline water electrolysis	• Well established Technology • Commercialized for industrial applications • Noble metal-free electrocatalysts • Relatively low cost • Long-term stability	• Limited current densities • Crossover of the gasses • High concentrated (5M KOH) liquid electrolyte
AEM water electrolysis	• Noble metal-free electrocatalysts • Low concentrated (1M KOH) liquid electrolyte.	• Limited stability • Under development
PEM water electrolysis	• Commercialized technology • Operates higher current densities • High purity of the gases • Compact system design • Quick response	• Cost of the cell components • Noble metal electrocatalysts • Acidic electrolyte
Solid oxide water electrolysis	• High working temperature • High efficiency	• Limited stability • Under development

2.5 Alkaline Electrolyser

On this chapter a more detailed assessment of the alkaline electrolyser will take place. On the Figure 23 the basic components on an alkaline electrolyser are visible.

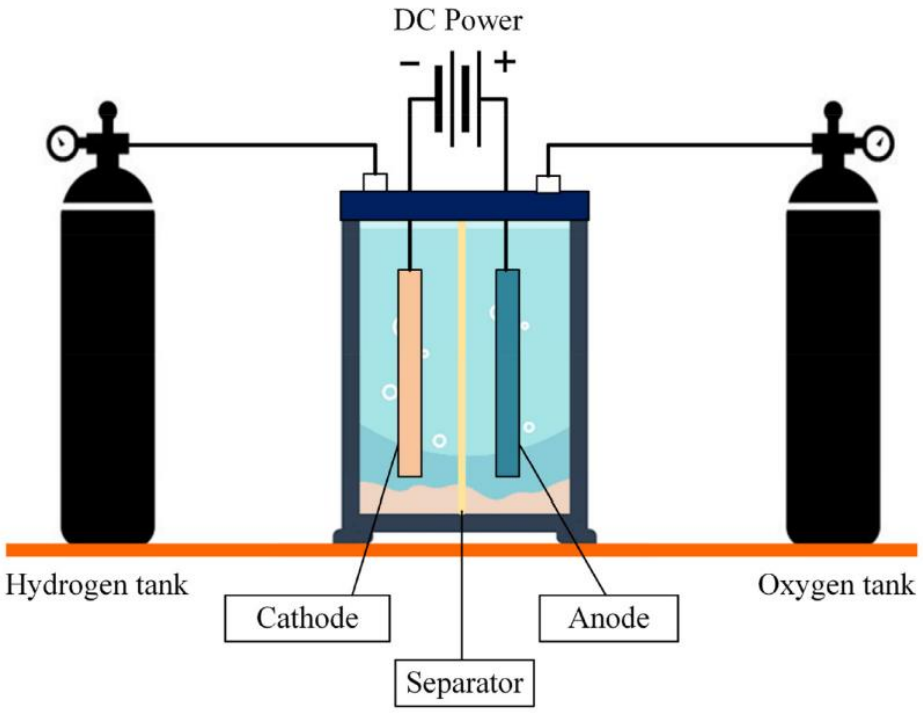

Figure 23: Basic components of alkaline electrolyser [36].

Alkaline electrolysers use an alkaline liquid solution based on KOH (around 32% w/w) or NaOH (around 18% w/w), while deionized water needs to be supplied constantly. Consequently, the environment is corrosive, the gases generated have low pressure and purification is needed for the produced hydrogen [33]. Also, low current density is necessary in order for acceptable efficiencies which results to larger plants [37].

2.5.1 Electrodes and catalysts

The electrodes are responsible for the electric current to the anode and cathode chambers. The anode, which is the positive electrode, produces OER when it interacts with the electrolyte. The cathode, or negative electrode, produces HER. These electrodes need to resist corrosion, possess excellent conductivity, appropriate catalytic properties, and maintain structural integrity. In alkaline electrolysis the use of noble materials is not necessary, due to increased pH levels. Nevertheless, when electrodes are coated or doped

with a more stable layer, lower activation energy and increased charge transfer is obtained [33].

- Cathode

For the cathode Ni is most usually used because of the significant electrocatalytic performance and the very good stability in alkaline environments. After some period, the overpotential increases due to the generation of a non-conductive nickel hydride resulting from the polarization of the cathode. In order to address this issue Ni is mainly used in combination with other metals (Mo, Zn, Fe, Co, Cr, W) and/or metallic oxides (MoO_2,MoO_3, CeO_2, IrO_2,RuO_2) [33].

- Anode

Anode is made from Ni as well while the increase of the overpotential is also observed due to the polarization, an issue that can be addressed by the use of electrocatalysts based on nickel and cobalt. Also, the inclusion of iron boosts the effectiveness of the produced oxygen [33].

- Electrodes morphology

The ohmic resistance of the electrolysis cell is affected by the electrodes morphology. The different morphologies that are used are screens, meshes, porous foams, etc., while bigger area of electrolyte means greater electrocatalytic activity. Ni foams initiate the lowest ohmic resistance [33].

2.5.2 Diaphragms

The diaphragms are placed one the electrolytic cell dividing it into the anode and the cathode chamber. The purpose of the diaphragm is to let only the hydroxyl anions to be transferred from the cathode to the anode, while it needs to be resilient with the alkaline nature of the electrolysis, the oxidizing environment of the anode and the reducing circumstances in the cathode [33]. The main material that was used on the diaphragms for the last decades was asbestos but due to high resistances and toxicity new materials have been studied such as Zirfon Perl [37].

2.5.3 Cell Designs

When it comes to the cell designs the electrodes of an alkaline electrolyser can be either distanced from the membrane in a range of microns to millimeters or in a very limited distance that optimizes the resistance. The first one is called gap cell and the second one zero-

gap cell. Zero gap configuration use porous electrodes and result to a higher current density, and it is most commonly used on the new alkaline electrolysers [33]. Those two configurations are illustrated on the Figure 24 below.

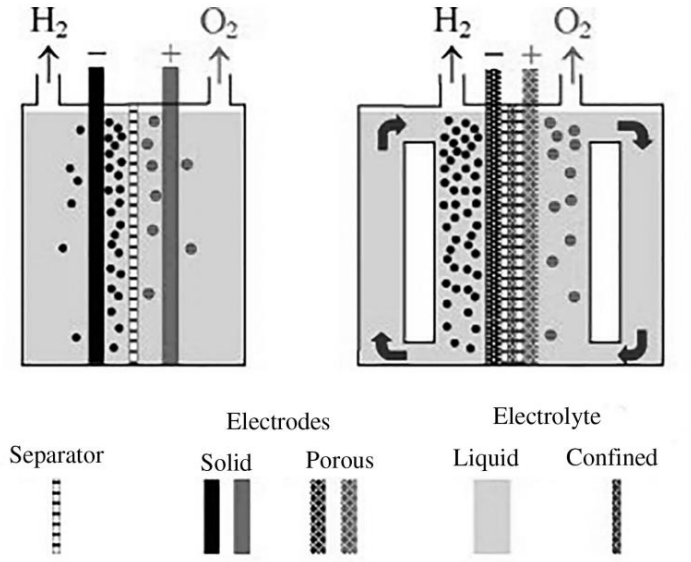

Figure 24:Gap cell and zero gap cell configurations [33]

2.5.4 Stack Configuration

Only one cell is not able to produce the mass flow of hydrogen that is desirable and for that a configuration of cells is necessary. Likewise other electric circuits the configuration of the stacks can be either in series or on parallel. When on parallel the stack is called monopolar and then the voltage is common while the total current is the sum of each current, while on series the stack is called bipolar, and the sum of the voltages give the total voltage while the current is the same for each cell and is not added up. A monopolar design makes the replacement of a part easier because it is not necessary to stop the electrolysis, the structure is simpler and the durability longer. On the other hand, the bipolar configuration is most commonly used on advertised technologies because of the smaller and more compact design while a broader range of operating temperatures and pressures takes place and the efficiency is higher [33], [38]. Figure 25 shows the monopolar and the bipolar structure of an alkaline electrolyser.

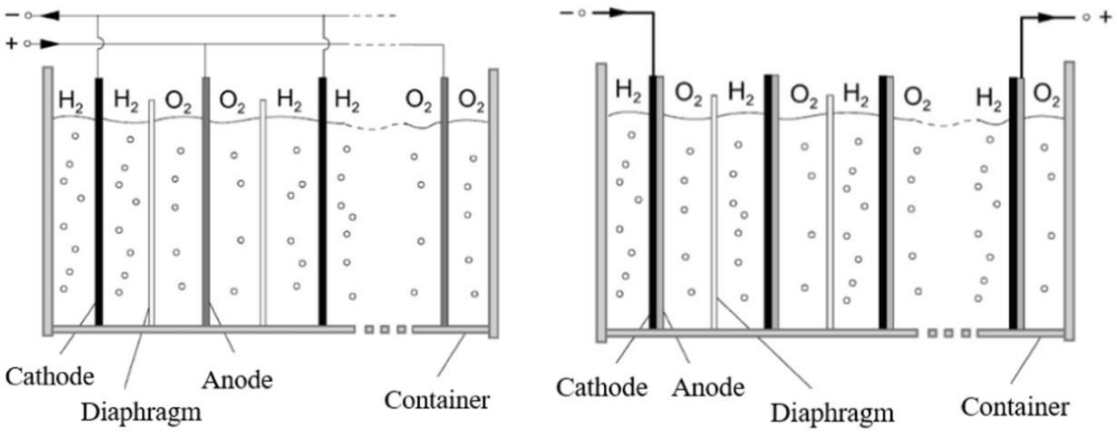

Figure 25: Monopolar and bipolar structure of alkaline electrolysis cells [38].

2.5.5 Summary

In summary alkaline electrolysers are mature and low cost when compare with the other alkaline electrolysers, although solutions on the low current density and the highly corrosive nature of the technology needs to be found [33]. The cathode and the anode are mainly produced from nickel but coating them with more stable layer the performance is better, they exist as screens, meshes and mainly Ni foams. The use of Zirfon Perl on the diaphragms is mainly observed on new models, while the diaphragm can be either almost in touch with the electrodes (zero gap) or in distance (gap cell) and when a lot of cells combine to make the plant monopolar or bipolar design can be used.

2.6 Storage methods

A challenge that needs to be addressed for the wide utilization of hydrogen on the forthcoming decades is the storage. REPowerEU sets a target of hydrogen storage capacity of 7,5 Mt by 2030 [39]. Hydrogen can be stored as solid, liquid or gas with the last one being the most usual. When in liquid or gas physical-based technologies are used while on solid material-based technologies are used [40].

2.6.1 Compressed hydrogen gas storage

Storing hydrogen as a compressed gas is the most usual and developed method [41]. It can be stored in vessels, on geological storages [42] and as linepack in gas pipelines.

2.6.1.1 Compressed hydrogen in vessels

When in vessels there are four different technologies (Types I,II,III,IV) that have developed during the last centuries.

- ***Type I***

Type I vessel is made from metal (steel or aluminum) and is capable to store hydrogen gas up to 175-200 bar [40]. It is very heavy compared to the hydrogen percentage it can store (around 1 wt %H_2) due to the thick walls that are necessary [41], but it is the cheapest technology of compressed gas storage and it is typically used for industrial works and was first introduced around 1874 [40].

- ***Type II***

Type II vessel is made from thick metallic liner hoop with the introduction of a fiber-resin composite that is wrapped around the cylindrical part of the vessel [41], [43] and it is capable of storing hydrogen up to 263-300 bar [40]. When compared to type I, it is 30-40% less heavy (still only 1,5 wt% of H_2) but 50% more expensive and it is also most commonly encountered on the industrial use. Both type I and II are very heavy and have hydrogen induced-cracking issues [40], [41].

- ***Type III***

Type III vessel is made from carbon fiber composite materials with a metal liner (such as aluminum) that blocks the hydrogen penetration. It can store hydrogen up to 450 bar and 25-75% lighter than the type I and II making it suitable for vehicle applications. On the downside it is expensive [40], [41].

- ***Type IV***

Type IV vessel is similar to type III, but the liner is polymeric, such as high-density polyethylene. Hydrogen can be stored up to 700 bar while it is the lightest and most expensive compared to the other types. High durability and long lifetime are also some of the characteristics of this type, while it is also suitable for vehicle applications [40], [41].
The Figure 26 below demonstrates those four types of vessels.

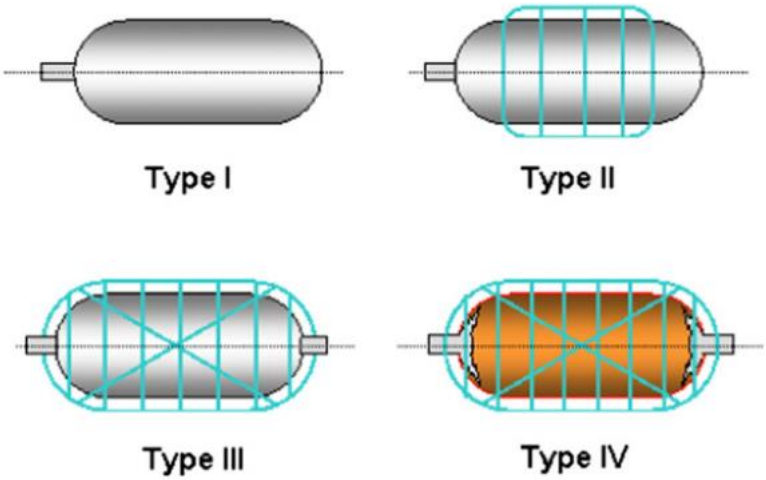

Figure 26: The four different types of gas hydrogen storing on vessels [43].

2.6.1.2 Underground geological storage

When in geological storage, salt caverns, aquifers, and depleted oil and gas fields are used although a wide variety of problems occur. In the EU if a retrofitting of the 204 TWh of the existing underground natural gas storage occur a total 49 TWh of hydrogen could be available [39].

- ***Salt caverns:***

Most of the salt caverns in the world are in North America and Europe, while only a few of them are used for large scale hydrogen storage and not all the countries have a lot of underground salt layers. In salt caverns, hydrogen can be stored up to maximum pressures 700 to 900 bar, while the depth and the geology affect the operating conditions and the cost [43]. One of the EU countries with the lowest salt cavern storage potential is Greece with around 100 TWh, while Germany has the highest salt cavern storage potential in the EU of around 35.610 TWh [39].

- ***Aquifers:***

Storing hydrogen into underground water-bearing formations in a similar way to natural gas in order to use it when necessary is environmentally friendly and possibly cost effective but problems such as limitation aquifer's capacity and flow rate, long-term stability and safety are some of the challenges that occur [43].

- ***Depleted oil and gas fields:***

Depleted oil and gas fields can be used to store hydrogen on a large capacity in a similar way to CO_2 and natural gas storage. Nevertheless, hydrogen has different behavior that could make long term storage of it on depleted oil and gas fields very difficult, while the cost could probably be higher than above ground storing [43].

2.6.1.3 Linepack Storage

Natural gas pipeline is a very mature technology that could be used for a cost-effective method to transport hydrogen on long distances [44]. In addition, pipeline can be used to store hydrogen in the form of linepack. Hydrogen could be injected as a blend with natural gas, or it could be moved entirely as 100% hydrogen gas. In the first scenario a lot of already used pipelines could be retrofitted to move hydrogen on percentages (till 20% hydrogen) but in the second scenario new dedicated pipelines that can move hydrogen under high pressures are necessary. When hydrogen is moved on blends sometimes deblending it would be necessary. Membranes that can separate hydrogen from methane exist and can achieve H_2 purities higher than 99,5 mol% [45]. In the most cases retrofitting already developed pipelines in order to move hydrogen on percentages is more cost effective than building new pipelines [42]. The Figure 27 below demonstrate the vision of 32 European network operators for their pipelines that could move hydrogen on 2040 under an accelerated and ambitious climate scenario. New pipelines are colored orange while repurposed are green.

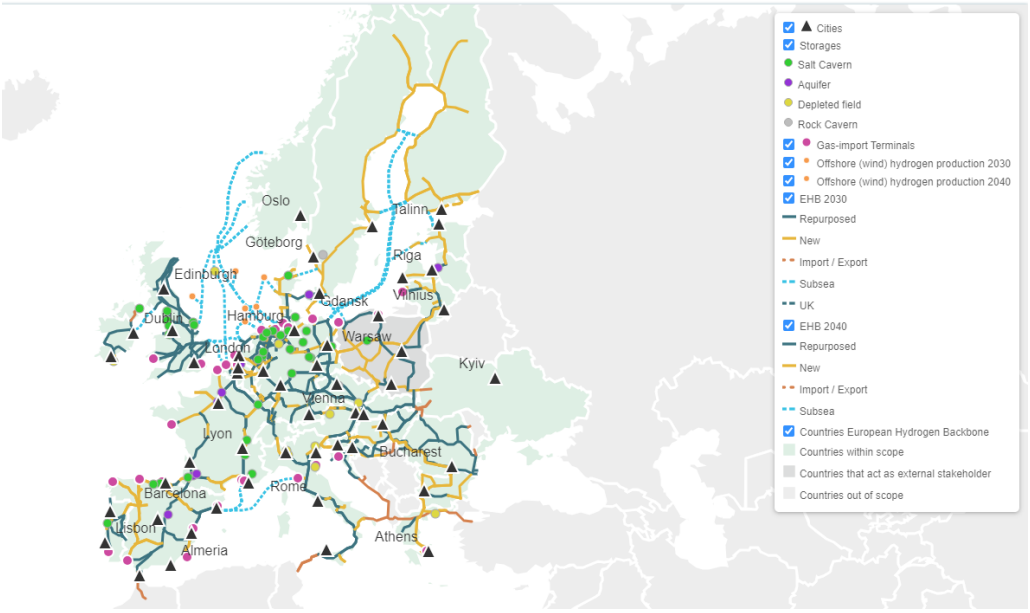

Figure 27: The gas pipeline infrastructure that can store and move hydrogen for 2040 as proposed form European hydrogen backbone [46].

2.6.2 Hydrogen stored in the liquid state

2.6.2.1 Liquid hydrogen (LH_2)

Cryogenic or liquid hydrogen (LH_2) is a safe and energy dense method (71 g/L). Hydrogen for normal temperature is liquified to -253 Celsius and is not corrosive making stainless steel and aluminum alloy vessels with a thick insulation cover capable for this kind of technology. The biggest drawbacks of this method are the high energy demand for the liquefaction (30-40% of net heating value of hydrogen), the loss of energy that comes constantly with the boil-off phenomenon (1,5-3% of hydrogen vaporizes per day) and the large containers that are necessary in order for the previous phenomenon to be less intense [41].

When hydrogen is under liquid phase and compressed (250-300 bar) cryo-compressed hydrogen has higher energy density (80 g/L) and the boil-off phenomenon is not a problem. On the other hand, more expensive type III vessels and even more energy demand is necessary [41].

2.6.2.2 Liquid Ammonia Hydrogen Storage (LAH_2)

On room temperature pure ammonia liquifies at 9,2 bar while it consists of 17,65 wt % of hydrogen and a 4,5 times larger volumetric density of hydrogen compared to liquid hydrogen [40]. Green hydrogen can be combined with nitrogen extracted from air to produce ammonia (power-to-ammonia P2A) that can be easily transported through already developed systems

and finally used either as a direct fuel or by decomposing hydrogen from ammonia (Figure 28). Some of the challenges that occur are the highly energy demand of the ammonia production process, the toxicity of ammonia in the case that it is released and the traces of ammonia that tend to remain in hydrogen after the decomposition [42].

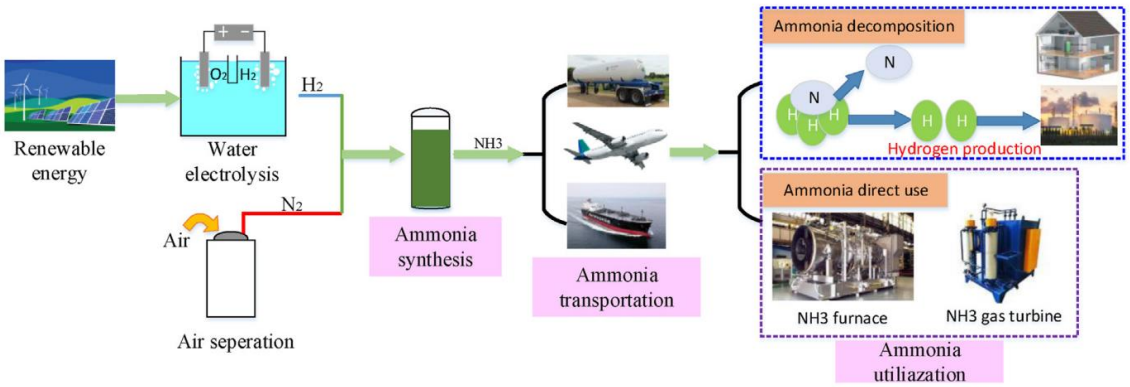

Figure 28: Storing hydrogen in the form of Liquid Ammonia [42].

2.6.2.3 Liquid Organic Hydrogen Carriers (LOHC)

Liquid hydrogen can react with a hydrogen deficient organic molecule to produce liquid organic hydrogen carrier (hydrogenation) that can easily be stored and transported and with the opposite reaction (dehydrogenation) hydrogen can be used when it is needed and the remained carbon atoms can be used again for another organic hydride cycle [40], [41]. High gravimetric and volumetric density, ambient operating temperatures and the exploitation of current infrastructure used for transporting gasoline are some of the biggest advantages, while the high energy demand for the dehydrogenation and the difficulty of developing catalysts that are used for dehydrogenation are some of the challenges [40], [47].

2.6.3 Hydrogen stored in solid state

2.6.3.1 Metal Alloy Hydrogen storage (MAH_2)

When there is chemical interaction between hydrogen and metals and metal alloys, metal hydrides can be formed [41]. The bulk of the metal or alloy structure chemisorbs at its surface the atomic hydrogen and the reverse reaction (when one decreases the pressure or increases the temperature) of desorption release hydrogen for it to be used as a fuel. Compared to compressed and liquified hydrogen, metal hydrides have higher storage capacity with less dangerous operating conditions. On the other hand, when hydrogen is released it has high temperature and undesirable gases can be formatted [41], while the density of hydrogen

storage per mass is low and it is not yet a grown and mature technology but rather an experimental one [47]. Two of the most promising alloys are LiH and MgH_2.

2.6.3.2 Carbon Material Hydrogen storage (CMH_2)

Carbon material hydrogen storage belongs to the materials-based technology of physisorption. High surface area of the material, low temperature (-198 Celsius) and high pressures are required for high hydrogen storage. To achieve this method high pressure cylinder and a cooling system rise the temperature or decrease the pressure of hydrogen [40]. Activated carbon and carbon nanotubes are some of the used materials and as an advantage the whole process is very fast but material preparation, cryogenic conditions and still on the research levels are some of the drawbacks [47].

A summary of the different technologies that can be used on hydrogen storing are represented on the Table 7. Highest hydrogen content is observed on ammonia and liquid hydrogen while high energy demand and safety are some of the disadvantages. Compresses gas is the most mature technology but not the most efficient. Ammonia and LOHCs can use already developed infrastructure providing cost effective solutions. Metallic hydrides give very good volumetric density but for the hydrogen to be realized high temperature is necessary. And lastly carbon-based material gives high storage capacity, while a lot of factors affect this capacity, and it is not yet commercialized [40].

Table 7: Comparison of different hydrogen storage technologies [47].

Types of technology	Key parameters	Hydrogen storage capacity	Advantages	Disadvantages	Current main applications
CH_2	20 MPa 70 MPa	11 kg H_2/m^3 39 kg H_2/m^3	1) Mature 2) Simple structure 3) Fast process	1) Low volumetric hydrogen storage capacity 2) Increased safety risks and transport costs as pressure increases	1) Common cylinders 2) Lightweight high-pressure hydrogen storage tanks
LH_2	<-253 °C	70.8 kg H_2/m^3	1) High hydrogen storage capacity 2) Safe	1) High vessel insulation requirements 2) High energy consumption in the liquefaction process	1) Mass- and long-distance transport 2) Rocket cryogenic propulsion
LOHCs	Toluene/ Methylcyclohexane Dibenzyltoluene/ Perhydro-dibenzytoluene	w_{H2} = 6.16 wt %, 47.4 kg H_2/m^3 w_{H2} = 6.2 wt%, 57 kg H_2/m^3	1) High hydrogen storage capacity 2) Closed carbon cycle 3) Long-cycle storage and transportation	1) High energy consumption for dehydrogenation 2) Difficulty in developing dehydrogenation catalysts 3) Short cycle life	1) Transoceanic transport 2) Bulk storage and transportation
LAH_2	NH_3	w_{H2} = 17.8 wt%	High hydrogen storage capacity	1) High toxicity 2) Trace amounts of ammonia tend to remain in the hydrogen gas	Proton exchange membrane fuel cells
MAH_2	LiH MgH_2	w_{H2} = 12.5 wt% w_{H2} = 7.65 wt%	1) High volumetric hydrogen storage capacity 2) Safe	1) Lack of technical maturity 2) Low efficiency of hydrogen storage and discharge 3) Low density of hydrogen storage per mass 4) High energy consumption	Laboratory research stage
CMH_2	Activated carbon Carbon nanotubes	w_{H2} = 3.8 wt% w_{H2} = 6.5 wt%	Fast process	1) Easily influenced by reaction conditions and material preparation processes 2) The hydrogen storage capacity is related to cryogenic conditions	Laboratory research stage

3. Simulation of an alkaline electrolyser

On this chapter the computational part of the thesis takes place. Firstly, a custom model for the stack of an alkaline electrlolyser is developed on the Aspen Custom Modeler that is later used to simulate on the Aspen Plus an alkaline water electrolysis system of 1,5 MW.

3.1 Alkaline Stack Modeling

The simulation of the alkaline electrolyser takes place in the Aspen Plus software, although specific components that describe the operation of the stack are not included on the program. Indirect methods could be used in order to simulate the operation of the stack but important operating variables such as V_{cell}, η_F, HTO (the percentage of hydrogen that immigrates to the anode from the cathode) would not be calculated in a dynamic way inside the software. Therefore, Aspen Custom Modeler (ACM), a quickly creating customized modeling for process equipment software that can later be used in Aspen Plus, was employed.

3.1.1 Operating Equations

The equations that were used to describe the working conditions of the stack were developed in the Sanchez et al. paper [48] where a 15 kW alkaline water electrolyser was modeled with a semi-empirical mathematical model predicting the electrochemical behavior of it. When the electrical input, the temperature and the pressure changes, operating voltage, Faraday efficiency (η_F[%]), HTO (%), electrical current (I_{cell}[A]) and hydrogen production ($\eta_{H2,prod}$ [mol/sec]) alternates. The equations that describe those operating conditions in a semi-empirical way are displayed on the following equations.

$$V_{cell} = V_{rev} + [(r_1 + d_1) + r_2 * T + d_2 * p] * i_{cell} + s * \log\left[\left(t_1 + \frac{t_2}{T} + \frac{t_3}{T^2}\right) * i_{cell} + 1\right] \quad (29)$$

$$\eta_F = \left(\frac{{i_{cell}}^2}{f_{11} + f_{12} * T + {i_{cell}}^2}\right) * (f_{21} + f_{22} * T) \quad (30)$$

$$HTO = \left[C_1 + C_2 * T + C_3 * T^2 + (C_4 + C_5 * T + C_6 * T^2) * \exp\left(\frac{C_7 + C_8 * T + C_9 * T^2}{i_{cell}}\right)\right] + \left[E_1 + E_2 * p + E_3 * p^2 + (E_4 + E_5 * p + E_6 * p^2) * \exp\left(\frac{E_7 + E_8 * p + E_9 * p^2}{i_{cell}}\right)\right] \quad (31)$$

$$W_{electrical,iput} = V_{stack} * I_{cell} = V_{cell} * N_{cell} * i_{cell} * A_{cell} \quad (32)$$

$$\eta_{H2,prod} = \frac{\eta_F * i_{cell} * A_{cell} * N_{cell}}{z * F} \quad (33)$$

Where i_{cell} [A/cm^2] is electrical current density, N_{cell} is the number of the cells, A_{cell} [m^2] is the area of each cell, z=2 is the number of electrons that are transferred per H_2 molecule and F=96485 C/mol is the Faraday constant. Table 8 shows the values of the coefficients that are used.

Table 8: Coefficients considered for the electrochemical model of an alkaline water electrolysis cell [48].

Model	Coefficient	Value	Unit
Polarization curve	r_1	4.45153×10^{-5}	$\Omega\ m^2$
	r_2	6.88874×10^{-9}	$\Omega\ m^2\ °C^{-1}$
	d_1	-3.12996×10^{-6}	$\Omega\ m^2$
	d_2	4.47137×10^{-7}	$\Omega\ m^2\ bar^{-1}$
	s	0.33824	V
	t_1	−0.01539	$m^2\ A^{-1}$
	t_2	2.00181	$m^2\ °C\ A^{-1}$
	t_3	15.24178	$m^2\ °C^2\ A^{-1}$
Faraday efficiency	f_{11}	478645.74	$A^2\ m^{-4}$
	f_{12}	−2953.15	$A^2\ m^{-4}\ °C^{-1}$
	f_{21}	1.03960	–
	f_{22}	−0.00104	$°C^{-1}$
Gas purity (hydrogen in oxygen)	C_1	0.09901	–
	C_2	−0.00207	$°C^{-1}$
	C_3	1.31064×10^{-5}	$°C^{-2}$
	C_4	−0.08483	–
	C_5	0.00179	$°C^{-1}$
	C_6	-1.13390×10^{-5}	$°C^{-2}$
	C_7	1481.45	$A\ m^{-2}$
	C_8	−23.60345	$A\ m^{-2}\ °C^{-1}$
	C_9	−0.25774	$A\ m^{-2}\ °C^{-2}$
	E_1	3.71417	–
	E_2	−0.93063	bar^{-1}
	E_3	0.05817	bar^{-2}
	E_4	−3.72068	–
	E_5	0.93219	bar^{-1}
	E_6	−0.05826	bar^{-2}
	E_7	−18.38215	$A\ m^{-2}$
	E_8	5.87316	$A\ m^{-2}\ bar^{-1}$
	E_9	−0.46425	$A\ m^{-2}\ bar^{-2}$

While HTO is an important variable that should be considered especially for safety reasons, 2% HTO emergency stop should take place and 1.6% HTO is the alarm value [49], the diffusion of oxygen to hydrogen (OTH) can be considered as negligible quantity around 0.1-0.5% [50]. The mass balance on the anode and cathode side generates the following equations.

$$\eta_{H2,cat} = \eta_{H2,prod} \tag{34}$$

$$\eta_{H2,an} = \eta_{HTO} \tag{35}$$

$$\eta_{O2,an} = \eta_{O2,prod} = 0.5 * \eta_{H2,prod} \tag{36}$$

$$\eta_{H2O} = \eta_{H2,prod} \quad (37)$$

3.1.2 Stack development on the Aspen Custom Modeler

In order to create the custom model of stack the familiarization with the program and the basic tools that it provides was necessary. On this context the tutorial from David Tremblay and Zachary Peer [51] was very useful.

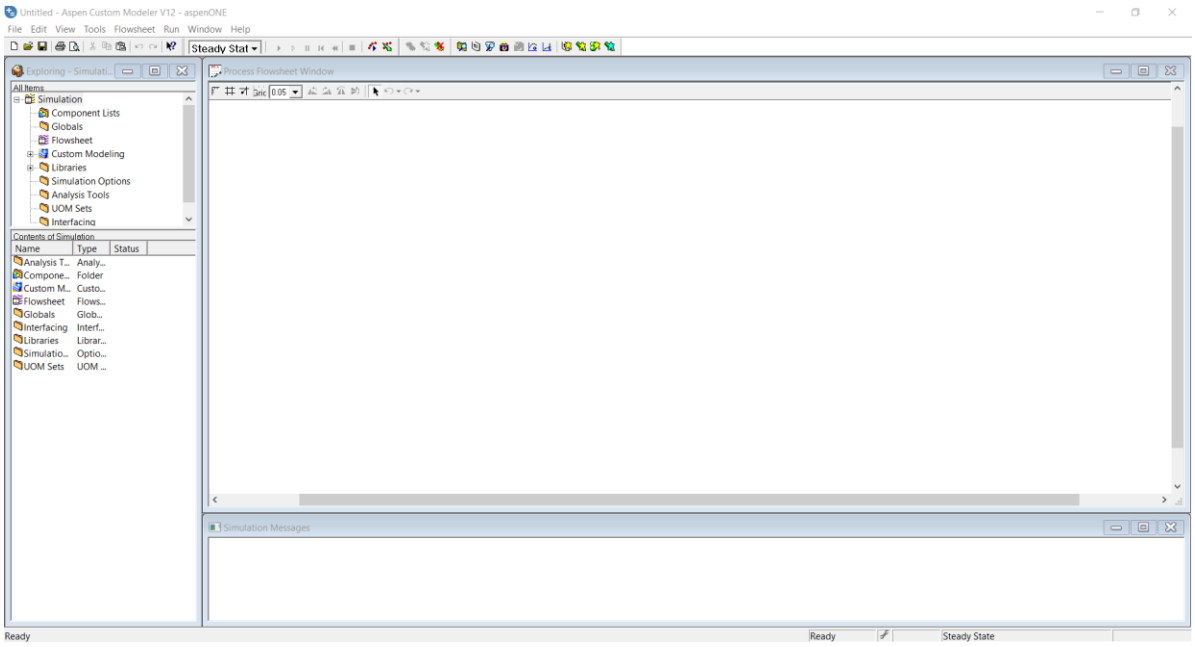

Figure 29: Aspen Custom Model basic environment.

Very useful for the creation of the custom model, that also recreates the custom model from the original paper [48], was also the paper [52]. The following steps were taken. Firstly, the Component List needs to be defined. To do so from the ''Component Lists'' the following components from Figure 30 were defined with the ''Edit using Aspen Properties'' function of ''Use Aspen property system''. The base method was Non Random Two Liquids (NRTL).

Component ID	Type	Component name	Alias	CAS number
WATER	*Conventional*	**WATER**	**H2O**	7732-18-5
H2	*Conventional*	**HYDROGEN**	**H2**	1333-74-0
O2	*Conventional*	**OXYGEN**	**O2**	7782-44-7
KOH	*Conventional*	**POTASSIUM-HYDROXIDE**	**KOH**	1310-58-3

Figure 30: Component List that was used in the ACM.

Next a new model needs to be defined from the ''Custom Modeling'' -> ''Models''. The code with the operating equations of the components will be written on the window that pop up. For the program to understand that one inlet and two outlet materials streams, one inlet work stream and one outlet heat stream are used, ports need to be added. The heat stream (Q_{loss} [W]) refers to the ambient loss of duty from the stack to the environment, the work stream (Wstack [W]) stands for the electrical power input, the inlet material refers to the inlet stream of the stack and the two outlet material ports refers to the anode and the cathode. The variables of pressure, temperature, current density, and everything that is going to be used needs to be defined, while the equations need to be applied as well. The whole code has been displayed on the chapter Code Annex at the end. Once all the variables of the equations have been defined the code can be compiled.

Next a simple flowsheet needs to be built. In order to create the desirable icon for the stack from the model on the simulation explorer ''Add Icon'' is selected and when the modifications are over the icon needs to be defined as default by right clicking and selecting ''Make Default''. Then by simply dragging the new model from the simulation explorer and dropping it into the workspace the icon pops up and from ''Libraries''->''Modeler''->''Stream Types'' the ports are dragged into the flowsheet.

Now the problem is ready to be solved inside the program simply by double clicking the icon for the AllVariables Table to open and from there the fixed variables with their known values are being set for the unknown free variables to be found. If the problem is well defined a green square should be visible at the bottom of the window (see Figure 31) and it can be solved.

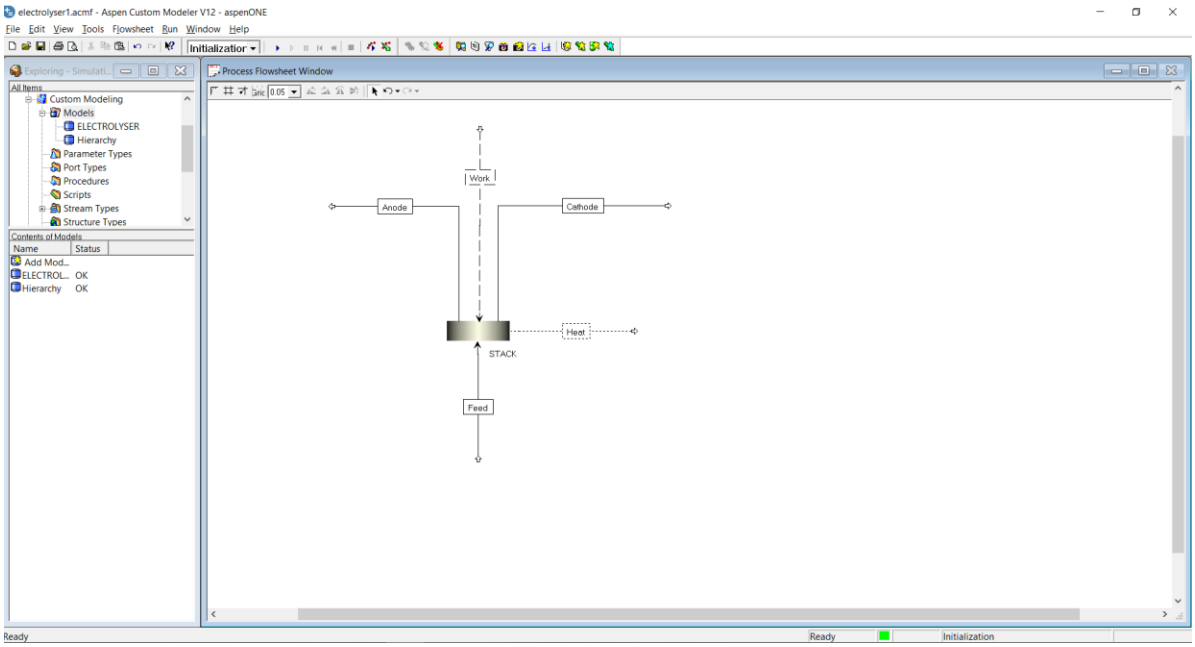

Figure 31: The Aspen Custom Modeler when the code and the icon has been defined.

By right clicking the new model and selecting the ''Package Model for Aspen Plus/HYSYS'' an export package can be created that can be later used from the Aspen Plus as a new component. Figure 32 shows the flowsheet of Aspen plus when the stack is inserted with 80 C inlet stack temperature and 7 bar stack pressure.

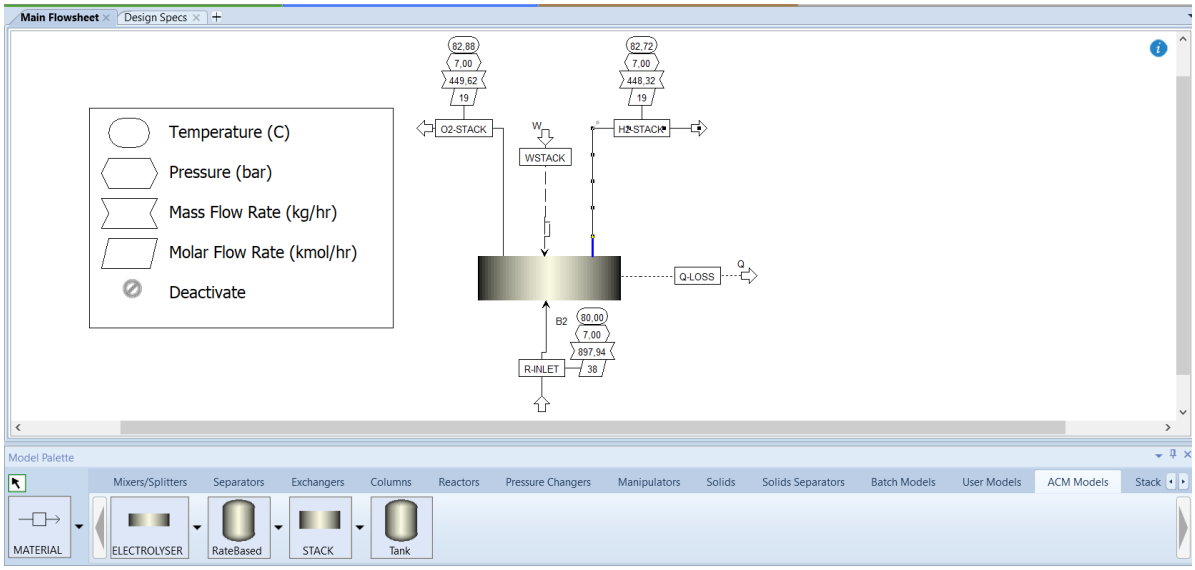

Figure 32: The stack component on the Aspen Plus environment.

There are some details about the function of the created stack on the Aspen Plus environment. Firstly, it is necessary to define the constant (fixed) and the calculated (free) variables. Constant variables are the inlet stream and its properties, the electrical power input, the number of the cells, the area of the cells and the reversible voltage, while calculated variables are the properties of the outlet streams, the stack temperature, the cell voltage and current density, the HTO, the η_F and all the others.

Table 9: Constant Variables of the stack

AllVariables | Constant | Calculated — Count: 15

Variable	Value	Units	Physical Type	Specification	Lower Bound	Upper Bound
INLET.F	38	KMOL/HR	MOLE-FLOW	Constant	0	1e+10
INLET.Z(KOH)	0,147407	FRACTION	CONTENTS	Constant	0	1
INLET.Z(O2)	4,72659e-05	FRACTION	CONTENTS	Constant	0	1
INLET.Z(H2)	4,26236e-05	FRACTION	CONTENTS	Constant	0	1
INLET.Z(WATER)	0,852503	FRACTION	CONTENTS	Constant	0	1
INLET.T	80	C	TEMPERATURE	Constant	-246	5000
INLET.P	7	BAR	PRESSURE	Constant	1e-30	5e+06
INLET.H	-3,06608e+08	J/KMOL	MOLE-ENTHALP	Constant	-1e+16	1e+12
INLET.V	0,0307703	CUM/KMOL	MOLE-VOLUME	Constant	0,0002	1e+30
WSTACK.W	10	KW	POWER	Constant	-1e+08	1e+08
WSTACK.SPEED	0	RPM	FREQUENCY	Constant	0	100000
PSTACK	7	BAR	PRESSURE	Constant	1e-30	5e+06
NCELL	12	*	UNTYPED	Constant	-1e+37	1e+37
ACELL	0,1	*	UNTYPED	Constant	-1e+37	1e+37
VREV	1,23	VOLT	VOLTAGE	Constant	0	1e+09

Table 10: Calculated Variables of the stack

AllVariables | Constant | Calculated — Count: 56

Variable	Value	Units	Physical Type	Specification	Lower Bound	Upper Bound
OUTCATHODE.F	19,0437	KMOL/HR	MOLE-FLOW	Calculated	0	1e+10
OUTCATHODE.Z(KOH)	0,147069	FRACTION	CONTENTS	Calculated	0	1
OUTCATHODE.Z(O2)	0	FRACTION	CONTENTS	Calculated	0	1
OUTCATHODE.Z(H2)	0,00470705	FRACTION	CONTENTS	Calculated	0	1
OUTCATHODE.Z(WATER)	0,848224	FRACTION	CONTENTS	Calculated	0	1
OUTCATHODE.T	82,8848	C	TEMPERATURE	Calculated	-246	5000
OUTCATHODE.P	7	BAR	PRESSURE	Calculated	1e-30	5e+06
OUTCATHODE.H	-72855,4	CAL/MOL	MOLE-ENTHALP	Calculated	-2,38846e+08	2,38846e+08
OUTCATHODE.V	30,8806	CC/MOL	MOLE-VOLUME	Calculated	0,2	1e+33
QLOSS.Q	707,396	WATT	ENTHALPY-FLO	Calculated	-2,77778e+10	2,77778e+10
TSTACK	82,8848	C	TEMPERATURE	Calculated	-246	5000
VCELL	1,98513	VOLT	VOLTAGE	Calculated	0	1e+09
ICELL	4197,88	*	UNTYPED	Calculated	-1e+37	1e+37
ETAF	0,940912	*	UNTYPED	Calculated	-1e+37	1e+37
HTO	0,00906512	*	UNTYPED	Calculated	-1e+37	1e+37
EXTENT	0,0884245	KMOL/HR	MOLE-FLOW	Calculated	0	1e+10

Table 11: Inlet streams of the 15 kW electrolyser

Inlet stack mole flow	38	[kmol/hr]
Inlet KOH mole fraction	14,74%	[kmol,i/kmol,tot]
Inlet O_2 mole fraction	0,0043%	[kmol,i/kmol,tot]
Inlet H_2 mole fraction	0,0047%	[kmol,i/kmol,tot]
Inlet H_2O mole fraction	85,25%	[kmol,i/kmol,tot]
Nominal power input	15	[kW]

The values for the variables that were used were similar to the original paper [48] and as Table 8, Table 9 and Table 11 shows the inlet material flow is 38 kmol/hr, the mass fraction is almost 35% KOH and 65% H_2O and it is translated to mole fraction of 14.7% KOH, 84.8% H_2O and some small fractions of oxygen and hydrogen ($4.7*10^{-5}$ oxygen and $4.3*10^{-5}$ hydrogen) that returns from the anode and the cathode. The number of cells N_{cell} is 12 and the area of each cell A_{cell} is 0.1 m^2.

3.1.3 Validation of the stack

To validate the stack that was created a comparison with the original paper figures takes place. More specific the diagrams that are compared are the hydrogen flow rate and HTO for different inlet stack temperatures and stack pressures. To extract the figures a similar work to the following chapter ‘’Operating diagrams’’ was done.

As it is illustrated on the following Figure 33-Figure 35 the produced hydrogen flow rate and the HTO for different current densities and stack inlet temperatures at 7 bar stack pressure are very similar for the case of the thesis and the original paper.

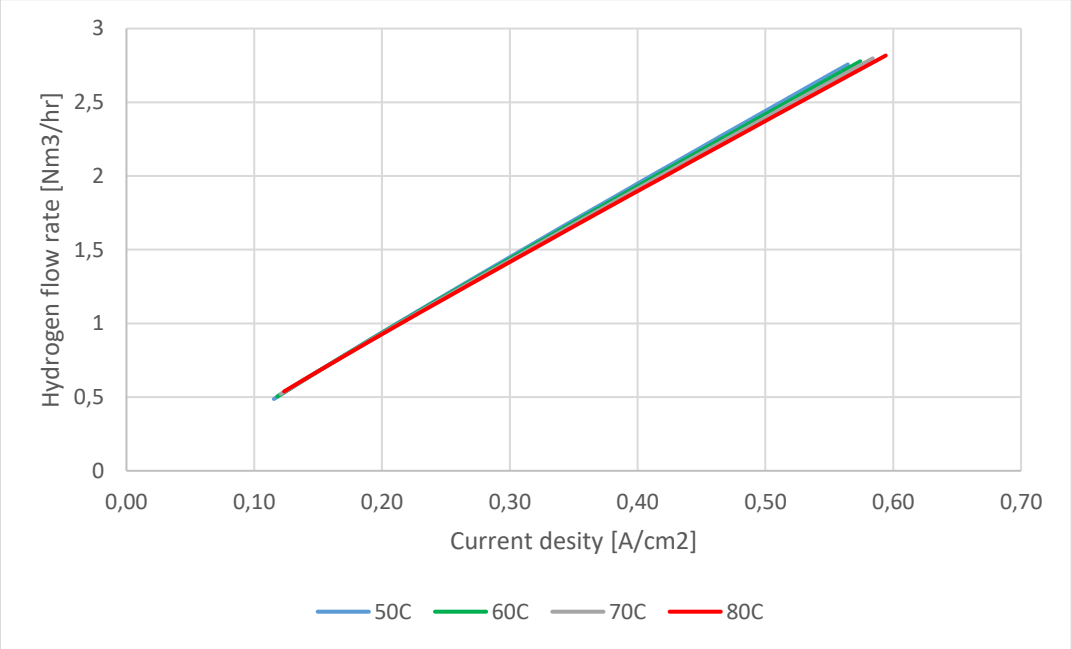

Figure 33: Hydrogen flow rate for different current densities and inlet temperatures for 7 bar stack pressure-Current Thesis.

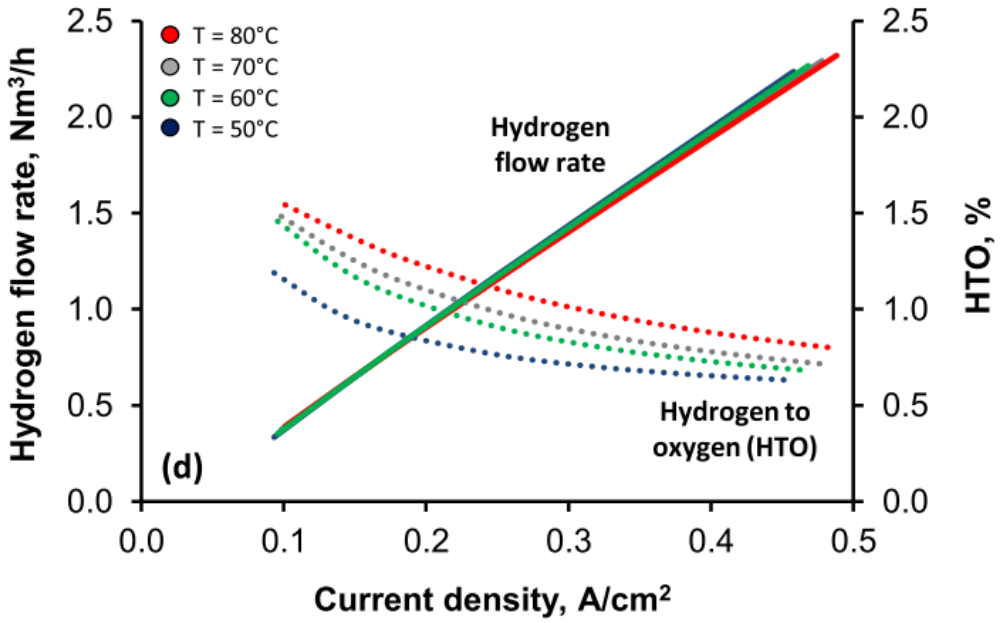

Figure 34: Hydrogen flow rate - HTO for different current densities and inlet temperatures for 7 bar stack pressure-Original Paper (figure 5(d) [48]).

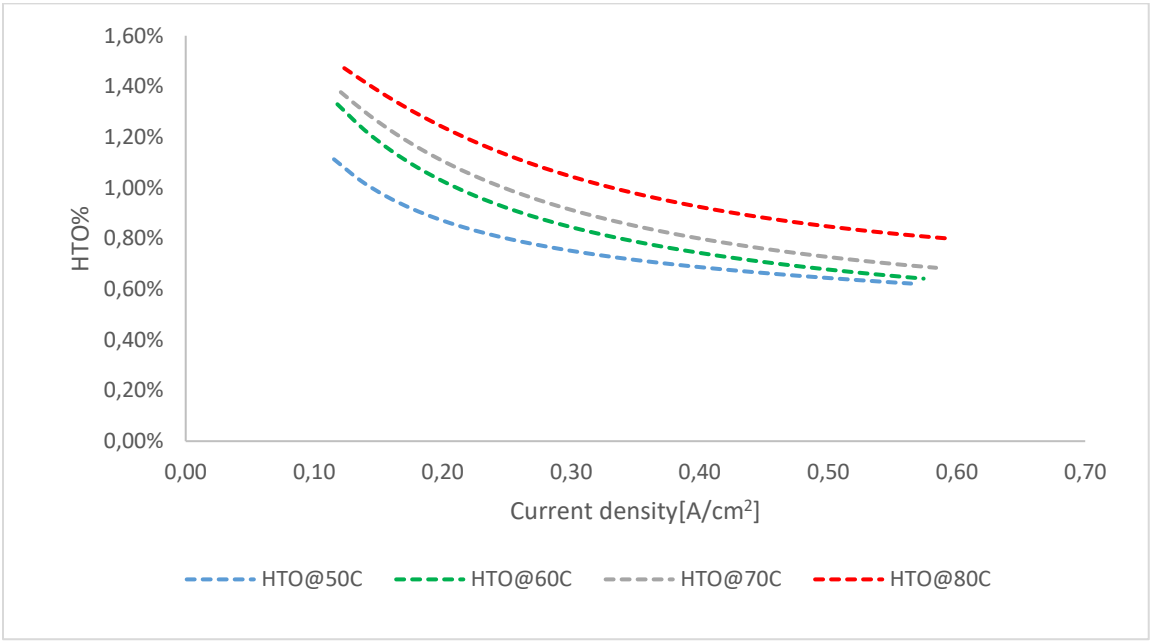

Figure 35: HTO for different current densities and inlet temperatures for 7 bar stack pressure-Current Thesis.

Figure 36 and Figure 37 demonstrate the produced hydrogen flow rate and the HTO for different current densities and stack temperatures at 72 Celsius inlet stack temperature are also very similar for the case of the thesis and the original paper.

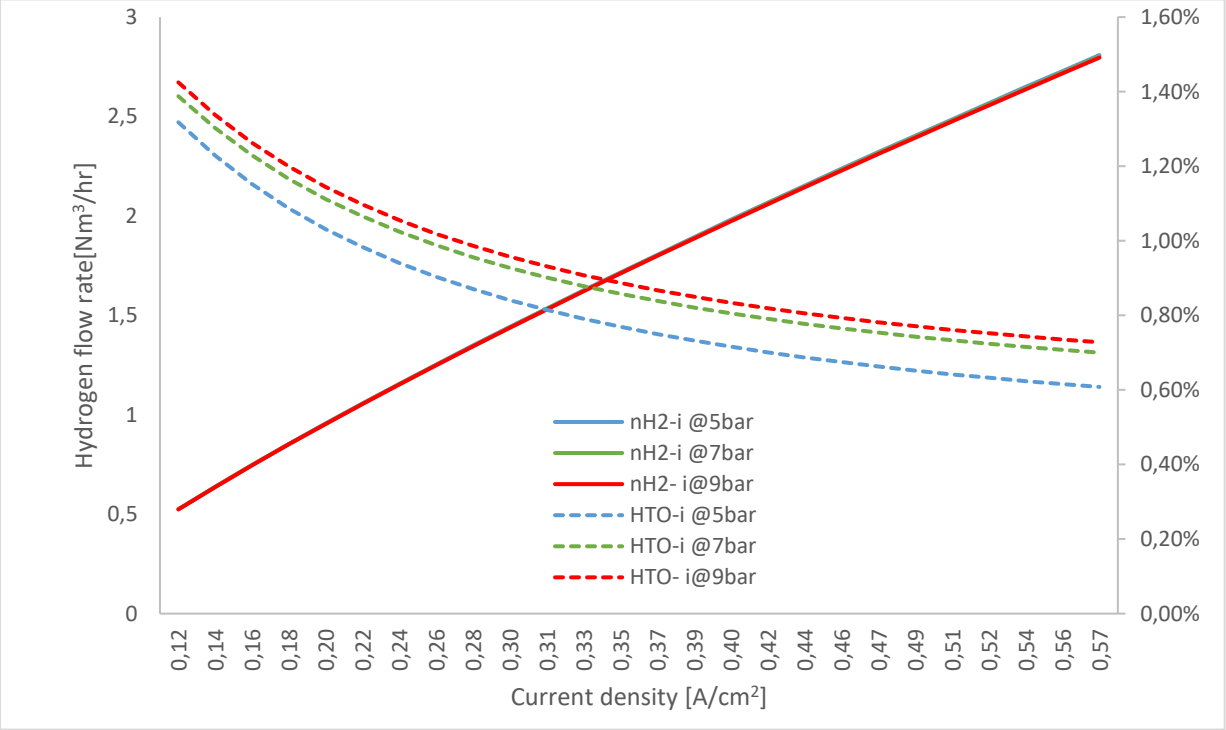

Figure 36: Hydrogen flow rate - HTO for different current densities and stack pressures at 72 C inlet stack temperature-Current Thesis.

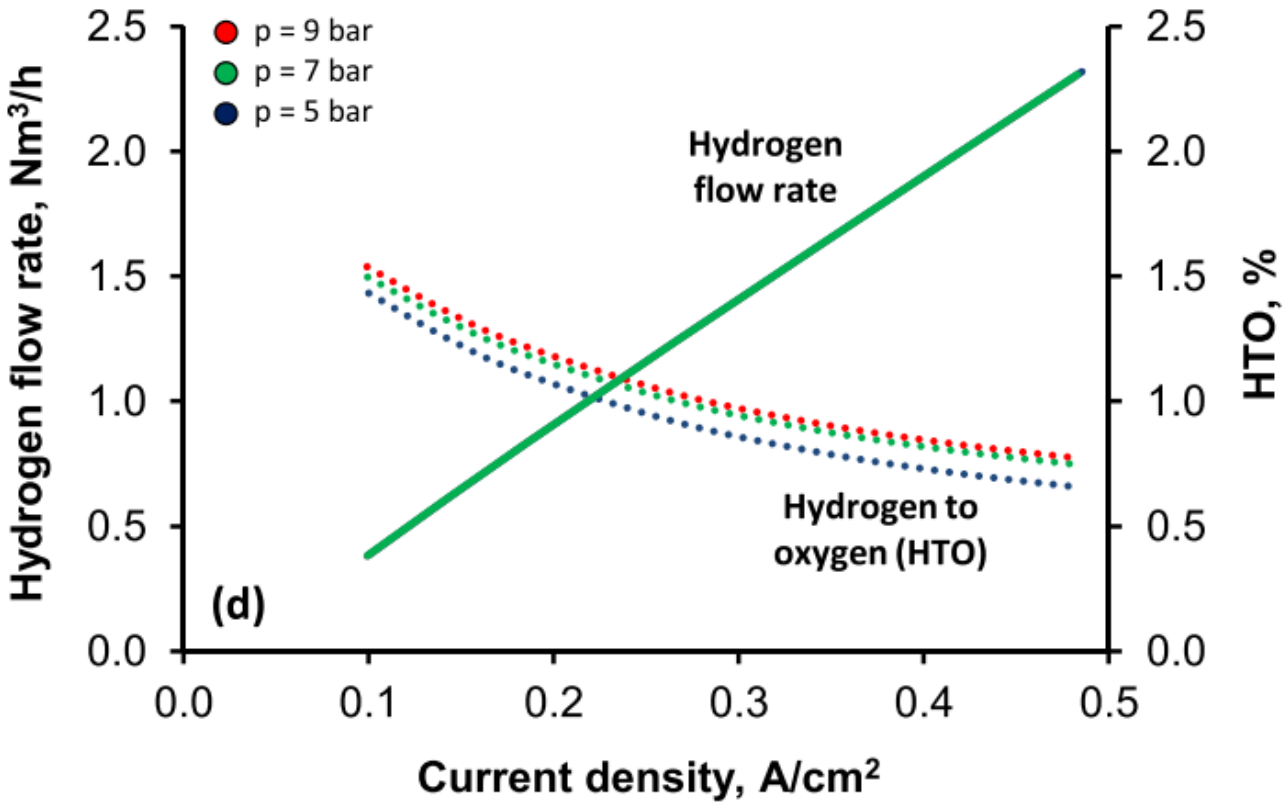

Figure 37: Hydrogen flow rate - HTO for different current densities and stack pressures for 72 C inlet stack temperature-Original Paper (figure 6(b) [48]).

3.2 Alkaline water electrolysis system

3.2.1 Scaling the stack on the desirable nominal power

Since the validation of the stack was finished the next step was to create a system of a 1.5 MW alkaline water electrolysis system in Aspen Plus, because higher nominal powers are more usually used on green hydrogen projects that require electrolysers with power greater than 1 MW. In order to scale the stack from 15 kW to 1.5MW the input power, the mass flow of the deoxidized water, the KOH electrolyte and the number of the cells was multiplied by 100. The next table shows some basic information about the inlet streams of the 1,5 MW electrolyser.

Table 12: Inlet streams of the 1.5 MW electrolyser

Inlet stack mole flow	3800	[kmol/hr]
Inlet KOH mole fraction	14,74%	[kmol,i/kmol,tot]
Inlet O_2 mole fraction	0,0043%	[kmol,i/kmol,tot]
Inlet H_2 mole fraction	0,0047%	[kmol,i/kmol,tot]
Inlet H_2O mole fraction	85,25%	[kmol,i/kmol,tot]
Deionized water flow	170	[kg/hr]
Nominal power input	1,5	[MW]

Since those configurations did not produce any problems, the other components of the system were necessary to be inserted. The next Figure 38 demonstrates the whole system on the program. The system was solved for three different stack pressures 5,7 and 10 bars at four different inlet stack temperatures 50,60,70 and 80 C each. Real life systems usually can work for lower and greater pressures too, but the way the stack was modeled that used the semi-empirical equation (31) forbids the usage of stack pressures apart from the 5-10 bars because very high percentages of HTO are being produced. For reasons that will be explained more detailed later, the maximum best operating conditions are succeed at 5 bar and 80 C stack inlet pressure and temperature for the maximum power input of 1.5 MW.

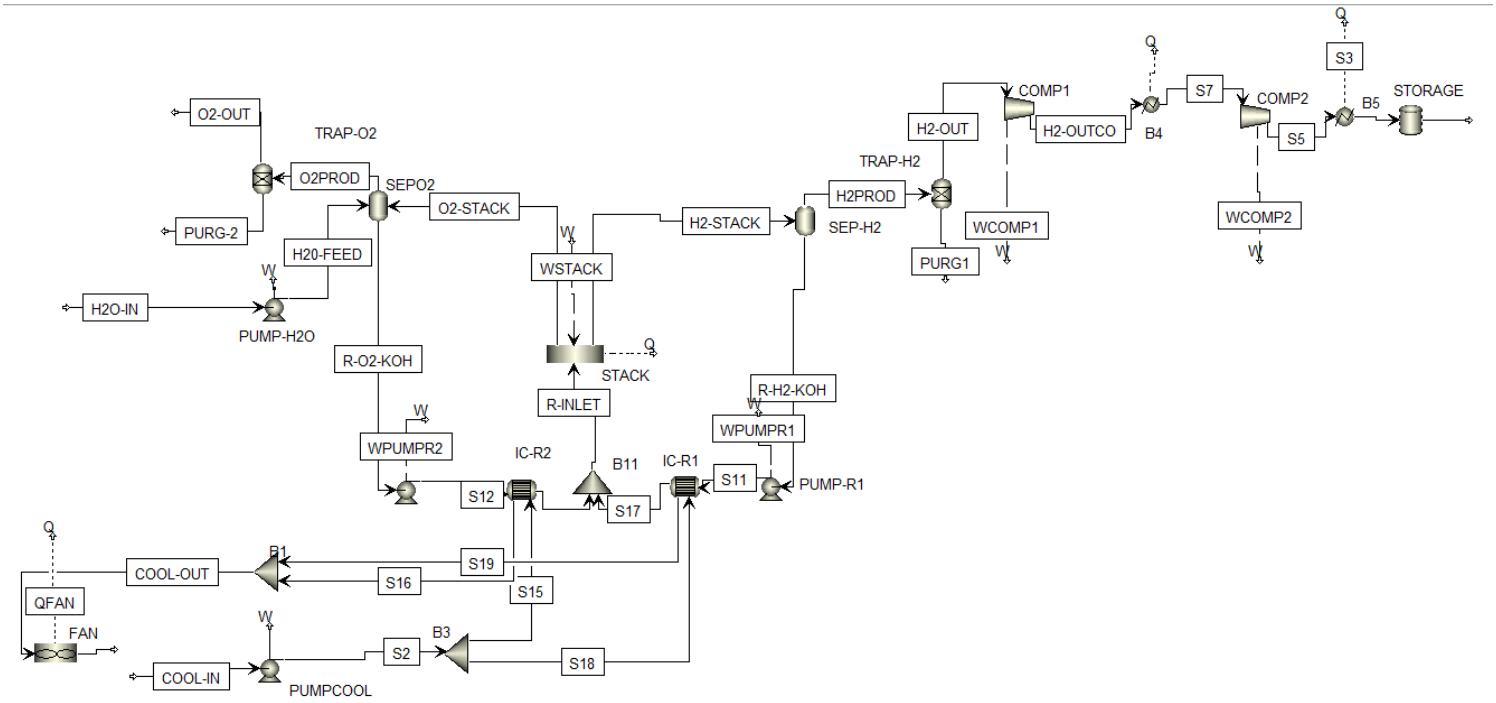

Figure 38: The alkaline water electrolysis system modeled on the Aspen Plus.

3.2.2 System components

- Gas-liquid separator

For the separation of the gas-liquid mixture of the anode and the cathode side, two simple flash separators were added (''SEPO2'', ''SEPH2''). The separators were modeled adiabatic with a 0.3 bar diminish. The water-KOH mixtures with very small quantities of hydrogen and oxygen R-O2-KOH, R-H2-KOH from the anode and the cathode respectively, in order to return to the stack with the initial operating conditions get through a pump (''PUMP-R2'', ''PUMP-R1'') and a heat exchanger.

- The cooling system

The two heat exchangers ''IC-R2'' and ''IC-R1'' were inserted for the cooling of the returning mixture from the anode and cathode respectively. The refrigerant that was used is water with an inlet temperature of 35 C and outlet temperature of 41 C. To target a specific inlet temperature a design spec was added that varies the mass flow of the

refrigerant water. The initial 35 C, 2.6 bar mass flow of the water split evenly (''B3'' splitter) to the two heat exchangers. For the calculations on the heat exchangers shortcut method was used, with the hot fluid (''IC-R1'',''IC-R2'') being on the shell side and a countercurrent flow direction. A 0.3 bar drop was added to the refrigerant (hot sides) and 0.5 bar drop to the mixtures (cold sides). After the heat exchangers, the mixtures from the anode and the cathode mix with a simple mixer (''B11'') and enters the stack again, while the cold sides mix with a simple mixer (''B1'') in order to be cooled down in the air cooler and be used again. The air cooler (''FAN'') was modeled with a simple Heater block that cools the water to the initial 35 C with a 0.3 bar pressure drop. The original paper from Sanchez et. al [50] does not refer a lot to the cooling loop, while for the fan they have probably developed their own component on the Aspen Custom Modeler that models their original fan. Also, in their Fig. 7, it is observed that from the 2392.8 Watt of the heat that is absorbed from the mixtures in the heat exchangers only the 718 Watt are absorbed away from the fan, while the fan uses only 592 Watt electric power input in order to absorb those 718 Watt. With a small market research, it seemed that this kind of cooling water - air cooler systems are being used on the industry. More specifically heat from process water is being absorbed from air cooled chillers that is then transferred to the air around the chiller unit, when the discharged heat is not a factory [53]. Although it does not seems logical that 592 electrical Watt can cause the absorption of 2392.8 thermal Watt a similar proportionality ratio was added to this thesis in order for the cooling system electrical consumption to be around 5-7% of the total electrical input of the system, because similar values was observed in such systems [53], [54].

- Purification system

The purification systems are added on this kind of systems to purify the produced hydrogen and oxygen. The produced oxygen can be used to medical or other applications. Real life purification systems are more complex but on the context of this thesis two simple separators (''TRAP-H2'',''TRAP-O2'') that fully separate the produced hydrogen and oxygen was added.

- Deionized water

For the inlet deionized water, the ''H2O-IN'' stream was added as pure water with 25 C and 1 bar that gets through a pump (''PUMP-H2O'') in order to get the pressure of the system. The inlet of the deionized water is 170 kg/hr. After the pump the water heads to the anode separator where it mixes with the mixtures to head to the stack.

- Pumps

All of the four pumps were modeled with an 89% efficiency and 99% driver efficiency.

- Compression and storage

After the purification system the produced hydrogen gets into the compression and storage part of the system. A two-stage compression system was added with two heat exchangers in order to produce 200 bar, 25 C hydrogen that is stored in a storage tank. The compressors were modeled with an isentropic efficiency of 87% and 99% mechanical efficiency. For the optimization of the compression the interstage pressure needs to be the geometric average of the initial and final pressures [55].

$$p_{opt} = \sqrt{p_i * p_f} \quad (38)$$

For this system p_f=200 bar and p_i=4.7,6.7,9.7 bar which translates to p_{opt}=30.65,36.6,44.05 bar. Those three pressures were the discharge pressures for the ''COMP1'' for each of the three different pressure scenarios, while for the ''COMP2'' the discharge pressure was 200 bar. The two heat exchangers were added to cool the hydrogen to 25 C after each compressor.

3.2.3 Validation of the alkaline electrolysis system

The next table compares some basic properties of the thesis modelled electrolyser at 80C, 5bar for maximum load of 1.5 MW input with the commercial alkaline electrolyser A300 with 1.5 MW nominal power of the company ecolyzer by Ecoclean [56] and the gateway 200 with 1.2 MW nominal power of the company stargate hydrogen [57].

Table 13: Comparison of the thesis electrolyser at 80C,5bar for 1.5 MW input with commercial alkaline electrolyser.

	Thesis electrolyser	**Commercial alkaline electrolyser A300 of Ecolyzer by Ecoclean**	**Commercial alkaline electrolyser gateway 200 of Stargate Hydrogen**	**Units**
Nominal Power Input	1,5	1,5	1,2	*[MW]*
Water consumption	206	300	328	*[L/hr]*
Hydrogen production	272	300	200	*[Nm3/hr]*
Stack efficiency	5,5	4,5	4,59	*[kWhr/Nm3]*
Hydrogen pressure (without compression system)	5	0,4	30	*[bar]*
Electrolyte	KOH	KOH	KOH	
Load	16-100%	20-100%	20-100%	

Although hydrogen production is similar, water consumption and efficiency are quite different. The reason for this mismatch of characteristics probably comes from the fact that the scaling of the thesis electrolyser is based on a small power of 15 kW electrolyser. Also, it is visible that the operating conditions are not the same since the working pressure differs and the electrolyte percentage is unknown. Nevertheless, it seems that the model responds to a satisfactory extent in generating realistic results for significant variables.

4. Results and Discussion

On this chapter the data from the simulation are taken in order to study the alkaline system behavior. Finally, a simple techno-economic analysis, from the exported data of the system, in order to calculate the LCOH for three different scenarios of primary electricity source (PV, wind turbine and grid connection), is done.

4.1 Operating diagrams

In order to study the operation of the system a sensitivity analysis for the different pressures and temperatures took place. In total 12 scenarios were studied for three different pressures at four different temperatures each. In each scenario the electrical input was changed from 250 to 1500 kW with a 50 kW step. In this way the system was studied from 16.66% to 100% of the nominal power input. When the electrical input increases the voltage and current density increases as well for each cell. For cell voltages higher than the thermoneutral, heat is generated (Q_{gen}). Some of this heat is transferred to the environment via heat radiation (Q_{loss}) and the remaining Q_{excess} result to the increase of the temperature on the anode and the cathode mixtures.

$$Q_{gen} = N * I_{cell} * (V_{cell} - V_{tn}) \quad (39)$$

$$Q_{excess} = Q_{gen} - Q_{loss} \quad (40)$$

The results from the Aspen sensitivity analysis were transferred to Excel in order to create some figures and study the behavior of the hydrogen plant.

4.1.1 Influence of temperature on the electrolysis system

For the influence of the temperature on the electrolysis system, only data from the 5 bar stack pressure scenario are reported, but for other pressures investigated, the results have similar behavior.

Figure 39 demonstrates that when the temperature increases the same current density generates lower hydrogen flow rate. That can be explained by the fact that greater temperatures result to lower faraday efficiency. That is something that was expected from the theory (Figure 18 B) because greater temperatures result to lower resistance and higher parasitic current losses.

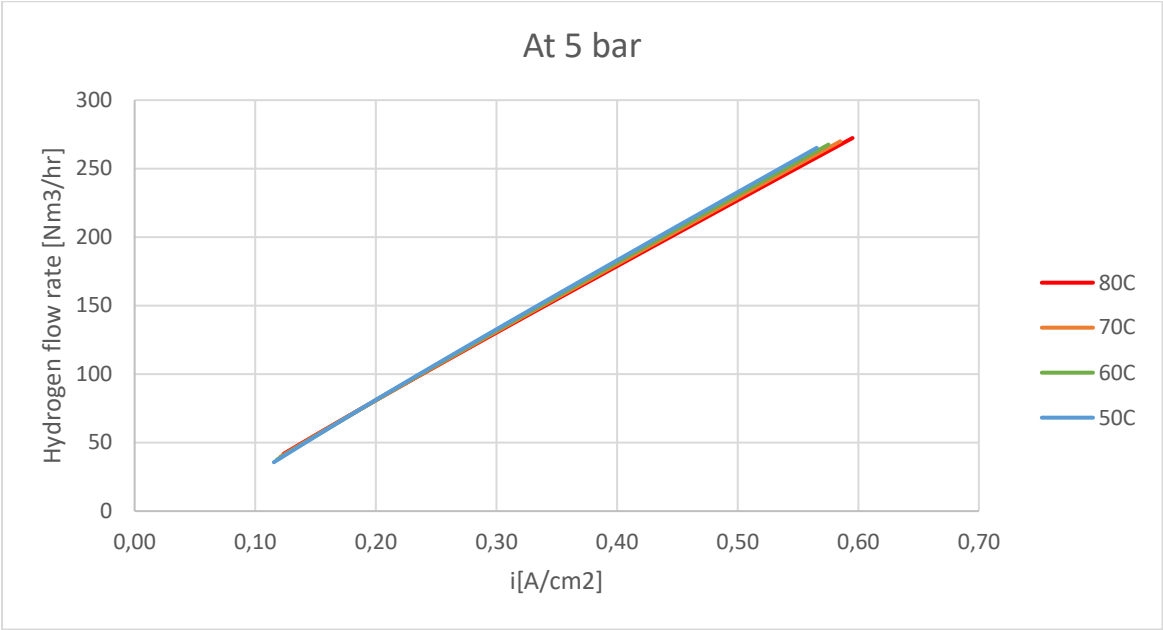

Figure 39: Hydrogen flow rate at 5 bar versus stack temperature and current density.

Although hydrogen flow rate for a specific current density is higher when the temperature is lower, that is not the case for specific power input. Figure 40 illustrates that for a specific power input, higher temperature leads to greater hydrogen flow rate.

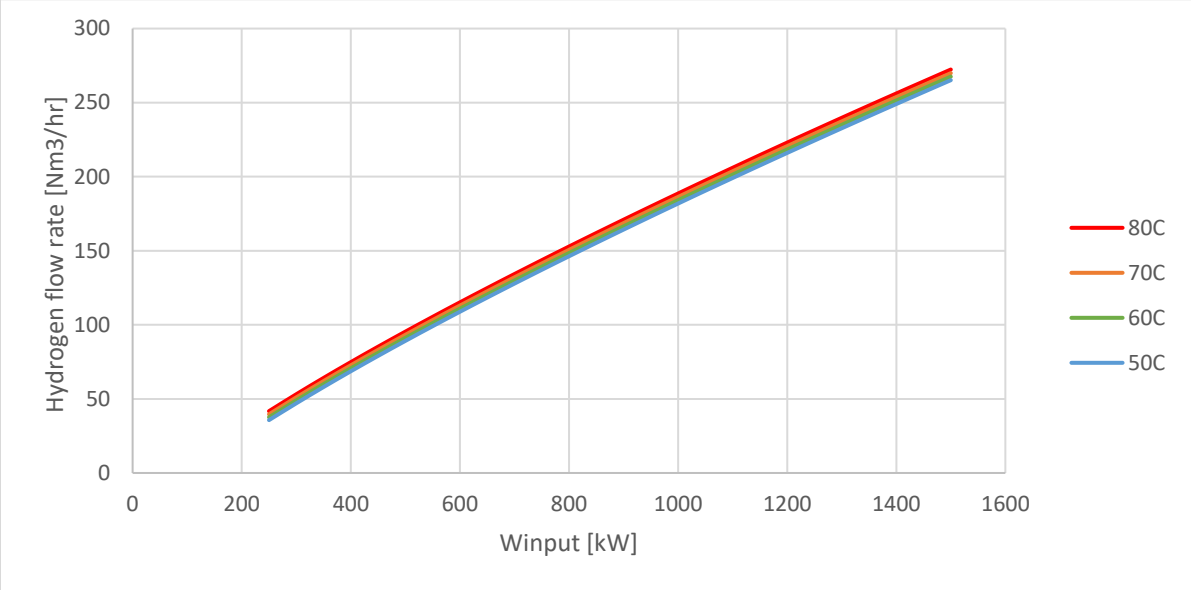

Figure 40:Hydrogen flow rate at 5 bar versus power input and stack inlet temperature.

On the other hand, Figure 41 shows that higher stack inlet temperatures lead to higher portions of hydrogen immigrated to the anode, which can be explained by the fact that diffusion and gas migration increases when the temperature increases. The phenomena that are responsible for the hydrogen migration are not connected to the electrolyser load (current density), meaning that when the produced gases are less during lower loads the portion of impurities is bigger, which is also visible in the Figure 41.

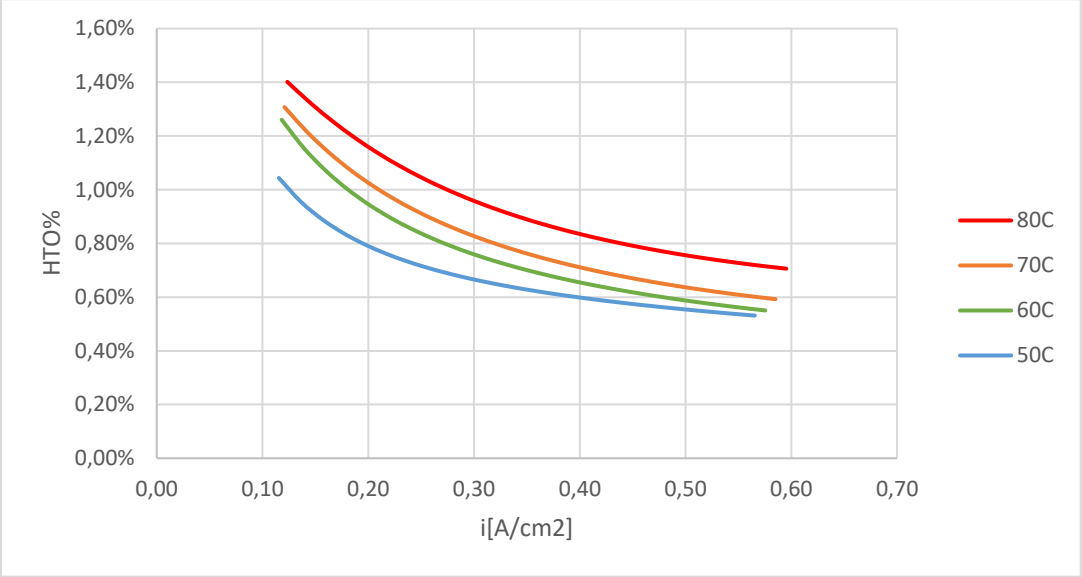

Figure 41: Hydrogen to oxygen percentage (HTO) at 5 bar versus stack inlet temperature and current density.

Next, Figure 42 shows how the different overpotentials and the cell voltage varies through different loads and temperatures. From the theory (Table 4) it is known that concentration overpotentials are also important but at higher current densities, and for that reason they were not included in the equation (29) that models the cell voltage. Higher temperatures produce lower activation overpotentials due to faster electrochemical reactions, while low ohmic overpotentials for every temperature have been succeed due to increased electrolyte conductivity (35% w/w KOH). Overall lower loads and higher temperatures lead to decreased cell potentials which contracts with the theory (Figure 18 A).

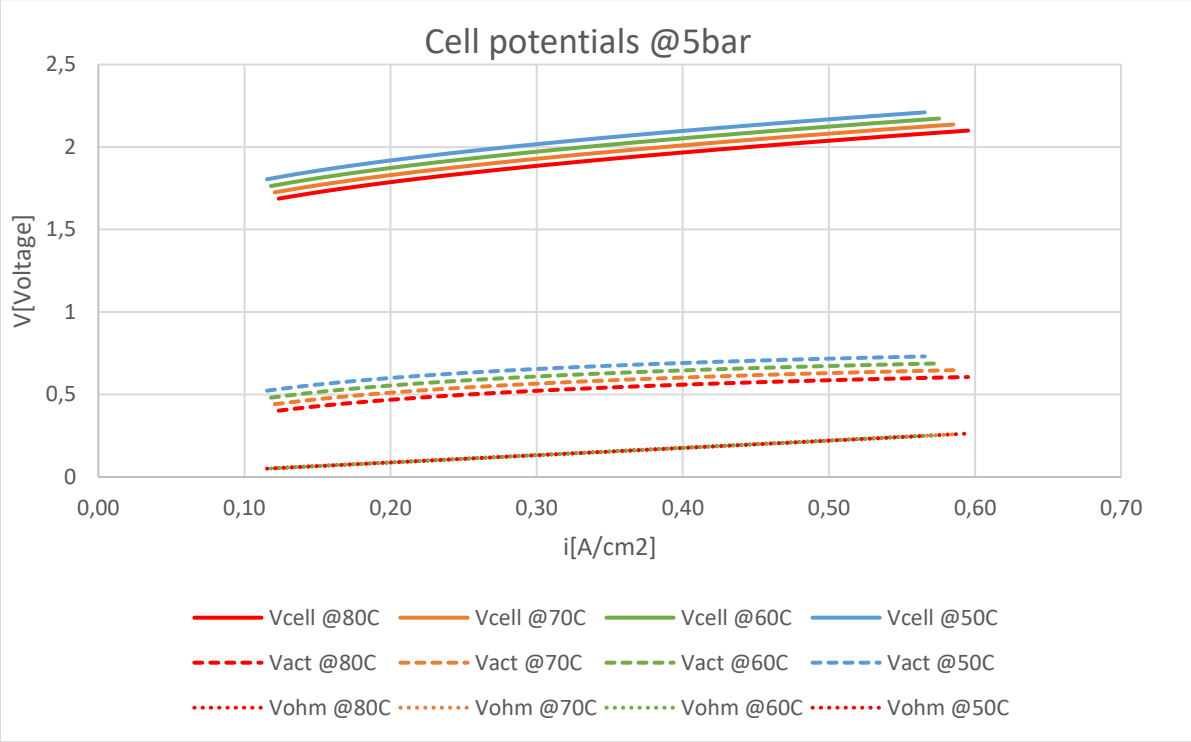

Figure 42: Ohmic, Activation and cell potentials versus load and stack inlet temperature.

The trends that were observed before for the hydrogen flow rate and the cell potential are illustrated in the Figure 43 as well were the voltage (etav-η_V) and the faraday efficiency (etaf-η_F) for different temperatures and loads are seen. It is also observed that the overall efficiency (e_{tot}-η_{tot}, see equation (19)) increases with higher temperature, while it increases for low loads, it then gets a pick and then decrease with a small rate.

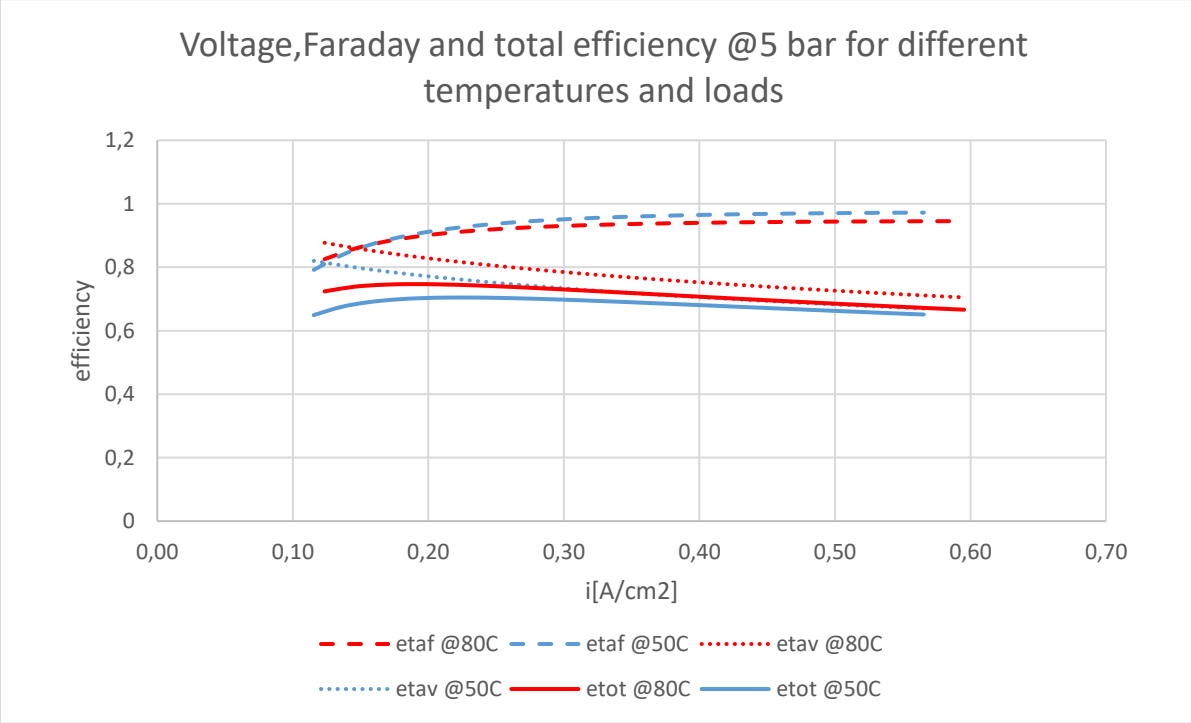

Figure 43: Voltage (etav), Faraday (etaf) and total (etaf) efficiency at 5 bar versus stack inlet temperature and load.

The previous efficiency refers to the efficiency of the electrolysis reaction but there is also the stack efficiency and the system efficiency that follow similar trends and are defined from the following equations

$$\eta_{stack} = \frac{\dot{m}_{H2} * LHV_{H2}}{\dot{W}_{electrical,stack,input}} \quad (41)$$

$$\eta_{system} = \frac{\dot{m}_{H2} * LHV_{H2}}{\dot{W}_{electrical,system,input}} \quad (42)$$

Where:

$$\dot{W}_{electrical,system,input} = \dot{W}_{electrical,stack,input} + \dot{W}_{fan} + \dot{W}_{comps} + \dot{W}_{pumps} \quad (43)$$

The following Figure 44 illustrates the stack efficiency for different current densities and pressures at stack pressure 5 bar. Higher temperature lead to higher stack efficiency while when the current density increases until around 0.2-0.4 A/cm^2 the stack efficiency increases and after that it decreases with a slower rate. The biggest stack efficiency is 57.4% at 80 Celsius inlet stack temperature, 5 bar stack pressure and 0.33 A/cm^2.

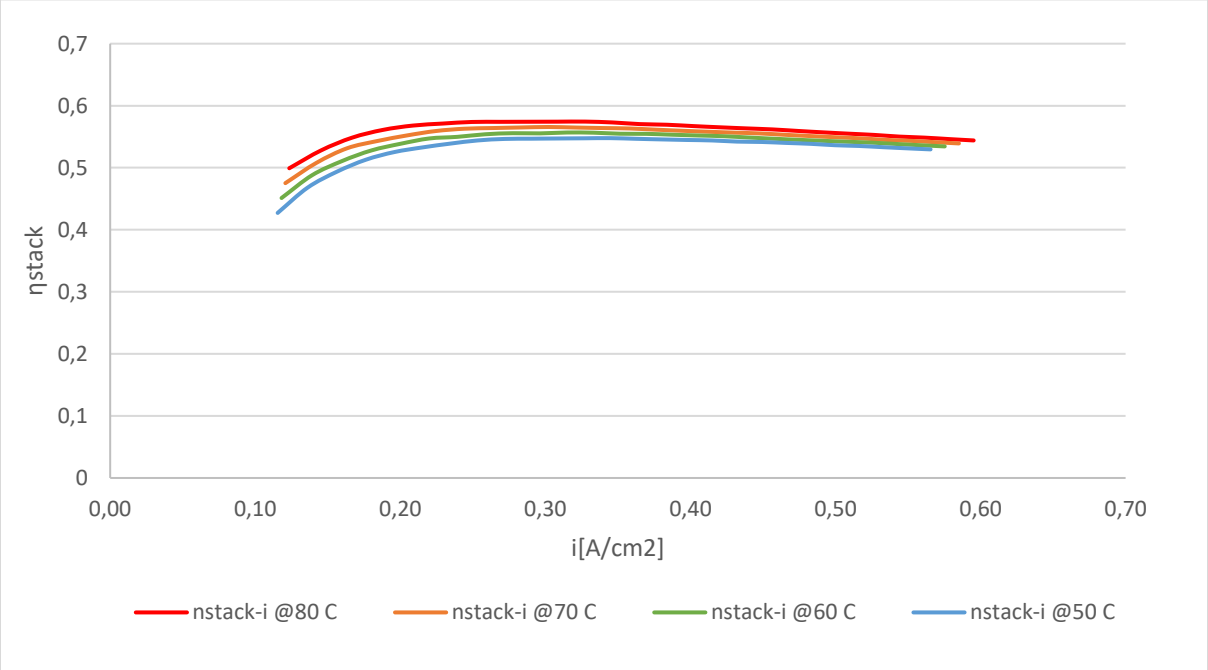

Figure 44: Stack efficiency at 5 bar stack pressure versus current density and stack inlet temperature.

Nevertheless, the system includes other components with electrical consumptions. The following Table 14 shows all the electrical consumptions at 80C, 5bar scenario and in order to better understand the influence of each component, a figure for this scenario at the maximum load is illustrated. W_{auxin} stands for the auxiliary consumptions of the fan the compressors and the pumps.

$$\dot{W}_{auxin} = \dot{W}_{fan} + \dot{W}_{comps} + \dot{W}_{pumps} \quad (44)$$

Table 14: Electrical consumptions at 80 C, 5 bar.

Wstack[kW]	Wfan[kW]	Wcomps[kW]	Wpumps[kW]	Wauxin[kW]	Wel,syst,input[Kw]
250	10.0	8.7	3.4	22.1	272.1
300	11.1	11.0	3.4	25.5	325.5
350	12.5	13.3	3.4	29.3	379.3
400	14.3	15.5	3.5	33.3	433.3
450	16.3	17.7	3.5	37.5	487.5
500	18.7	19.8	3.5	42.0	542.0
550	21.1	21.9	3.5	46.5	596.5
600	23.7	23.9	3.6	51.3	651.3
650	26.5	26.0	3.6	56.1	706.1
700	29.5	27.9	3.6	61.1	761.1
750	32.6	29.9	3.7	66.1	816.1
800	35.7	31.8	3.7	71.2	871.2
850	39.0	33.7	3.7	76.5	926.5
900	42.4	35.6	3.8	81.8	981.8
950	45.9	37.5	3.8	87.2	1037.2
1000	49.5	39.3	3.9	92.6	1092.6
1050	53.2	41.1	3.9	98.2	1148.2
1100	57.1	42.9	3.9	104.0	1204.0
1150	61.0	44.7	4.0	109.7	1259.7
1200	64.6	46.5	4.0	115.2	1315.2
1250	68.6	48.3	4.1	120.9	1370.9
1300	72.6	50.0	4.1	126.8	1426.8
1350	76.7	51.8	4.2	132.6	1482.6
1400	80.8	53.5	4.2	138.5	1538.5
1450	85.0	55.2	4.3	144.5	1594.5
1500	89.3	56.9	4.3	150.5	1650.5

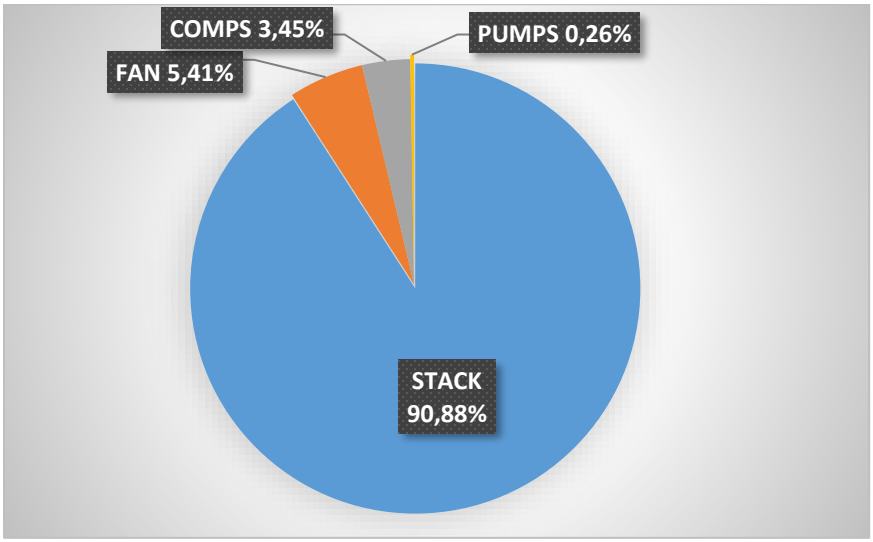

Figure 45: Electrical consumptions at 80 Celsius, 5 bar and maximum load

To better understand how temperature influence electrical consumptions Figure 46 illustrates electrical consumptions at 80 and 60 Celsius at 5 bar for different loads. It is understood that lower temperatures influence the fan and demand higher electrical consumptions and for that reason lower temperatures needs greater electrical input.

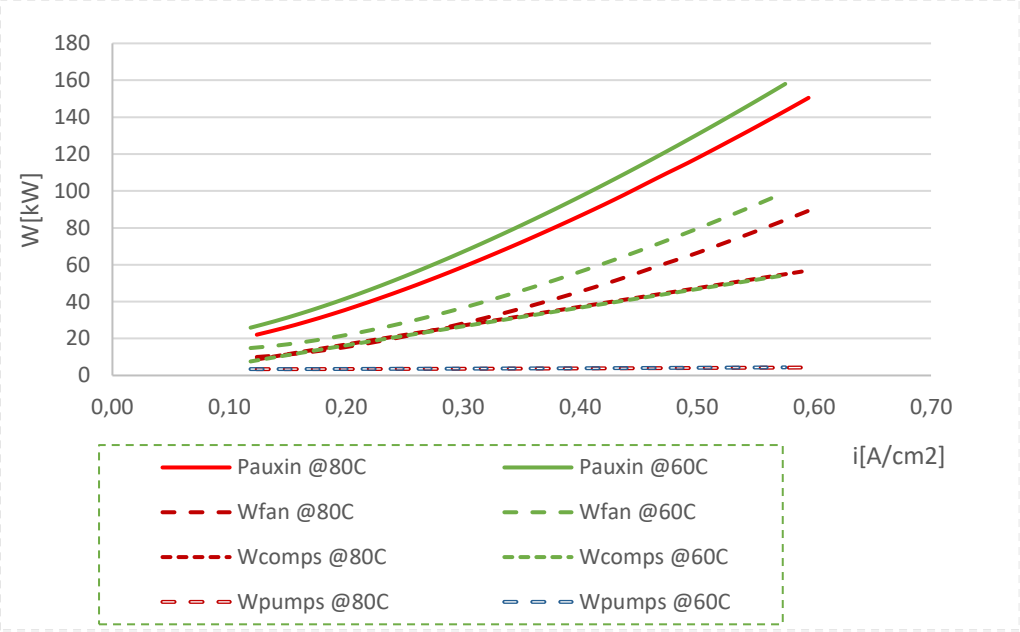

Figure 46: Electrical consumptions at 5 bar versus stack temperature and load.

Figure 47 shows how the system efficiency and the specific consumption changes at 5 bar for different temperatures and loads. The specific consumption is defined by the following equation:

$$Spec.cons[\frac{kWhr}{Nm^3}] = \frac{\dot{W}_{electrical,system,input}[kW]}{\dot{V}_{H2}[\frac{Nm^3}{hr}]} \quad (45)$$

It is shown that when the specific consumption is at the lowest that system efficiency is at the maximum 54.9% while it is spotted once again at 80 Celsius inlet stack temperature, 5 bar stack pressure and 0.33 A/cm^2 current density.

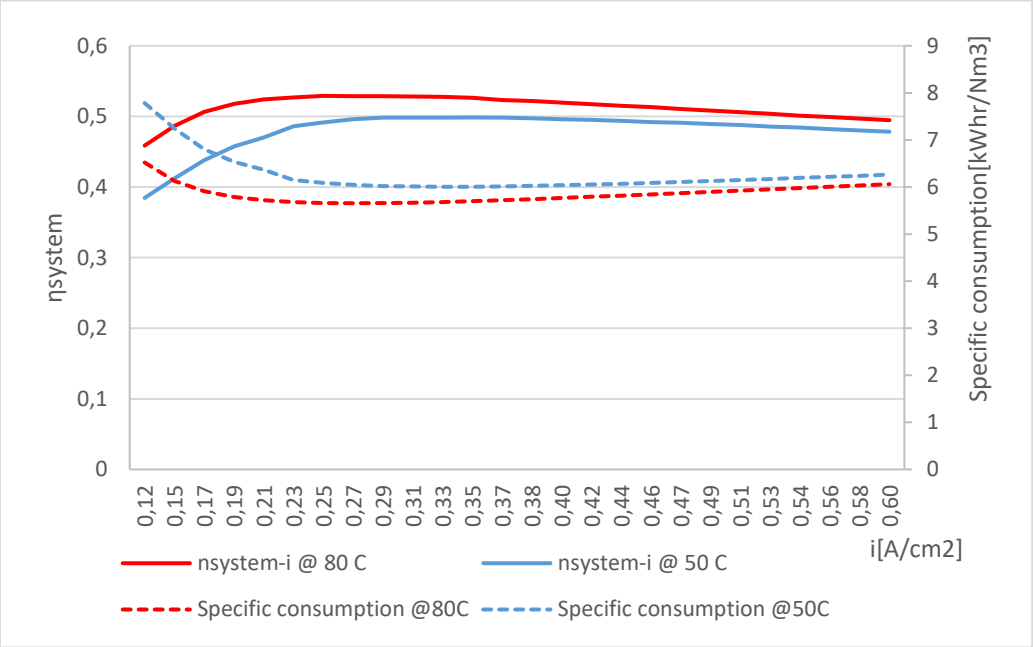

Figure 47: System efficiency and specific consumption versus stack temperature and load at 5bar.

4.1.2 Influence of pressure on the electrolysis system

In order to study the influence of the pressure on the function of the system, the data from the three different stack pressures 5, 7 and 10 bars and for 70 Celsius inlet stack temperature were studied and some figures were extracted. Overall smaller pressures lead to greater efficiencies and hydrogen production.

On the chapter 3.1.3 we saw that pressure does not influence the hydrogen quantity that exits the stack but that is not the case for the system analysis because the way gas-liquid

separator was modeled influence the hydrogen that returns to the stack from the cathode. For higher pressures more hydrogen returns to the stack in the liquid phase and less hydrogen leads to the purification system. That is something that is illustrated on the Figure 48 along with the influence of pressure on the HTO. Lower pressure result to lower HTO because less gas moves from the cathode to the anode inside the cell due to diffusion.

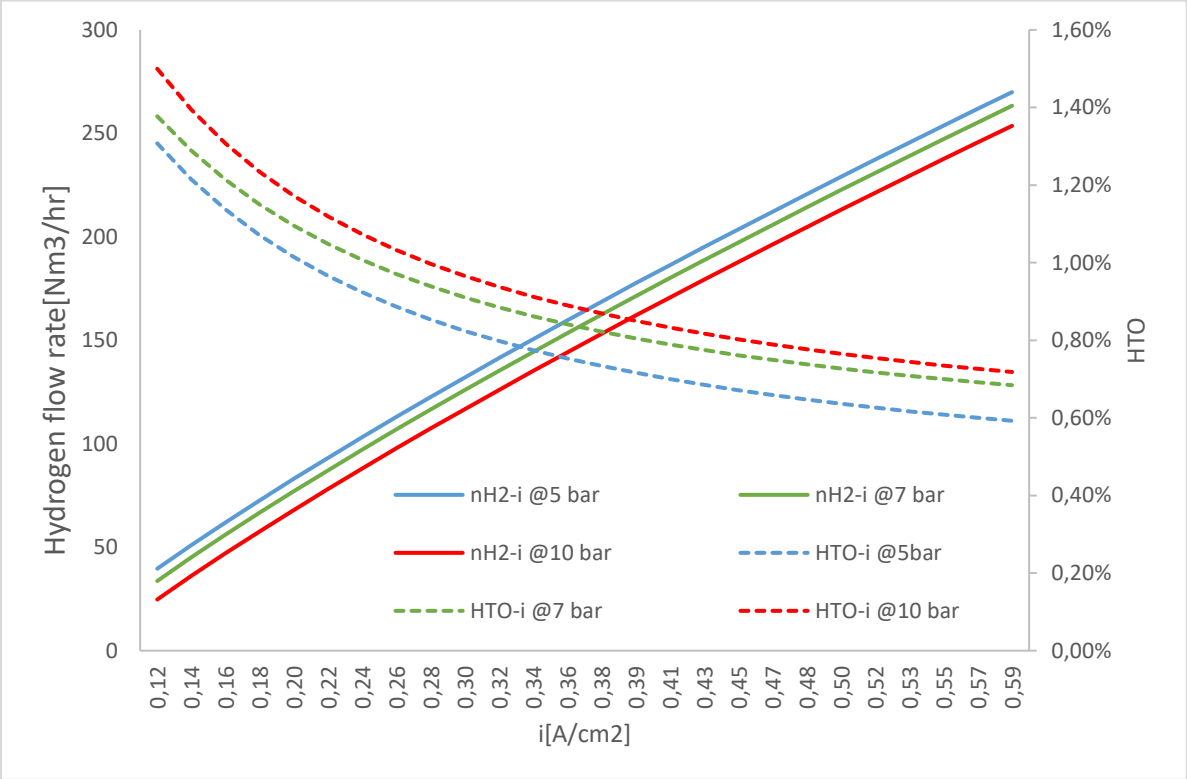

Figure 48: Hydrogen flow rate and HTO versus stack pressure and load for 70 Celsius inlet stack temperature.

Next Figure 49 shows how the cell voltage, activation and ohmic overpotentials change for different stack pressures and loads. It is shown that there is no perceptible influence, although theoretically ohmic overpotentials increase slightly with pressure [48].

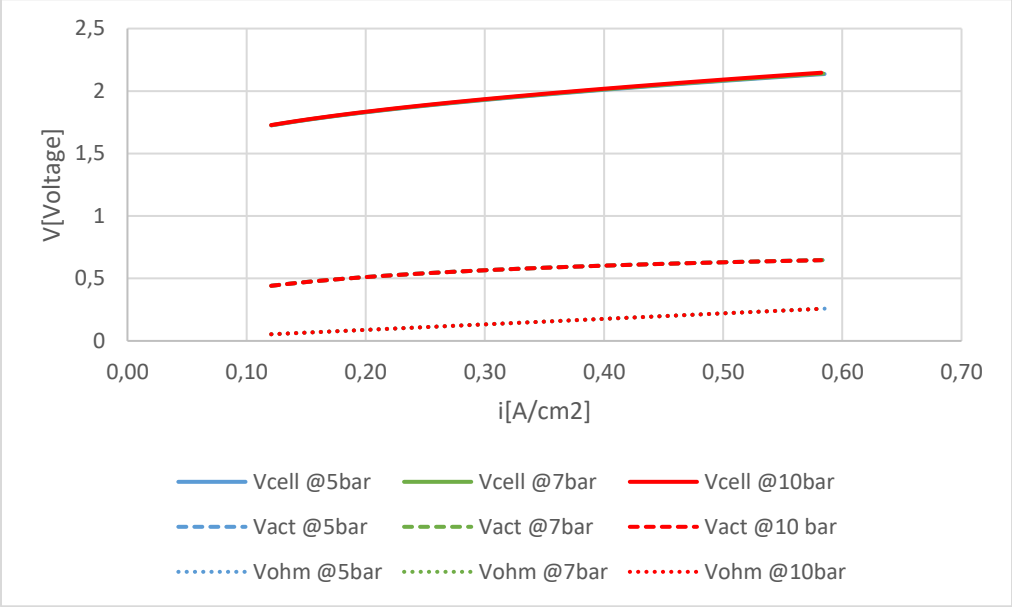

Figure 49: Cell voltage, activation and ohmic overpotentials at 70C inlet temperature verus stack pressure and load.

Since cell voltage and hydrogen produced on the cathode does not change with pressure the following trends on the Figure 50, where faraday, voltage and total efficiency at 70 C for different pressures are displayed, were expected.

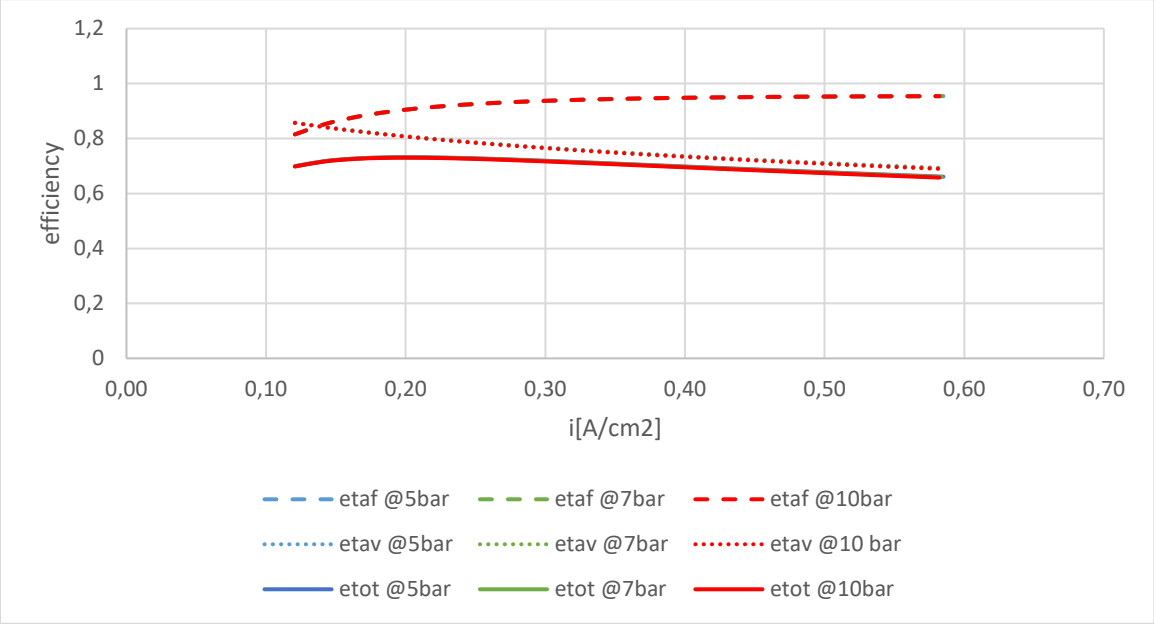

Figure 50: Faraday(etaf), voltage(etav) and total efficiency(etot) at 70C inlet temperature versus stack pressure and load.

Figure 51 demonstrates that stack efficiency decreases when the stack pressure increases as expected from Figure 48.

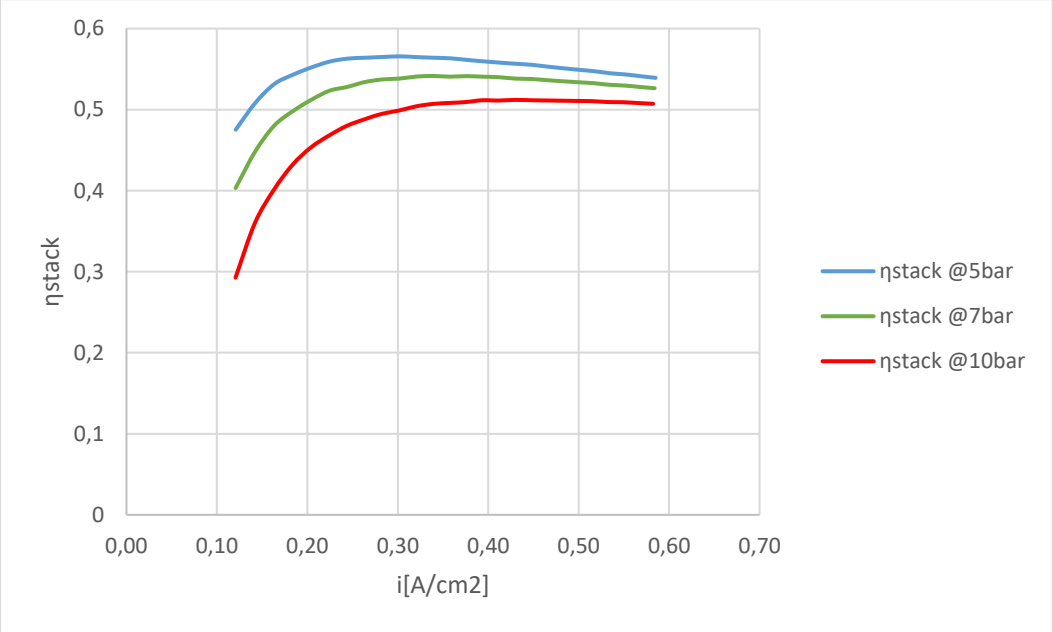

Figure 51: Stack efficiency at 70C inlet stack temperature versus stack pressure and load.

Figure 52 illustrates the electrical consumptions at 5 and 10 bar stack pressure. Pumps consumption does not change with pressure. Bigger stack pressure leads to lower compressor consumptions since the initial pressure of the first compressor increases and less work needs to be applied. On the other hand, bigger stack pressure seems to demand more consumption on the fan. From these two counterbalanced trends the influence from the compressor lead to lower total auxiliary consumptions for higher stack pressure. Nevertheless, the influence of the exported hydrogen production is greater than the auxiliary consumptions and lower pressure achieve greater system efficiency. System efficiency along with the specific consumptions at different pressures are shown on the Figure 53.

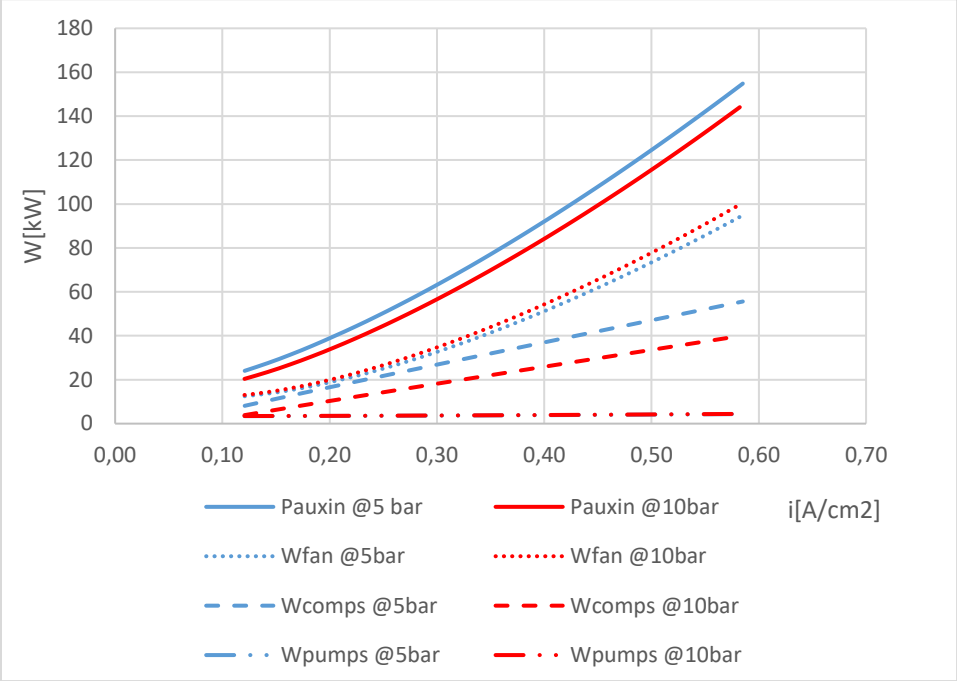

Figure 52: Electrical consumptions for 70 C inlet stack temperature versus stack pressure and load.

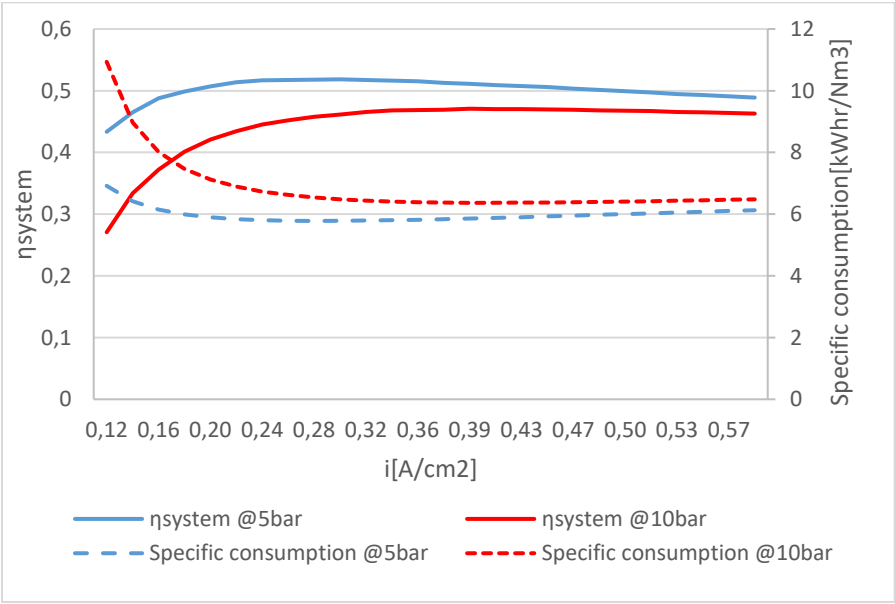

Figure 53: System efficiency and specific consumption versus stack pressure and load at 70C inlet stack temperature.

4.1.3 Combined influence of temperature and pressure on the electrolysis system

At this point it seems useful to display some charts that sums up the influence of the temperature and the pressure on the system.

Figure 54 displays how the auxiliary electricity consumptions varies with stack inlet temperature and stack pressure. Pumps consumption stay constant with temperature and pressure, compressor work decreases for lower temperature and higher pressure but consumptions from the fan decrease when temperature increase and when and the pressure decrease. All those trends combined lead to the total auxiliary electrical consumptions being decreased when stack inlet temperature and pressure increases.

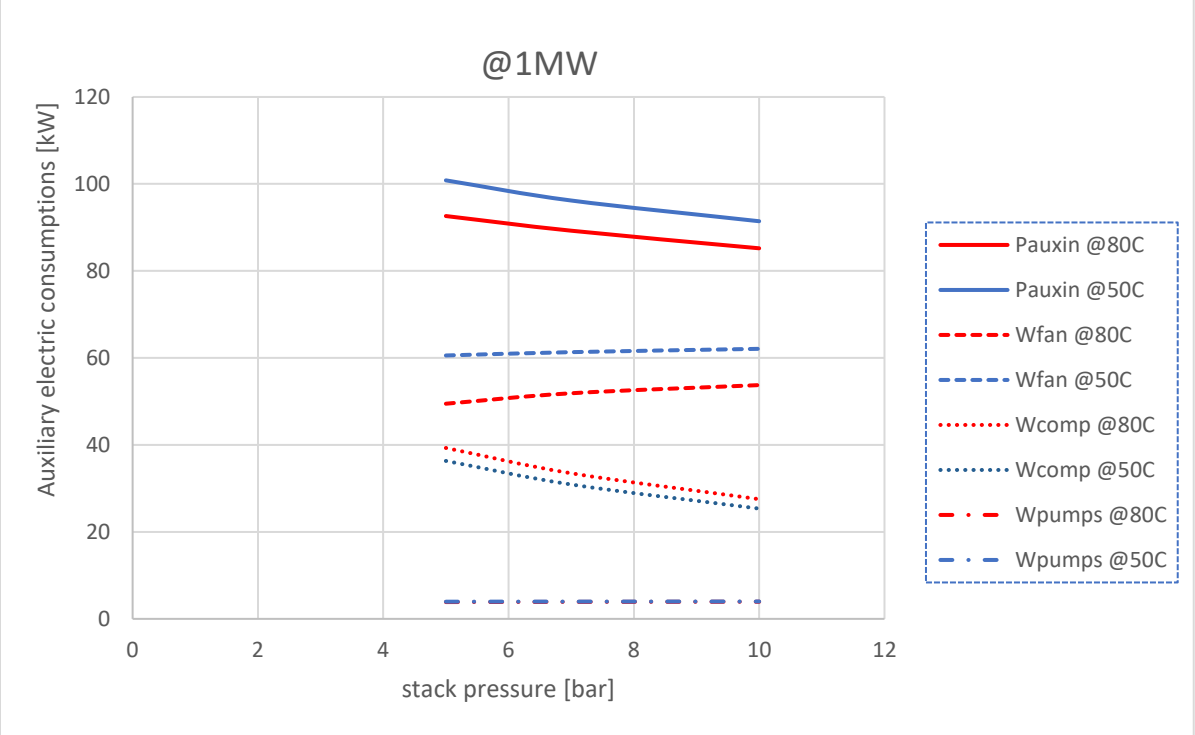

Figure 54: Electricity consumptions versus stack pressure and stack inlet temperature at 1MW.

Nevertheless, Figure 55 illustrates that hydrogen production increases for lower pressures and higher stack inlet temperatures and that trend is more powerful for the operation of the whole system leading to better system efficiency for lower pressures and higher stack inlet temperatures. This conclusion is expressed at Figure 56 and Figure 57 in different ways. In Figure 57 power output is defined through the following equation:

$$P_{H2,thermal} = \dot{m}_{H2} * LHV_{H2} \quad (46)$$

Figure 56 illustrate that when inlet temperature increases, and pressure decreases the thermal power output of hydrogen increases and specific consumptions decreases and Figure 57 shows that the system efficiency increases for higher inlet stack temperatures and lower pressures.

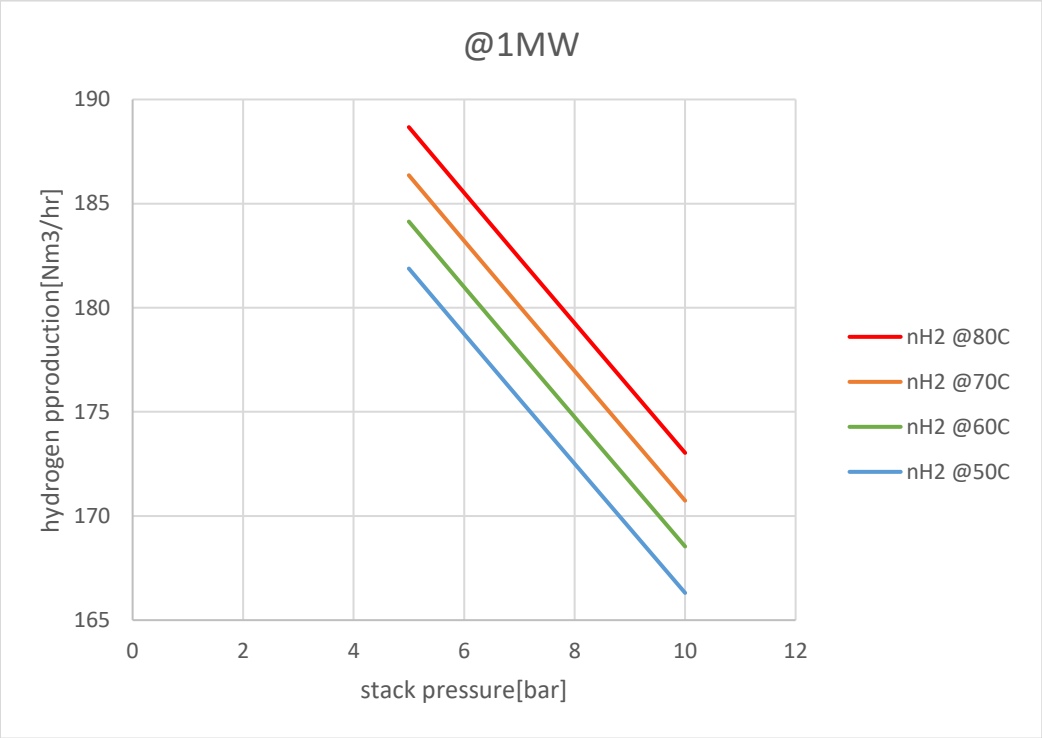

Figure 55: Hydrogen production versus stack pressure and inlet stack temperature.

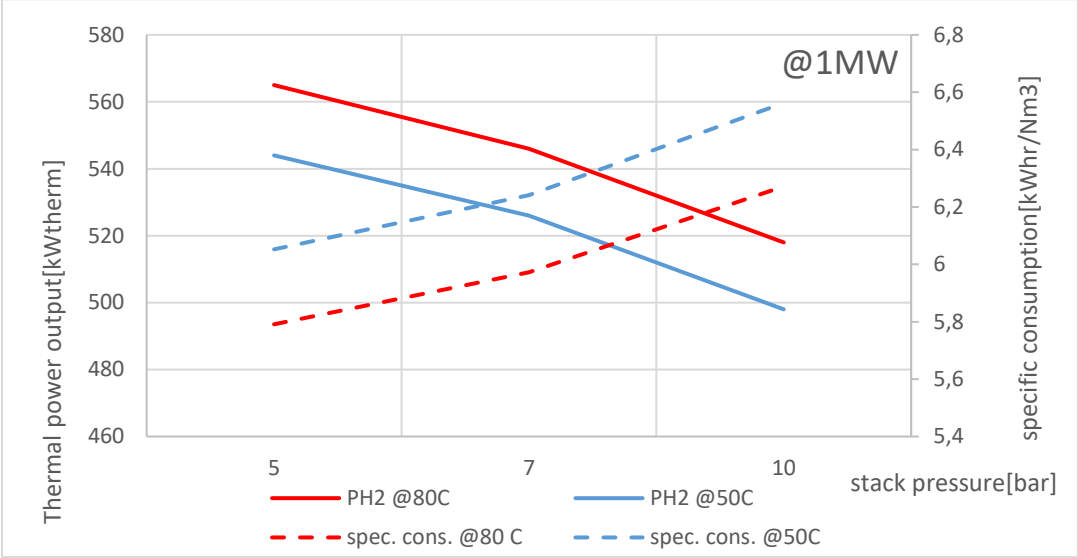

Figure 56: Power output and specific consumptions versus stack pressure and inlet stack temperature.

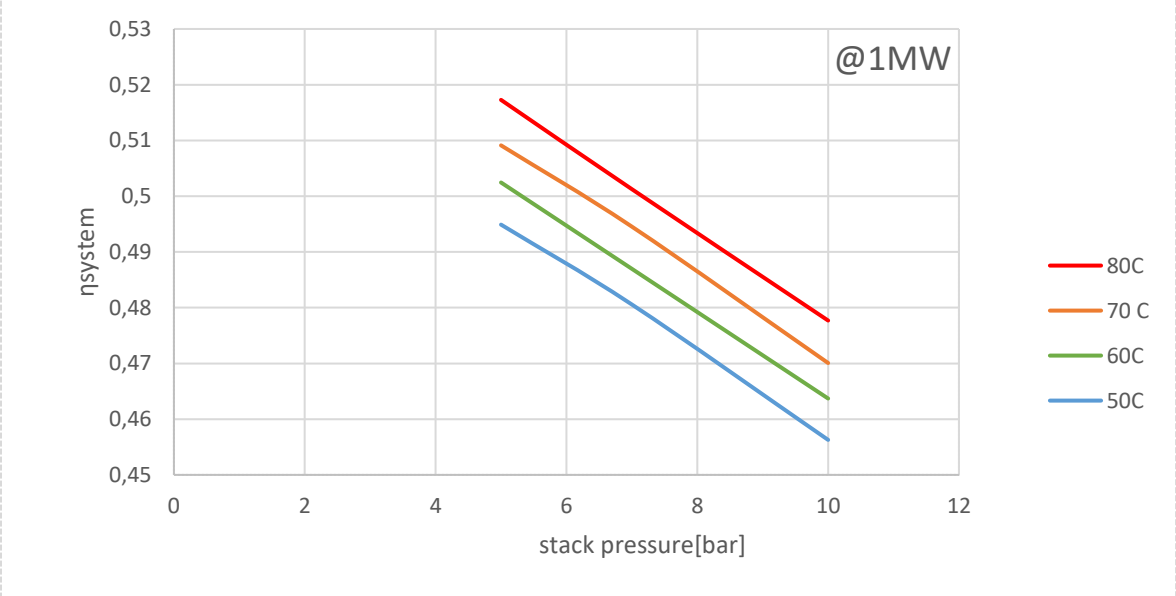

Figure 57: The system efficiency increases for lower pressures and higher stack inlet temperatures.

4.2 Tecno-economic analysis for the LCOH calculation

On this subchapter a simple techno-economic analysis takes place, in order for the LCOH of the simulated electrolyser system to be calculated. The LCOH is calculated for three different sources of electricity solar photovoltaic PV (Scenario 1), onshore wind park (Scenario 2) and grid connected (Scenario 3) at best (80C, 5bar) and worst (50C, 10bar) operational parameters in present time (2024) and at best operational parameters (80C, 5bar) for the renewable source scenarios 1 and 2 in the case of construction in 2030. Finally, the LCOH was calculated also for the third scenario of grid connection, at the best operational parameters for half of the operating time to secure the minimum prices from the grid in off-peak hours. In total nine different LCOH calculations where deployed. For the green hydrogen production, Scenarios 1 and 2, the power of the renewable energy park that is directed coupled to the electrolyser system is assumed to be equal the electrolyser power, in order for the capacity factor of the electrolyser to be around 20% for the 1st Scenario and 35% for the 2nd [39]. For the first two scenarios, in order to calculate the total hydrogen production, the average hydrogen production from all the loads is assumed. For the third scenario of grid connected system it is assumed that the electrolyser works 8000 hours (CF=91,32%) or 4000 hours (CF=45,66%) yearly. The lifetime of each system is assumed to be 25 years.

For the calculation of the LCOH the following formula was used:

$$LCOH = \frac{CAPEX[€] * Annuity + OPEX[\frac{€}{year}] + WaterCost[\frac{€}{year}] + LCOE[\frac{€}{year}]}{H_{2,production}} \quad (47)$$

Where

$$Annuity = \frac{(1+i)^n * i}{(1+i)^n - 1} \quad (48)$$

i is the discount ratio and it is assumed to be 5%, and n is the lifetime of the system 25 years.

- **Stack Costs**

For the CAPEX of the present time and the 2030 construction scenario the following equations were used [58].

$$CAPEX_{stack,2024} = 600\left[\frac{€}{kW}\right] * 1500[kW] = 900000\ € \quad (49)$$

$$CAPEX_{stack,2030} = 400\left[\frac{€}{kW}\right] * 1500[kW] = 600000\ € \quad (50)$$

The OPEX was calculated as 4% of the CAPEX [58].

The stack needs replacement every 80000 working hours due to degradation and it adds an 30% of the CAPEX cost [59]. Only the third scenario of grid connected electrolyser surpass the 80000 working hours.

- **Compressor Costs**

For the calculation of the compressors costs the following equation was used, and because compressors are a mature technology, it is assumed that their costs are not going to decrease any further during the following years [60].

$$CAPEX_{comp} = 4948 * W_{stack}[kW]^{0.66} = 4948 * 1500^{0.66} = 617518€ \quad (51)$$

The compressors OPEX was assumed to be 2% of the CAPEX [60].

- **Water Costs**

The cost of the water is calculated as 3.8 €/m^3 [59].

- **Storage**

For the storage it is assumed that a total capacity of 1000 kg H_2 is available, since similar capacity to nominal power ratios are being used in such systems [59]. Also a capacity of 1000 kg H_2 would ensure a two days nominal hydrogen production, since 24.5 kg/hr is the nominal hydrogen production, in the case electrolyser could not work due to luck or renewable dynamic (no wind or cloudy day) or maintenance activities. The CAPEX cost of the storage is calculated as 400 €/kg and the OPEX is 3% of the CAPEX [59].

- **Electricity cost (LCOE)**

For the present time calculations, the primary energy costs assumptions are the following:

$LCOE_{PV}$=0.045 €/kWhr [61],

$LCOE_{onshorewind}$=0.031 €/kWhr [61],

$LCOE_{grid}$=0.16176 €/kWhr ,for this value the average European electricity price with all taxes and levies included for non-household consumers with energy consumption 2000-19999

MWhr for the period of the second semester of 2018 till first semester of 2023 was assumed [62]. For the half operating hours case that work in off-peak hours, when the wholesale electricity prices are lowest, an 30% reduction at the electricity prices was assumed that result to a $LCOE_{grid,CF=45.66}$=0.1132 €/kWhr.

For the 2030 calculations, the primary energy costs assumptions are the following:

$LCOE_{PV}$= $LCOE_{grid}$=0.023€/kWhr [63]

The previous assumptions lead to the calculation of the costs that are visible on the following Table 15.

Table 15: Economical parameters for the three different scenarios.

BOP stands for Best Operational Parameters (80C,5bar) and WOP for Worst Operational Parameters (50C,10bar).

Scenario		**1 (PV conn.)**			**2 (Wind conn.)**			**3 (Grid conn.)**			***Sources***
BOP/WOP,present time/2030		**BOP, present time**	**WOP present time**	**BOP 2030**	**BOP, present time**	**WOP present time**	**BOP 2030**	**BOP, present time**	**WOP present time**	**BOP, present time half CF**	
Hydrogen production	***kg/hr***	14,7	12,7	14,7	14,7	12,7	14,7	24,5	12,7	24,5	
CF	***%***	20			35			91,32		45,66	
CAPEXstack	***€***	900000		600000	900000		600000	900000			[58]
OPEXstack	***€/year***	36000	36000	24000	36000	36000	24000	36000			[58]
Stack replacement every 80k hours	***€***	-			-			270000			[59]
CAPEXcomp	***€***	617518									[60]
OPEXcomp	***€/year***	12350									[60]
CAPEXstorage	***€***	400000									[59]
OPEXstorage	***€/year***	12000									[59]
Water Cost	***€/year***	1135			1987			5183		2592	[59]
LCOE	***€/kWhr***	0,045		0,023	0,033		0,023	0,1618		0,1132	[61], [62], [63]

To better understand how much each cost affects the total cost of the system, the following charts for each scenario at the best operational parameters, 2024 construction, are illustrated

(Figure 58-Figure 60). Stack is responsible for the 41.1-47% of the capital costs, compressor is the next with a 28.2-32.2% influence and finally the storage is responsible for the 18.2-20.7% of the capital costs. The stack replacement after 80000 hours adds another 12.3% to the capital costs to the third scenario only. For the operational costs electricity plays the most important role (55.1%, 60.8%, 97% for the first, second and third scenario respectively) while stack (26.3%, 22.6%, 1.6%), compressor (9%, 7.8%, 0.56%), storage (8.8%, 7.5%, 0.55%) and finally water purchases (0.83%, 1.3%, 0.24%) follows.

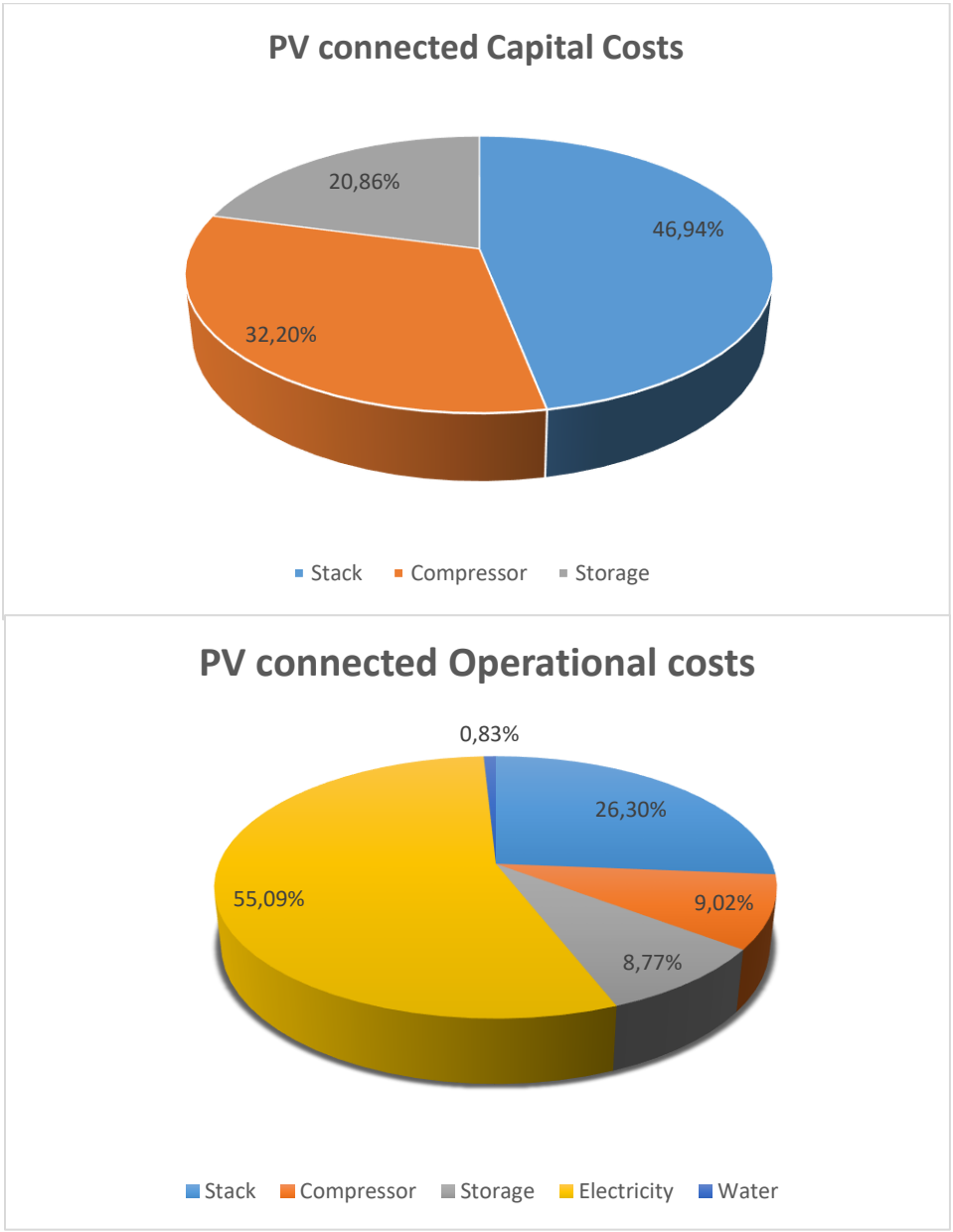

Figure 58: Capital and operational costs at best operating parameters for 2024 in the first scenario of PV connection.

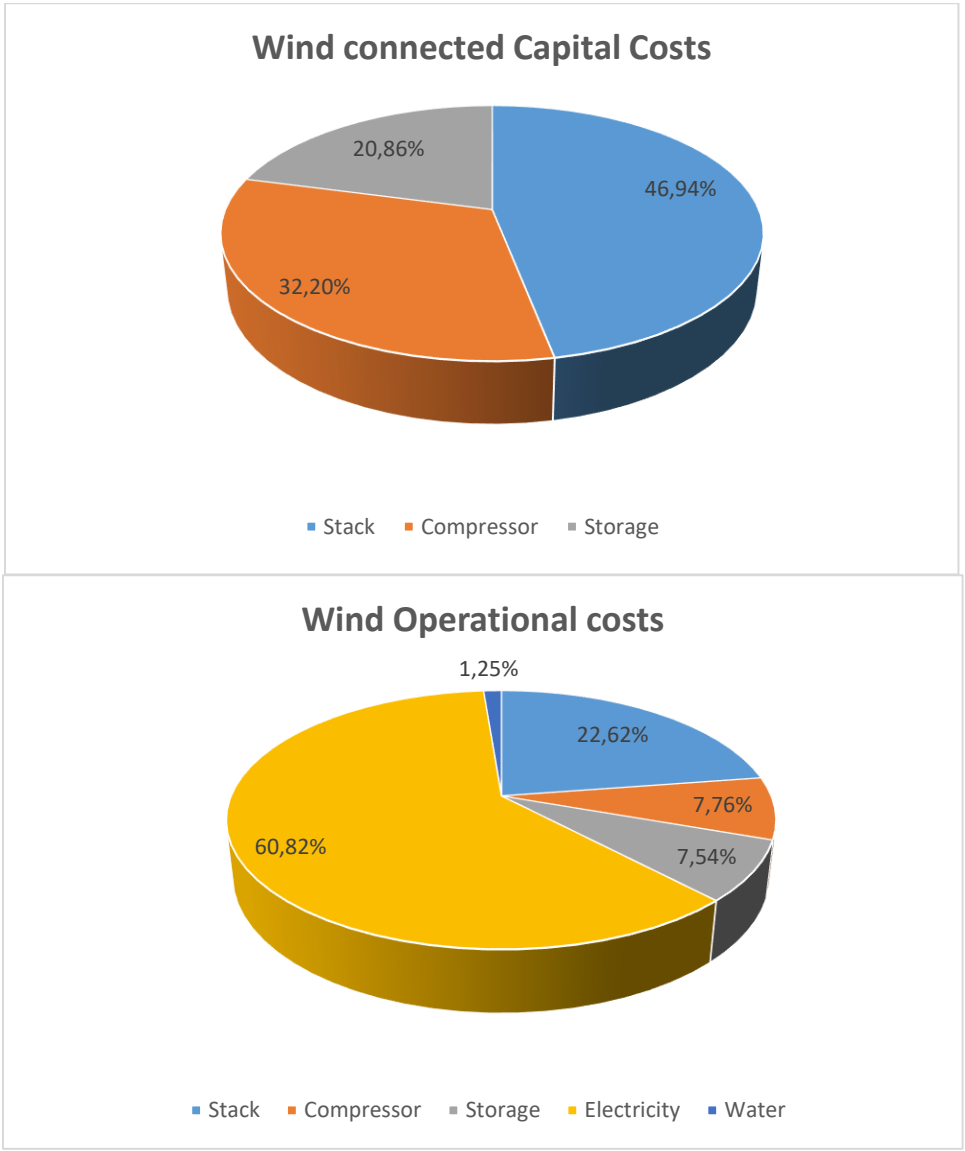

Figure 59: Capital and operational costs at best operating parameters for 2024 in the second scenario of wind turbine connection.

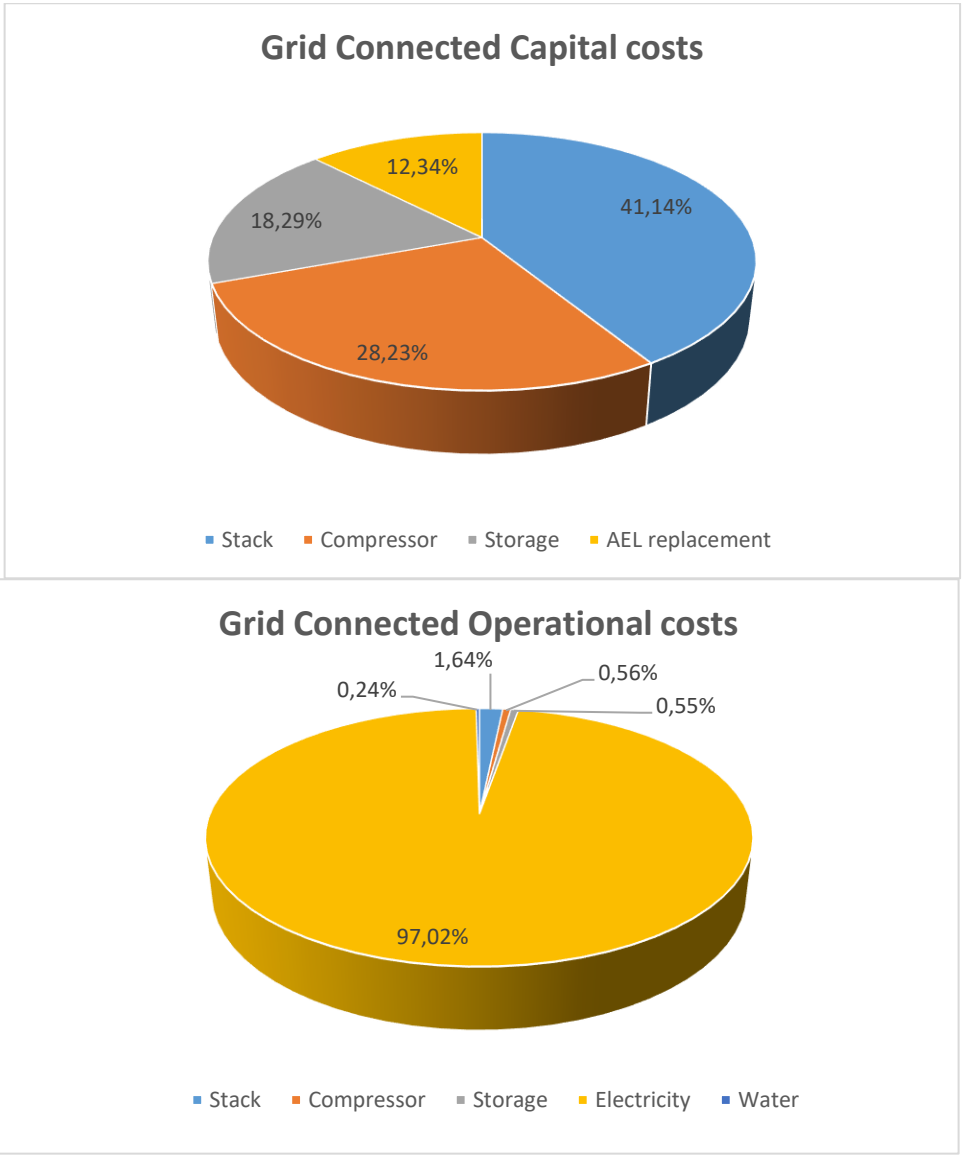

Figure 60: Capital and operational costs at best operating parameters and CF=91,32% for 2024 in the third scenario of grid connection.

Then the calculation of the LCOH is done for the nine different circumstances. The results are shown on the following Table 16. The minimum primary source price comes from the wind turbine scenario and for the best operating parameter at the 2024 calculation it results to the minimum LCOH of 6.6 €/kg. For the 2030 calculations, the primary source of PV and wind are equally low-cost, and for the wind turbine, that has higher capacity factor, the lowest LCOH of 5.2 €/kg is ensured. There is a decrease of 1.4-2.7€/kg for the 2030 scenarios compared to

2024, that is the result of the expected renewables LCOE further reduction and the cost reduction of the capital cost of the alkaline electrolyser. For the grid connection scenario, it is more efficient to work for less hours in order to secure lower electricity prices, although the impact of CAPEX on the LCOH for lower capacity factors is more intense. Finally, it is observed that working at the best operating parameters of 80C and 5 bar can decrease the LCOH from 1-1.7 €/kg, which is not neglected. It should be noted that the resulted levelized costs of hydrogen for each scenario are on the calculated regions from formal sources [39].

Table 16: LCOH of the three different scenarios.

BOP stands for Best Operational Parameters (80C,5bar) and WOP for Worst Operational Parameters (50C,10bar).

Scenario	BOP/WOP,present time/2030	tonnes of hydrogen/year	LCOH[€/kg]
1 (PV conn.)	BOP, present time	26	10,6
	WOP, present time	22	12,3
	BOP, 2030	26	7,9
2 (Wind conn.)	BOP, present time	45	6,6
	WOP, present time	39	7,6
	BOP, 2030	45	5,2
3 (Grid conn.)	BOP, present time	196	12
	WOP, present time	179	13,1
	BOP,present time half CF	98	9,8

To get a clearer picture of how the LCOH is structured for the different scenarios and cases the following Figure 61-Figure 63 are illustrated. For the first two scenarios of renewable connections the biggest influence comes from the initial capital expenditure. Next electricity expenses play a vital role with the operational expenditures following. Finally, water purchasers have the least influence on the final levelized cost. On the other hand, for the grid connection the most crucial role is played from the electricity and CAPEX, OPEX and water purchases follow on that order.

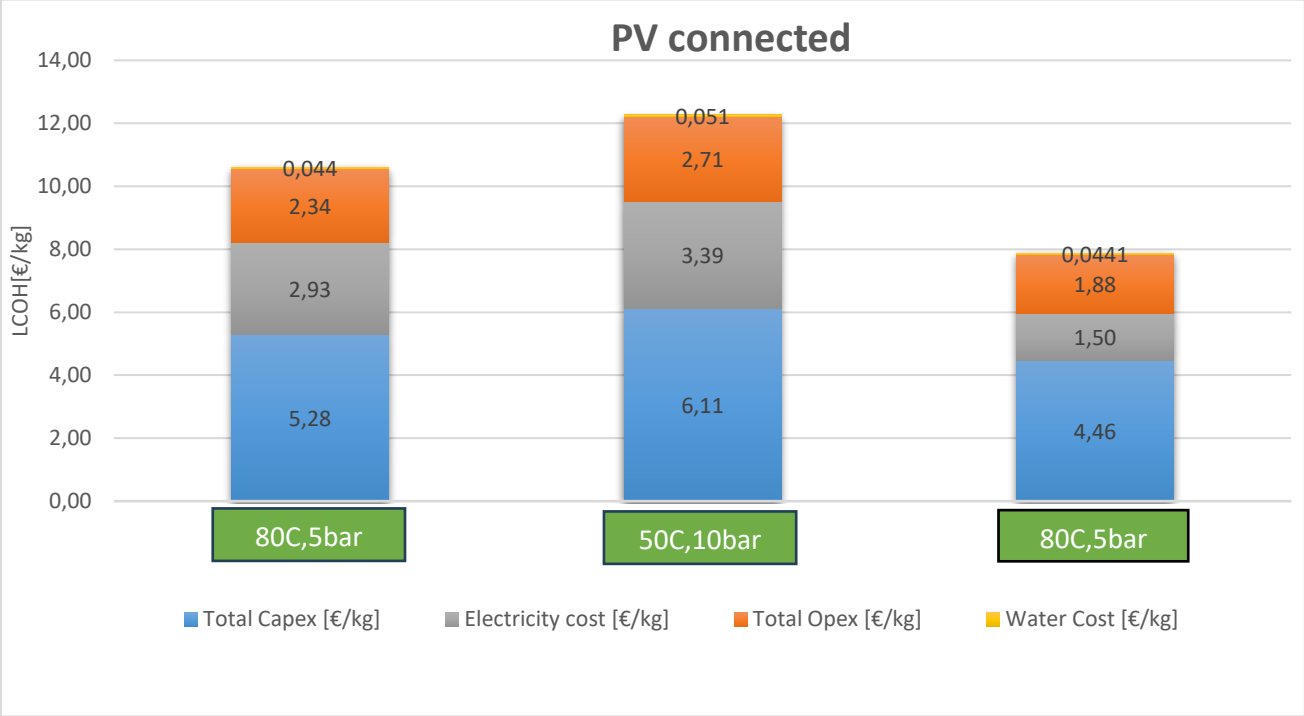

Figure 61: The LCOH for the first scenario of PV connection for the three different cases.

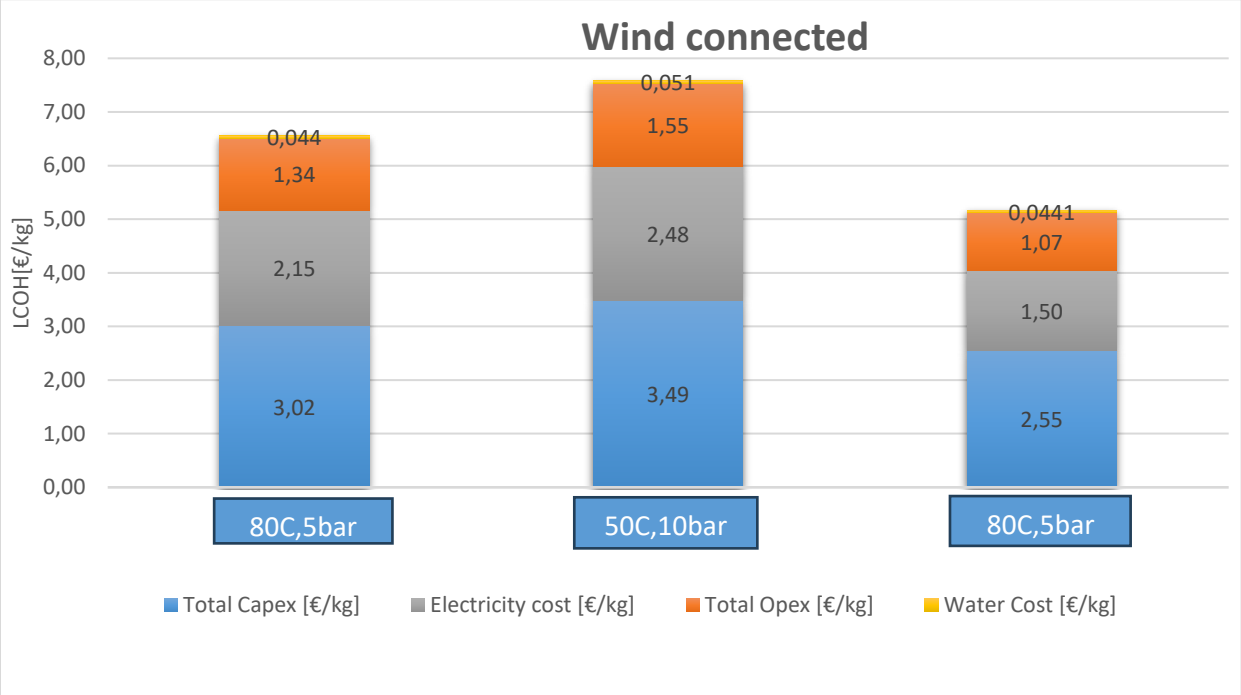

Figure 62: The LCOH for the second scenario of wind turbine connection for the three different cases.

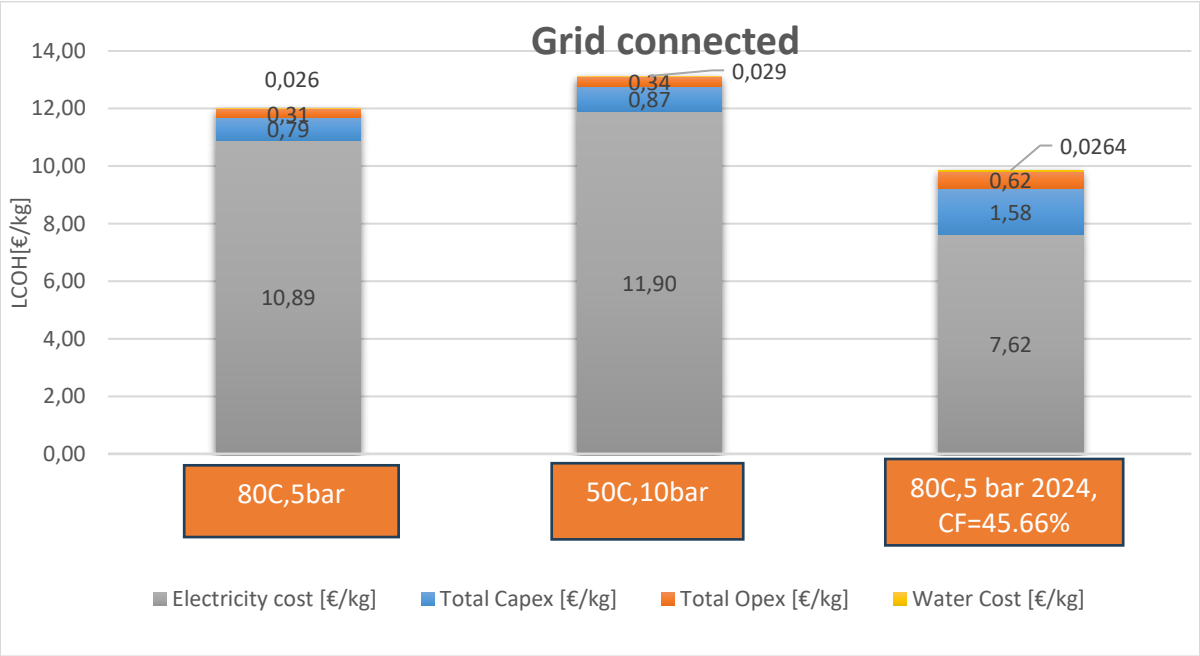

Figure 63: The LCOH for the third scenario of gird connection for the three different cases.

5. Conclusion and future work

5.1 Conclusion

Summarizing, hydrogen could play an important role on the forthcoming worldwide efforts of solving the climate change problem. Hydrogen can work as an energy battery that charges from the renewable energy when it surplus and gives back the energy on multiple hard to decarbonize sectors. As a fuel it has some big advantages such as the big higher heating value and the variety of ways to produce it on different methods and with different kind of primary sources, even with just water and green electricity making it a green fuel that could replace fossil fuels. Nevertheless, efficient ways to store it and move it from point A to point B or safety issues, are some of the most crucial challenges.

When hydrogen is made from water electrolysis the voltage applied to the cell should be greater than the reversible and the overvoltages and if thermal energy is not applied as well it should also be greater than the thermoneutral. Alkaline, SOEC, PEM and AEM are the most usual water electrolysis technologies with the first being the most mature and cheap but not as efficient as the others. Some other challenges with alkaline electrolysers are their corrosives and inability to work efficiently for high current densities (greater than 600 mA/cm^2). Hydrogen can be stored as solid, liquid or most usually as a gas in vessels reaching the 700 bar or in underground geological storage and even in already used pipelines pure or mixed with naturel gas.

Since alkaline water electrolysis could be used in a variety of projects in the near future, it is considered appropriate to develop detailed models that can predict important variables for different operating parameters such as load pressure and temperature. The use of Aspen Custom Modeler to develop a custom model for the stack seemed promising from the writer perspective. It can help for the development of very versatile and personalized components that can describe perfectly the behavior of the stack since Aspen Plus™ does not include components that simulate the water electrolysis. Equations (31)-(33) are the main part of the component development and have been made to perfectly simulate an 15 kW alkaline electrolysis system. If it was not for ACM a flowsheet in Aspen Plus™ that allows the interface with the current, voltage and the efficiencies would not be possible. Even though the validation of the stack with the original paper of Sanchez et al. [48] was successful, the validation of the developed 1.5 MW electrolysis system with a commercial alkaline electrolyser was not perfect since the efficiency and deionized water differ. For the simulation of the alkaline electrolyser apart from the stack two gas-liquid separators, the colling system, the purification system the deionized water, the pumps and the compression and storage components-streams were added. The colling system works with water as a refrigerator and includes two heat exchangers that cools down the returning form the anode and cathode

mixes. To close the loop of the colling system a fan is added that returns the refrigerator water at the initial 35 C. In the compression a two-stage compression system was added that works at an interstage pressure of $p_{opt} = \sqrt{p_i * p_f}$, that secures the least power compressor input, and produce hydrogen of 200 bar and 25 Celsius with the help of two heat exchangers. The inlet stack stream of 3800 kmol/hr is mainly KOH and H_2O with a 35 and 65% w/w respectively and some very small quantities of hydrogen and oxygen that returns from the anode and cathode.

To study the behavior of the modelled system 12 different scenarios for different stack pressures (5,7,10 bars) and inlet stack temperatures (50,60,70,80C) were solved. In each system to vary the load of the stack the electrical input was modified from 250 to 1500 kW and the results were transferred to the excel. Higher power input and stack inlet temperature lead to higher hydrogen flow rates (Figure 39), HTO increases for higher stack inlet temperatures and smaller loads (Figure 41), cell potentials increase with the load and decrease with the temperature (Figure 42), total efficiency η_{tot} of electrolysis reaction increase with stack inlet temperature (Figure 43), stack efficiency η_{stack} increases with stack inlet temperature and when the load changes it increase until it gets to the maximum and the decreases (Figure 44). The highest stack efficiency is 57.4% at 0.33 A/cm^2 (0.75 MW power iput) and 80C inlet stack temperature. Nevertheless, even though stack is responsible for the 90.88% of the electrical consumptions of the system, the fan, the compressors and the pumps consume power as well. Fans are responsible for the 5.41% of the total electrical consumptions, compressors are responsible for the 3.45% and pumps for the 0.26% (see Figure 45). Overall electrical consumptions decrease with the stack inlet temperature and increase with the load (Figure 46). The combination of stack efficiency and the auxiliary consumptions lead to the system efficiency η_{system} that increase with inlet stack temperature and when load increase it reach a maximum (the highest system efficiency Is 54.9% at 0.33 A/cm^2) and then it slowly decreases (Figure 47). Stack pressure does not really affect cell voltage and electrolysis reaction efficiency (Figure 49,Figure 50) but it affects hydrogen flow rate and HTO with highest pressures leading to lower hydrogen flow rates and higher HTO (Figure 48). The reason pressure influence hydrogen flow rate which results to affection of stack efficiency as well, is not the properties of the stack but the liquid gas separator and for lower stack pressure less hydrogen returns to the stack inlet after the cathode which result to greater efficiency (Figure 51). Although higher stack pressure leads to lower consumptions on the auxiliary consumptions (Figure 52), the influence of pressure on hydrogen flow rate is more powerful and overall system efficiency is higher for lower pressure (Figure 53). Overall, the modelled electrolysis system works better for lower stack pressures and higher stack inlet temperatures as Figure 55 demonstrates. Figure 55 can also work like an operating map which describes how the system efficiency can be kept constant. For example, if the current density at 10 bar and 70 Celsius gets higher than 0.40 A/cm^2, which result to the maximum efficiency

for those parameters, in order to maintain the efficiency, the pressure should decrease and or the stack inlet temperature should increase.
The techno-economic analysis lead to the calculation of the LCOH for different primary energy source, working operating parameters and construction year. The primary sources of PV, wind turbine and grid result to different capacity factors and electricity costs. The lowest LCOH, for the 2024 construction scenario at the best operational parameters, is 6.6 €/kg and comes from the wind turbine connection. Next grid connection with 4000 annual working hours result to 9.8 €/kg LCOH, PV connection leads to a similar 10.6 €/kg, while the worst scenario both from economically and environmentally perspective is the grid connection with 8000 annual working hours that result to 12 €/kg. If the system is worked instead of the best operating parameters of 5 bar, 80 C stack inlet temperature, at the worst of 10 bar, 50 C stack inlet temperature, a 1-1.7 €/kg increase can occur to the LCOH due to lower hydrogen production. In the 2030 construction year scenarios that were calculated for the renewable sources only, wind turbine connection leads to the all-time minimum of 5.2 €/kg and the only reason it is better than the 7.9 €/kg of PV connection is the higher capacity factor of 35% instead of 20%. This reduction in the 2030 scenario is a result of the further expected reduction on the LCOE of renewable sources, and the reduction of 200 €/kW on the stack capex. Finally, when it comes to the capital and operational costs the biggest influence comes from the stack capital cost and the electricity operational cost. Compressor and storage capex follows for the capital costs, while stack, compressor, storage and water purchases follow for the operational costs. For the grid connection scenario only, another 12.3% is added to the capital costs due to the stack replacement after the 80000 working hours.

5.2 Future work

From the writer perspective there are some thoughts about the future work.
Firstly, the custom model that was developed on the Asen Custom Modeler should be alternate in order for the system to predict realistic HTO for pressures outside the 5-10 bars scenario as well.
Also, a better mismatch with the commercials alkaline electrolysers data of similar powers could be reached if important components of the system like the fan and the purification system could be simulated more accurately. If those two conditions change, a very versatile and efficient simulation could be succeeded and a wide variety of alkaline electrolysis projects could be studied for different and even dynamic conditions.
Even though the techno-economic analysis lead to the calculation of realistic levelized costs of hydrogen, a more analytical model could be used that calculates other important economic variables that describe the evaluation of the investment, such as the net present value, the internal rate of return and the payback period.

Finally, since hydrogen production is most logical when it comes from renewable sources and considering that Europe countries like Greece possess substantial wind and solar potential, a more detailed analysis on the green hydrogen production, studied on the scale of minutes, could produce very important results that could be used on the forthcoming efforts of European states to reach the net zero emissions by 2050.

6. Intellectual property – Plagiarism

I have read and understood the rules on plagiarism and how to properly cite sources contained in the Guide to Writing Dissertations. I declare that, to the best of my knowledge, the content of this thesis is the product of my own work and there are references to all the sources I have used.

The opinions and conclusions contained in this Thesis are those of the author and should not be interpreted as representing the official positions of the School of Mechanical Engineering or the National Technical University of Athens.

Kyriakos Palamidis

Έχω διαβάσει και κατανοήσει τους κανόνες για τη λογοκλοπή και τον τρόπο σωστής αναφοράς των πηγών που περιέχονται στον Οδηγό συγγραφής Διπλωματικών Εργασιών. Δηλώνω ότι, από όσα γνωρίζω, το περιεχόμενο της παρούσας εργασίας είναι προϊόν δικής μου δουλειάς και υπάρχουν αναφορές σε όλες τις πηγές που χρησιμοποίησα.

Οι απόψεις και τα συμπεράσματα που περιέχονται σε αυτή τη Διπλωματική εργασία είναι του συγγραφέα και δεν πρέπει να ερμηνευθεί ότι αντιπροσωπεύουν τις επίσημες θέσεις της Σχολής Μηχανολόγων Μηχανικών ή του Εθνικού Μετσόβιου Πολυτεχνείου.

Κυριάκος Παλαμίδης

7. List of Abbreviations

AEL	Alkaline Electrolyser
ATR	Autothermal Reforming
AEM	Anion Exchange Membrane
ACM	Aspen Custom Modeler
BOP	Best Operational Parameters
CF	Capacity Factor
CCS	Carbon Capture and Storage
CCU	Carbon Capture and Utilization
CCUS	Carbon Capture Utilization and Storage
CMH_2	Carbon Material Hydrogen Storage
CAPEX	Capital Expenditure
FID	Final Investment Decision
HER	Hydrogen Evolution Reaction
HTO	Hydrogen To Oxygen
HHV	Higher Heating Value
LH2	Liquid Hydrogen
LAH2	Liquid Ammonia Hydrogen Storage
LOHC	Liquid Organic Carriers
LCOH	Levelized Cost Of Hydrogen
LCOE	Levelized Cost Of Energy
LHV	Lower Heating Value
MAH2	Metal Alloy Hydrogen
NRTL	Non Random Two Liquids

OTH	Oxygen To Hydrogen
OER	Oxygen Evolution Reaction
OPEX	Operational Expenditure
POX	Partial Oxidation
PV	Photovoltaics
PEM	Proton Exchange Membrane
SOEC	Solid Oxide Electrolyser
SMR	Steam Methane Reforming
WOP	Worst Operational Parameters
WGS	Water Gas Shift

8. List of Tables

9. List of Graphs

10. Code Annex

On this chapter the code from the Aspen Custom Modeler for the stack component is presented.

```
Model ELECTROLYSER

//adding ports

INLET As Input MoleFractionPort;

OUTanode As Output MoleFractionPort;

OUTcathode As Output MoleFractionPort;

Wstack as Input WorkPort;

QLOSS as Output HeatPort;

Pstack as pressure(value:7,description:"Stack Pressure", units: "bar");

Qlossf as realparameter(value:0.1,description:"Fraction of heat lost to surroundings");

Ncell as realvariable(value:12,description:"Number of cells in stack");

Acell as  realvariable(value:0.1,description:"Area of cell", units: "m2"); //m2

r1 as hidden realparameter (value:4.45153E-5);

r2 as hidden realparameter (value:6.88874E-9); //ohm-m2/C

d1 as hidden realparameter (value:-3.12996E-6); //ohm-m2

d2 as hidden realparameter (value:4.47137E-7); //ohm-m2/bar

s as hidden realparameter (value:0.33824); // V

t1 as hidden realparameter (value:-0.01539); // m2/A

t2 as hidden realparameter (value:2.00181); // m2-C/A

t3 as hidden realparameter (value:15.24178); // m2-C2/A

f11 as hidden realparameter (value:478645.74); // A2/m4

f12 as hidden realparameter (value:-2953.15); // A2/m4-C
```

f21 as hidden realparameter (value:1.03960);

f22 as hidden realparameter (value:-0.00104); // 1/C

C1 as hidden realparameter (value:0.09901);

C2 as hidden realparameter (value:-0.00207); // 1/C

C3 as hidden realparameter (value:1.31064e-5); // 1/C2

C4 as hidden realparameter (value:-0.08483);

C5 as hidden realparameter (value:0.00179); // 1/C

C6 as hidden realparameter (value:-1.13390e-5); // 1/C2

C7 as hidden realparameter (value:1481.45); // A/m2

C8 as hidden realparameter (value:-23.60345); // A/m2-C

C9 as hidden realparameter (value:-0.25774); // A/m2-C2

E1 as hidden realparameter (value:3.71417);

E2 as hidden realparameter (value:-0.93063); //1/bar

E3 as hidden realparameter (value:0.05817); //1/bar2

E4 as hidden realparameter (value:-3.72068);

E5 as hidden realparameter (value:0.93219); // 1/bar

E6 as hidden realparameter (value:-0.05826); // 1/bar 2

E7 as hidden realparameter (value:-18.38215); // A/m2

E8 as hidden realparameter (value:5.87316); // A/m2-bar

E9 as hidden realparameter (value:-0.46425); // A/m2-bar2

//variables definition

Vrev as hidden voltage (value:1.23, spec:Fixed);

Tstack as temperature;

Vcell as voltage;

icell as realvariable;

etaF as realvariable;

HTO as realvariable;

extent as flow_mol; //h2 produced in kmoles/hr

inflow(ComponentList) as flow_mol; //inlet stream

products(ComponentList) as flow_mol;

products_H as enth_mol;

products_z(ComponentList) as molefraction;

anodeflow(ComponentList) as flow_mol;

cathodeflow(ComponentList) as flow_mol;

anodedens as hidden dens_mol;

cathodedens as hidden dens_mol;

MW(ComponentList) as hidden molweight;

WstackQ as enthflow;

Qinp as enthflow;

Qout as enthflow;

aaMBzero as realvariable;

aaHBone as realvariable;

//equations

Call (MW) = pMolWeights() ComponentList; //MW procedure call

//Cell voltage (equation 3 from Sanchez et. al, paper)

EQ_1:Vcell=Vrev+(r1+d1+r2(Tstack)+d2*Pstack)*icell+s*log10((t1+t2/(Tstack)*
*+t3/(Tstack)^2)*icell+1);*

// Faraday efficiency (equation 5)

*EQ_2: etaF = (icell^2/(f11+f12*Tstack+icell^2))*(f21+f22*Tstack);*

//HTO is the mole fraction of H2 in the O2 stream (dry basis) from the equation 6

*EQ_3:HTO=(C1+C2*Tstack+C3*Tstack^2+(C4+C5*Tstack+C6*Tstack^2)*exp((C7+ C8*Tstack+C9*Tstack^2)/icell))+(E1+E2*Pstack+E3*Pstack^2+(E4+E5*Pstack+E6*Pstack^2)* exp((E7 + E8*Pstack+E9*Pstack^2)/icell));*

//work required for electrolyte stack -in kW

*EQ_4: Wstack.W*1000 = Vcell*Ncell*icell*Acell;*

//extent = # of moles produced in moles/hr, factor of 2 accounts for two electrons transferred //per hydrogen, 96485 = Faradays constant, 3600 accounts for time unit conversion

*EQ_5: extent*1000 = etaF*icell*Acell/2/96485*Ncell*3600;*

//cell stack operates adiabatically except from the ambient loss stream factored to the //reaction heat generated formation of liquid water

EQ_6: QLOSS.Q = Qlossf.288*extent; //*

//Generic equations follow

*inflow = INLET.F*INLET.z;*

//enthalpy flow calculation based on power/work provided Factor .0036 accounts for kW to //J/hr calculation

WstackQ = Wstack.W.0036;*

//Following code is for component balance. Water is permeable through diaphragm so //cathode and anode water flows are divided equally.

//KOH flow is also divided equally

anodeflow("KOH")= inflow("KOH")/2;

anodeflow("WATER")= (inflow("WATER")-extent)/2;

*anodeflow("H2")= extent/2*HTO/(1-HTO);*

anodeflow("O2")= inflow("O2")+extent/2;

cathodeflow("KOH") = inflow("KOH")/2;

cathodeflow("WATER") = anodeflow("WATER");

```
cathodeflow("H2") = inflow("H2") + extent - anodeflow("H2");
cathodeflow("O2") = 0;
products("KOH") = inflow("KOH");
products("WATER") = inflow("WATER")-extent;
products("H2") = inflow("H2")+extent;
products("O2") = inflow("O2")+extent/2;
//mole fraction calculation
products_z = products/sigma(products);
//energy balance
sigma(products)*products_h = Qinp-QLOSS.Q;
//molar enthalpy calculation for product stream based on mole-fractions
call(products_h) = pEnth_Mol(Tstack, OUTcathode.P, products_z);
//duty input calculation
Qinp = INLET.F*INLET.h+WstackQ;
//equate outcathode port variables to model variables
OUTcathode.F = sigma(cathodeflow);
OUTcathode.z = cathodeflow/OUTcathode.F;
OUTcathode.T = Tstack;
OUTcathode.P=Pstack;
OUTcathode.V*cathodedens = 1; // here V is molar volume for the port not voltage
//the following code is for the OUTcathode port enthalpy and density
call(OUTcathode.h) = pEnth_Mol_liq(OUTcathode.T,OUTcathode.P,OUTcathode.z);
call(cathodedens) = pDens_Mol_liq(OUTcathode.T,OUTcathode.P,OUTcathode.z);
//the following code is for OUTanode port
```

OUTanode.F = sigma(anodeflow);

OUTanode.z = anodeflow/OUTanode.F;

OUTanode.T = Tstack;

OUTanode.P = Pstack;

*OUTanode.V * anodedens = 1;*

call(OUTanode.h) = pEnth_Mol_liq(OUTanode.T, OUTanode.P, OUTanode.z);

call(anodedens) = pDens_Mol_liq(OUTanode.T, OUTanode.P, OUTanode.z);

//aaMBzero is defined as the difference between (sum of anodeflow and cathode flow) and //(inflow) variables, aaMBzero value needs to be close to zero

*aaMBzero =-sigma(inflow*MW) + sigma(anodeflow*MW) + sigma(cathodeflow*MW);*

// aaHBone is the ratio of inlet enthalpy calculated using port variable and duty converted //from power provided, aaHBone should be close to one

*aaHBone=(OUTanode.F*OUTanode.h+OUTcathode.F*OUTcathode.h+Qloss.Q)/(INLET.F*INLET.h+WstackQ);*

End

11. List of References

[1] L. A. WHITE, *ENERGY AND THE EVOLUTION OF CULTURE,* 1943.

[2] H. Ritchie, *How have the world's energy sources changed over the last two centuries,* 2021.

[3] "NASA," [Online]. Available: https://climate.nasa.gov/vital-signs/carbon-dioxide/.

[4] M. Barral, "Open Mind," 2019. [Online]. Available: https://www.bbvaopenmind.com/en/science/leading-figures/svante-arrhenius-the-man-who-foresaw-climate-change/.

[5] S. Arrhenius, On the Influence of Carbonic Acid in the Air upon the Temperature of the Ground, Philosophical Magazine and Journal of Science, 1896.

[6] "NASA," [Online]. Available: https://climate.nasa.gov/vital-signs/global-temperature/.

[7] S. I. R. G. S. VijayaVenkataRaman, "A review of climate change, mitigation and adaptation," *Renewable and Sustainable Energy Reviews,* 29 10 2011.

[8] "The Paris Agreement".

[9] *Renewable energy targets,* European Commission (Energy, Climate change, Environment).

[10] S. V. E. T. J. Evans Annete, "Evans A, StrezoAssessment of utility energy storage options for increased renewable energy penetration.," *Renewable and Sustainable Energy Reviews,* pp. 4141-4147, 2012.

[11] *The hydrogen ecosystem,* ITK. The Art of Digital Engineering..

[12] The European Hydrogen Path, European Commission.

[13] H. L. C. G. TEAM, *h21 Leeds City Gate.*

[14] N. Skordoulias, "Ανάλυση και προσομοίωση συστημάτων αποθήκευσης και αξιοποίησης πλεονάζουσας (curtailed) ηλεκτρικής ενέργειας από ΑΠΕ μέσω παραγωγής πράσινου υδρογόνου και σύζευξηςμε αεριοστρόβιλο (Power-to-H2-to-Power)," Athens, 2021.

[15] S. Antonis, "Τεχνοοικονομική μελέτη ολοκληρωμένου οικοσυστήματος παραγωγής και αξιοποίησης πράσινου Υδρογόνου στην Κύπρο," LSBTP NTUA, ATHENS, 2023.

[16] B. S. O. J. G. A. L. C. K. P. C. B. B.-M. H. Burcin Cakir Erdener, "A review of technical and regulatory limits for hydrogen blending in natural gas pipelines," *HYDROGEN ENERGY,* 2022.

[17] ENTSOG, *DECARBONISING THE GAS VALUE CHAIN,* 2021.

[18] D. P. P. M. G. B. P. B. A. Valera-Medina, "Preliminary study on lean premixed combustion of ammonia-hydrogen for swirling gas turbine," Gas Turbine Research Centre, Cardiff University, Wales, UK, Siemens Industrial Turbomachinery Ltd, Lincoln, England, UK, 2017.

[19] "Connecticut Hydrogen-Fuel Cell Coalition," [Online]. Available: https://chfcc.org/hydrogen-fuel-cells/about-hydrogen/hydrogen-properties/.

[20] "THE PATH TOWARDS A ZERO-CARBON GAS TURBINE," ETN GLOBAL.

[21] "Hydrogen: The future fuel today".*ICheme.*

[22] k. a. partners, "HyHouse". 2015.

[23] S.-L. J. e. al., "Enabling the injection of hydrogen in high-pressure gas grids: Investigation of the impact on materials and equipment,".*International Journal of Hydrogen Energy.*

[24] J. G. e. al., "Hydrogen embrittlement in hydrogen-blended natural gas transportation systems: A review".*International Journal of Hydrogen Energy.*

[25] M. S. R. H. A. Ajanovic, The economics and the environmental benignity of different colors fo hydrogen, Vienna University of Technology (TU WIEN), Vienna, Austria, 2022.

[26] J. W. Mengdi Ji, "Review and comparison of various hydrogen production methods based on costs and life cycle impact assessment indicators," *International Journal of Hydrogen Energy,* 2021.

[27] A. P. Pavlos Nikolaidis, "A comparative overview of hydrogen production processes," *Renewable and Sustainable Energy Reviews,* 2016.

[28] The colors of hydrogen, Hydrogen Europe.

[29] B. J, " Blue hydrogen 20% worse for GHG emissions than natural gas in heating: study.," *S&P Global Platts,* 2021.

[30] Global Hydrogen Review 2022, International Energy Agency, 2022.

[31] Global Hydrogen Review 2023, International Energy Agency.

[32] P. B. Z. F. Junbo Huang, Technical and economic analysis of different colours of producing hydrogen in China, 2022.

[33] S. F. T. Handbook.

[34] M. El-Shafie, "Hydrogen production by water electrolysis technologies: A review," *Results in Engineering,* 2023.

[35] H. L. S. Shiva Kumar, "An overview of water electrolysis technologies for green hydrogen production," *Energy Reports,* 2022.

[36] S. S. e. al., "A review of recent advances in alkaline electrolyzer for green hydrogen production:Performance improvement and applications".*International Journal of Hydrogen Energy.*

[37] A. W. V. Matheus T. de Groot, "Ohmic resistance in zero gap alkaline electrolysis with a Zirfon diaphragm," *Electrochimica Acta,* 2020.

[38] S. H. e. al, "A comprehensive review of alkaline water electrolysis mathematical modeling," *Applied Energy ,* 2022.

[39] Hydrogen Europe, *CLEAN HYDROGEN MONITOR 2022.*

[40] G. A. e. al., "An overview on the technologies used to store hydrogen," *ENERGY REPORTS,* 2022.

[41] M. R. Usman, "Hydrogen storage methods: Review and current status".*Renewable & Sustainable Energy Reviews.*

[42] N. M. e. al., "Large scale of green hydrogen storage: Opportunities and challenges".*Hydrogen Energy.*

[43] H. Barthelemy, "Hydrogen storage - Industrial prospectives," *Hydrogen Energy,* 2012.

[44] EUROPEAN HYDROGEN BACKBONE, *Analysing future demand, supply, and transport of hydrogen,* 2021.

[45] J. S.-L. e. al., "Enabling the injection of hydrogen in high-pressure gas grids: Investigation of the impact on materials and equipment," *HYDROGEN ENERGY,* 2023.

[46] European Hydrogen Backbone, *European Hydrogen Backbone Maps.*

[47] C. C. e. al., "Hydrogen storage by liquid organic hydrogen carriers: Catalyst, renewable carrier, and technology – A review," *Carbon Resources Conversion,* 2023.

[48] M. S. e. al., "Semi-empirical model and experimental validation for the performance evaluation of a 15 kW alkaline water electrolyzer," *International Journal of HYDROGEN ENERGY,* 2018.

[49] M. T. d. G. e. al., "Optimal operating parameters for advanced alkaline water electrolysis," *Hydrogen Energy,* 2022.

[50] M. S. e. al, "Aspen Plus model of an alkaline electrolysis system for hydrogen production," *International Journal of HYDROGEN ENERGY,* 2019.

[51] Z. P. David Tremblaym, *Jump Start: Aspen Custom Modeler V8,* Aspen Technology.

[52] aspentech, *Integrated Custom Model of Alkaline Electrolysis System for H2 Production.*

[53] "LNEYA Air Cooled Chiller," [Online]. Available: https://www.lneya.com/air-cooled-chillers?productid=YDYLaircoolingchiller&gad_source=1&gclid=CjwKCAiAqY6tBhA

tEiwAHeRopdb6XlXF7-3Xf0_NXCM57_viVruiIdtWwjVM8wCoZ2OLPEotxIAlwBoCO4gQAvD_BwE.

[54] S. D. e. al., "Experimental and modeling study on energy flow of 250 kW alkaline water electrolysis system under steady state conditions and cold start process," *The science and technology of Fuel and Energy,* 2023.

[55] S. Jarungthammachote, "Optimal interstage pressures of multistage compression with intercooling processes," *Thermal Science and Engineering Progress ,* 2022.

[56] Ecolyzer by Ecoclean, "ecolyzer.com," [Online]. Available: https://ecolyzer.com/fileadmin/files/EcoLyzer_Data-Sheet_technical_EN_2023_08.pdf.

[57] stargate hydrogen, [Online]. Available: https://stargatehydrogen.com/wp-content/uploads/2023/12/Spec_sheet_Electrolyser_stargate_hydrogen-2024.pdf.

[58] Clean Hydrogen Partnership, Strategic Research and Innovation Agenda 2021 – 2027.

[59] G. M. e. al., "Techno-economic model and feasibility assessment of green hydrogen projects based on electrolysis supplied by photovoltaic PPAs," *HYDROGEN ENERGY,* 2022.

[60] C. M. e. al., "A flexible techno-economic analysis tool for regional hydrogen hubs e A case study for Ireland," *HYDROGEN ENERGY,* 2023.

[61] International Renewable Energy Agency, "Renewable Power Generation Costs in 2022," 2023.

[62] *Electricity prices for non-household consumers - bi-annual data (from 2007 onwards).*

[63] WORLD ECONOMIC FORUM, "Wind and solar PV will keep taking the lead, Energy Technologies 2030," 2020.

[64] B. T, M. G and A. R. J, Global, Regional, and National Fossil-Fuel CO2 Emissions (1751 - 2014), Carbon Dioxide Information Analysis Center (CDIAC), Oak Ridge National Laboratory (ORNL), Oak Ridge, TN (United States). , 2017.

[65] Global Energy Review: CO2 Emissions in 2021, International Energy Agency, 2022.

[66] Total energy consumption, World Energy & Climate Statistics- Yearbook 2023.

[67] BP Statistical Review of World Energy, 2019.

[68]